공학박사학위논문

Design and Optimization of Low Carbon Emitting Combined Rankine Cycle using LNG Cryogenic Exergy

액화 천연가스의 냉열을 이용한 저탄소 복합 발전 시스템의 설계 및 최적화

2014 년 8 월

서울대학교 대학원

화학생물공학부

이 웅

Abstract

Design and Optimization of Low Carbon Emitting Combined Rankine Cycle using LNG Cryogenic Exergy

Ung Lee
School of Chemical & Biological Engineering
The Graduate School of Seoul National University

Recent climate change and related consequences have attracted worldwide attention and increased global efforts to reduce the emission of greenhouse gases, particularly CO_2. Among the various sources of the CO_2 emission, power plants combusting fossil fuel such as coal, oil and gas contribute the CO_2 emission the most. Several methods of removing CO_2 from power plant flue gas have been proposed, and amine-based CO_2-absorbing systems are considered to be one of the most suitable options because they have been demonstrated to be mature and less expensive technologies[1]. However, high energy consumption and corresponding electricity cost increment have been pointed out as an obstacle of the commercialization. The estimated

electricity production cost increase from introducing a CO_2 capture process is 40–85% for a supercritical pulverized coal (PC) power plant [2]. In this study, a low carbon emitting combined Rankine cycle is proposed. In this cycle, the CO_2 generated from the coal combustion unit is captured through the post combustion capture process using mono-ethanol amine (MEA). This capture process consumes only 73% of the conventional capture plant operation energy by employing advanced process configuration such as vapor recompression. An organic Rankine cycle (ORC) utilizing both low-grade heat from a pulverized coal power plant and liquefied natural gas (LNG) cold exergy is also installed and optimized in order to minimize the power de-rate. The ORC uses R601-R23-R14 ternary mixture as its working fluid and is integrated with a steam cycle as a bottoming cycle. By utilizing the hot and cold exergy of low-pressure steam and LNG that were initially wasted, the ORC is able to generate additional power without consuming fossil fuel. The CO_2 captured from the capture process is liquefied by utilizing its latent heat as a heat source for the working fluid. Consequently, an energy intensive liquefaction process can be avoided by CO_2 utilization. 74.1 MW of additional electricity can be produced from ORC without consuming additional coal, thus both cycle efficiency and power de-rate resulted from CO_2 capture process installation are greatly improved. To fine

the optimum composition of the ternary working fluid, Scattered Search algorithm is developed. Based on the single variable local optimum information, this method selects deterministic starting point and find the global optimum using sequential quadratic programming iteration method. With this algorithm, optimum composition can be found within the half of the iteration steps with improved accuracy as compared with Genetic Algorithm

Keywords: Carbon Capture, CO_2, LNG, ORC, Scattered Algorithm, Ternary, Exergy optimization,

Student ID: 2010-21006

Contents

Abstract i

CHAPTER 1. Introduction 2

1.1. Research motivation 2

1.2. Research objective 7

1.3. Outline of the thesis 11

CHAPTER 2. Base Case Modeling and Simulation 13

2.1. Process Overview 13

2.2. PC power plant modeling 13

2.3. Post combustion CO_2 capture process modeling 21

2.4. CO_2 liquefaction process modeling 30

2.5. Base case simulation result 40

CHAPTER 3. Modified CO_2 Capture Process Design and Optimization 55

3.1. Overview 55

3.2. Lean vapor recompression process 56

3.3. Mechanical vapor recompression process 60

3.4. Modified CO_2 capture process simulation result 66

3.4.1. Lean vapor recompression 66

3.4.2. Mechanical vapor recompression 76

CHAPTER 4. Combined Rankine Cycle Design and Optimization 84

4.1. Overview 84

4.2. Working fluid selection 85

4.3. Process modeling and simulation 94

4.3.1. Design basis 94

4.3.2. ORC process description 94

4.4. Mathematical modeling 97

4.4.1. Condenser/evaporator 97

4.4.2. Reheater 98

4.4.3. Preheater 98

4.4.4. Pump 99

4.4.5. Turbine 99

4.4.6. System efficiency 100

4.5. Result and Discussion 101

4.5.1. Cycle performance and optimization 101

4.5.2. Cycle performance of different ternary mixtures 113

4.5.3. Sensitivity analysis 115

4.6. Performance summary of the combined rankine cycle 123

CHAPTER 5. Implementation of Scattered Search for Simulator Based Non Convex Problem 125

5.1. Overview 125

5.2. Local optima calculation: Sequential Quadratic Programming 126

5.3. Scattered search for global optimum 128

5.4. Case study with Rastrigin's fucnction..... 131

5.5. Implementation of scattered search on irreversibility minimization 136

CHAPTER 6. Concluding Remarks 140

6.1. Conclusions..... 140

6.2. Future work..... 142

List of Figures

Fig. 1-1 Process flow diagram of combined Rankine cycle 9

Fig. 2-1 Process flow diagram of steam cycle 17

Fig. 2-2 Process flow diagram of coal combustion process..... 20

Fig. 2-3 Process flow diagram of post combustion CO2 capture process 26

Fig. 2-4 Flow diagram of CO2 liquefaction process..... 34

Fig. 2-5 T-S diagram of the steam cycle 43

Fig. 2-6 CO_2 capture process column temperature profiles..... 46

Fig. 2-7 Exergy loss of the unit operations in CO_2 capture process 48

Fig. 2-8 Pressure enthalpy diagram of CO_2 and the operating line of the CO_2 liquefaction process..... 51

Fig. 2-9 Operation energy consumption of CO_2 liquefaction process 54

Fig. 3-1 Process flow diagram of the CO2 stripper lean vapor recompression 58

Fig. 3-2 T-S diagram of typical MVR process..... 62

Fig. 3-3 Process flow diagram of the CO2 stripper with mechanical vapor compression process 65

Fig. 3-4 Stripper temperature profile of LVR process 68

Fig. 3-5 Effect of the minimum temperature approach on the reboiler energy consumption and the steam consumption 70

Fig. 3-6 Heat curves of the HE-202 with minimum temperature approach of 16.5 and 5˚C 72

Fig. 3-7 Stripper operating pressure effect on the solvent regeneration and lean vapor compressor energy..... 75

Fig. 3-8 Total energy consumption of the base case and modified capture process..... 80

Fig. 3-9 Exergy loss of each unit operation, and total exergy loss of the system 82

Fig. 4-1 T-S diagram of organic Rankin cycles 87

Fig. 4-2 Heat curve of the ternary mixture working fluid and LNG within the condenser..... 92

Fig. 4-3 Process flow diagram of ORC using ternary mixture working fluid..... 96

Fig. 4-4 T-S diagram of ORC using ternary mixture working fluid. 102

Fig. 4-5 Total power generation vs. P1 discharge pressure change and corresponding T-S diagram of the ORC..... 104

Fig. 4-6 Heat curve of evaporator and reheater 106

Fig. 4-7 Irreversibility of unit process. 108

Fig. 4-8 Net power generation of ORCs using ternary mixture working fluids. 114

Fig. 4-9 Power generation of combined Rankine cycle depending on the steam extraction location. 117

Fig. 4-10 Power generation and thermal efficiency of ORC according to the T1 discharge pressure..... 119

Fig. 4-11 Gross power generation according to the composition of working fluid..... 122

Fig. 5-1 Starting point grid of Rastrigin's function..... 130

Fig. 5-2 3D plot and contour of Rastrigin's function..... 132

Fig. 5-3. Single variable responds and starting points of Rastrigin's function optimization..... 134

Fig. 5-4 Single variable respond of objective function f 138

List of Tables

Table. 2-1 Basic input and simulation result of the steam cycle 15

Table. 2-2 Design coal characteristics 19

Table. 2-3 Flue gas composition and its condition 22

Table. 2-4 Henley's constant parameters of light gases 23

Table. 2-5 Gas Quality and Input Data for CO_2 Liquefaction Process 33

Table. 2-6 Power cycle performance of base case 42

Table. 2-7 Optimized Compression ratio and pressure on each compressor stage 53

Table. 3-1 Input parameters and results of the stripper with LVR process 67

Table. 3-2 Composition of the stripper overhead stream 78

Table. 3-3 Composition of the stripper overhead stream 79

Table. 4-1 Composition of LNG 86

Table. 4-2 Refrigerants for ternary mixture working fluid combination .. 91

Table. 4-3 Composition and pressure of the ternary mixture working fluid 93

Table. 4-4 Evaluation result of ORC with R601-R23-R14 working fluid 110

Table. 4-5 Performance of ORCs with pure, binary and ternary mixture working fluid 112

Table. 4-6 Performance summary of the base case and the combined Rankine cycle 124

Table. 5-1 Results of Rasfrigin's function optimization with different algorithms 135

CHAPTER 1. Introduction

1.1. Research motivation

The depletion of fossil fuel due to increasing energy consumption has been accelerating, thus the energy crisis is becoming more severe. Moreover, the need to reduce fossil fuel consumption has been attracting more attention recently due to concerns related to global warming. Pulverized coal (PC) power plants are one of the largest consumers of fossil fuel, and they produce a significant amount of CO_2. Therefore, much research has been focused on improving the efficiency of PC power plants and reducing their CO_2 emission in order to address both fossil fuel depletion and greenhouse gas reduction.

Several methods of removing CO_2 from power plant flue gas have been proposed, and amine-based CO_2-absorbing systems are considered to be one of the most suitable options because they have been demonstrated to be mature and less expensive technologies [1]. However, high energy consumption and corresponding electricity cost increment have been pointed out as an obstacle of the commercialization. The estimated electricity production cost increase from introducing a CO_2 capture process is 40–85% for a supercritical pulverized coal (PC) power plant [2].

To reduce the energy penalty, several studies have been conducted on more-efficient power generation processes with CO_2 capture. Research on minimizing the de-rate of the power cycle includes optimization of the steam extraction point for the CO_2 stripper reboiler [3-6], advanced process configuration, and parameter optimization. Mimura, Romeo, and Desideri indicated that steam for the CO_2 stripper can be extracted from midway through the low-pressure (LP) section of the turbine. Alie also advocated steam extraction from the power cycle as the best approach, and it can be extracted from IP/LP crossover pipe[3].

Wagener et al. suggested the ulitization of geothermal energy for solvent regeneration through advanced stripper configuration [7]. Jassim et al. proposed the complex absorber and stripper configuration and reduce the solvent regeneration energy by 0.12 GJ/ton CO_2 [8]. Abu-Zahra et al. presented effects of main parameters on solvent regeneration energy and suggested the optimum operation condition [1]. Despite of these studies, the plant de-rate ranged from 17% to 30% compared to similar plants without a capture process.

In order to compensate the power derate due to the CO_2 capture process, various thermodynamic cycles such as organic Rankine cycle, supercritical Rankine cycle, Kalina cycle and Goswami cycle can be installed to produce electricity from low grade heat. Among these cycles, the organic Rankine

cycle (ORC) has been identified as an efficient low temperature heat recovery method because of its high efficiency and simplicity [9].

The bottoming ORC is able to produce additional power without consuming fossil fuel through utilization of waste heat generated from the steam cycle. Although many studies have focused merely on improving the efficiency of the topping cycle, it is also important to improve the bottoming cycle's efficiency in order to produce more power from power plants. Because the waste heat from the steam cycle (the temperature of which is too low to be utilized for other purposes within the steam cycle) is used, the combined cycle can produce more power without generating additional CO_2.

Many researchers have proposed a power cycle using low-grade heat sources, which can be applied to the bottoming cycle. These studies included working fluid selection, optimization of low-grade heat source utilization, and novel power cycle design. Chacartegui et al. [10] studied an organic Rankine cycle (ORC) as a bottoming cycle of a combined cycle using six different pure working fluids. The combined cycle using toluene as an ORC working fluid exhibited the highest efficiency of all the working fluids they tested. Vélez et al. [11] showed that a transcritical power cycle using CO_2 can maximize power generation when the heat source temperature is below 150 ℃. Baik et al. [12] proposed a transcritical cycle using a zeotropic mixture working fluid for geothermal power generation. The results of their

study showed that the proposed transcritical cycle generates 11% more power than that of the R134a subcritical cycle when R125-R245fa mixture is used as the working fluid. A parametric study and performance analysis of the ORC for waste-heat recovery was performed by Roy et al. [13]. The flue gas, which had a temperature of 140 ℃, was utilized as a heat source and evaluated with three different working fluids. The result showed that the ORC using R-123 can generate power up to 19.09 MW. Parametric optimization and a comparative study of the ORC were performed by Dai et al. [14]. They assumed that a 140 ℃ heat source is available taking into account both geothermal and solar energy, and they tested 10 different working fluids including water. Hung [15] studied the factors that affect the net power produced by the ORC using low-grade heat. In this study, the efficiency of the ORC and the sum of all the irreversibility from each unit (e.g., the evaporator) have opposite curves, and the power cycle was optimized at the crossover point of the two curves. Xi et al. and Wang et al. [16, 17] performed the optimization of ORC for low-grade heat recovery by using an optimization algorithm (a genetic algorithm and an evolutionary algorithm, respectively). Xi et al. [17] compared three kinds of ORCs: basic, single-stage regenerative, and double-stage regenerative. It was concluded that the basic ORC produces maximum power, but the double-stage regenerative ORC has better thermal and exergy efficiency. Wang et al. [16]

also performed an optimization of the ORC by selecting both exergy efficiency and capital cost as objective functions. Using an evolutionary algorithm, they found that the ORC exhibits an exergy efficiency of 13.98% and a capital cost of 129.28×10^4 USD at the optimum state.

There have been other noteworthy studies performed to recover low-grade heat using liquefied natural gas (LNG) as a heat sink. In this way, the temperature difference between the heat source and the heat sink is increased because the condensation of the working fluid takes place at a point lower than ambient temperature. Consequently, the bottoming cycle can produce more power with the same heat source utilization. Qiang et al. [18] investigated the parameters of the ORC for LNG cold exergy recovery, and the temperature of the low-grade heat source, condensing temperature, and turbine inlet pressure were determined to be the essential parameters. Shi and Che [19] suggested an ammonia-water mixture Rankine cycle combined with LNG power generation. The turbine inlet pressure, ammonia mass fraction, and heat source temperature were investigated to find the optimum operating condition that leads to maximum electric and exergy efficiency. Wang et al. [20] also proposed an ammonia-water power cycle utilizing LNG cold exergy. Exhaust gas at 200 ℃ was used as a low-grade waste-heat source in this study. They also performed a multiobjective optimization to achieve the optimum condition of the water-ammonia power cycle using key parameters.

Liu and Guo [21] reported that the availability of LNG depended on its pressure, and they proposed a combined cycle comprised of the ORC and a direct expansion of LNG. The effects of the LNG utilization temperature and the LNG vaporizing pressure on the efficiency of the proposed combined cycle were also presented in this study. Liu and Guo [22] proposed a modified ORC using a tetrafluoromethane-propane mixture as the working fluid. By utilizing seawater and LNG cryogenic exergy, the proposed power cycle generated much more power than a single-component ORC. Szargu and Szczgiel [23] performed analyses of three variant ORCs using LNG cold exergy and a heat source at 15 ℃ . Choi et al. [24] performed optimization of a cascade ORC to recover LNG cryogenic exergy effectively. The three-stage ORC using propane as a working fluid generates the largest amount of power and exhibits high thermal and exergy efficiency compared to other power cycles they examined. Rao et al. [25] proposed a combined cycle using low-grade heat from solar energy and cryogenic exergy from LNG. Sixteen working fluid candidates were examined to obtain the optimum performance.

1.2. Research objective

In this work, an innovative combined Rankine cycle is designed and optimized. The combined Rankine cycle consists of the coal combustion unit, steam cycle, CO_2 capture process, and organic Rankine cycle with

ternary mixture. Both the coal combustion unit and the steam cycle are modeled based on the DOE/NETL report and their coal consumption and gross power output are 219 t/h, and 661 MW, respectively. The amount of flue gas production from the coal combustion process is 2,307 t/h. Since single CO_2 capture process can handle about 460 t/h flue gas in this study, five CO_2 capture processes in parallel are required in order to capture 92% of CO_2 from the flue gas. The LNG regasification process is designed based on the operation data of Incheon LNG terminal in Republic of Korea. The amount of available LNG for the regasification process is 1,620 t/h. In the combined Rankine cycle, the energy consumption of the CO_2 capture process is reduced through vapor recompression process and the power production is enhanced by waste heat recovery using bottoming ORC. The process flow diagram of the combined Rankine cycle is presented in Fig. 1-1.

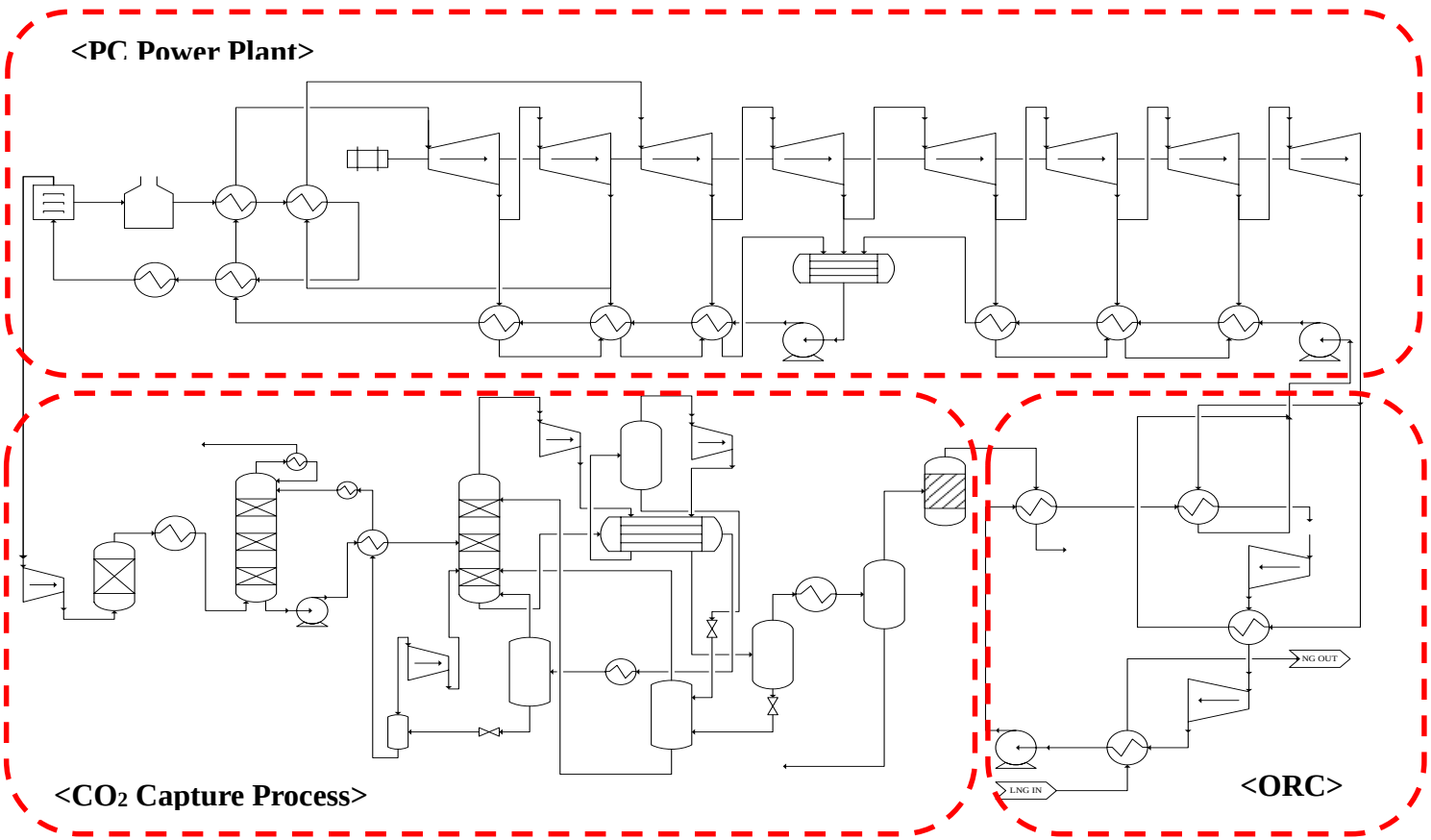

Fig. 1-1 Process flow diagram of combined Rankine cycle

Most of the previous CO_2 capture process studies mainly focused on the solvent regeneration energy. In this study, however, we emphasize more on the exergy loss of the entire system. In order to reduce the exergy loss of the system, vapor recompression processes are employed. By adopting vapor recompression, both the solvent regeneration energy and exergy loss can be greatly reduced. Additionally, product pressure of CO_2 capture process increases to 6.5 bar with vapor recompression process, thus the CO_2 compression process which consumes considerable amount of energy can be avoided.

The multicomponent organic Rankine cycle utilizes LNG cryogenic exergy and wasted heat from steam cycle. Although previous research has improved the performances of ORC significantly, some points still need to be improved. Since LNG is a multicomponent mixture comprised of more than eight components, the evaporation process of LNG is not isothermal. Therefore, the exergy recovery of the LNG through the ORC working fluid can be significantly improved by utilizing multicomponent working fluids, which have a nonisothermal condensing nature. Also, the proposed ORC is designed to recover the entire evaporation enthalpy of LNG by using a multicomponent working fluid in order to maximize the power generation within the cycle. To illustrate the performance of the ternary mixture ORC quantitatively, ORCs with single and binary components were also examined

in this study.

Another important point of this study is the integration of the ORC with a PC power plant with a CO_2-capture unit. The proposed power cycle utilized low-pressure steam from a PC power plant to enhance the total power generation. In addition, captured CO_2 from the PC power plant was utilized to preheat the working fluid. In this manner, the proposed power cycle can preheat the working fluid and eliminated the energy requirement for liquefaction of CO_2.

Through the novel configuration and process integration of the combined Rankine cycle, Energy penalty of CO_2 capture process can be greatly improved. The power reduction of the cycle is reduced from 23% to 9% and consequent thermal efficiency increases from 32.1% to 37.6%. While the combined Rankine cycle operation, 1620 t/h LNG is evaporated without consuming additional energy.

1.3. Outline of the thesis

The thesis is organized as follows. Chapter 1 presents the motivation and objective of the research as introduction. A complete power cycle with CO_2 capture and liquefaction process is suggested as the base case in the Chapter 2. The base case process is modeled and optimized according to the literature survey and pilot plant operation data. Chapter 3 presents modified CO_2 capture process based on the exergy analysis. Since the most exergy

loss and energy consumption are occurred at the lean rich amine heat exchanger and the stripper, efficient energy recovery and exergy loss minimization on these units were mainly considered. Chapter 4 suggests wasted heat recovery from both the steam cycle and LNG regasification process by integrating them with multi component ORC. In order to maximize energy recovery from the cycle, the best working fluid mixture was proposed and exergy loss minimization was performed. In addition, parameter sensitivity analysis was performed in order to give optimal operation condition of the cycle. Heuristic approach to find global optimum is also presented in chapter 5. Using sequential quadratic programming algorithm and scattered search method, the global optimum of non-convex problem can be solved with reliable efficiency and accuracy. In chapter 6, the conclusion of this thesis and future work are presented.

CHAPTER 2. Base Case Modeling and Simulation

2.1. Process Overview

The base case of this study is consisted of pulverized coal (PC) power plant, post combustion CO_2 capture process using aqueous mono-ethanol amine (MEA), and CO_2 liquefaction process. CO_2 generated from the 661 MW PC power plant is captured through the capture process with 92.8% recovery and liquefied into complete liquid in the liquefaction process. For the modeling and simulation of these process, a commercial process simulator Aspen Plus^{TM} was used. Three thermodynamic properties were used in the simulation: the National Bureau of Standards (NBS) steam table equation of state (STEAMNBS) for the PC power plant, the electrolyte NRTL method with the Redlich–Kwong (RK) equation of state for the CO_2 capture process [26], and the Soave–Redlich–Kwong (SRK) equation of state with the modified binary interaction parameter for the gas conditioning process [27]. These thermodynamic models have been widely employed in previous studies [28-30] and demonstrate good agreement with the experimental data within target plant operating conditions.

2.2. PC power plant modeling

A 661MW PC power plant was modeled based on the supercritical pulverized coal power system in DOE/NRTL report [31]. Steam conditions

for the Rankine cycle were selected based on the NETL Advanced Materials for Supercritical Boilers program. This program specifies the steam condition of both supercritical and ultra-supercritical steam cycle process.

- For supercritical cycle cases – 3500 psig/1110°F/1150°F
- For ultra-supercritical cases – 4000 psig/1350°F/1400°F

It has been indicated that it does not necessary to increase the steam pressure beyond 3500 psig to increase process efficiency because increasing pressure has small impact on the efficiency and it proportionately increases the thickness of all the pressure part. This added thickness not only directly increases material cost for the pressure parts, but also cause additional building and foundation costs to support the additional weight and causes the surface metal temperatures to increase requiring more costly alloy materials [31].The basic input of the steam cycle is summarized in Table 2-1.

Table. 2-1 Basic input and simulation result of the steam cycle

Items	Value/Unit
SH steam	598.9℃, 242.35bar
RH steam	621.1.℃, 49bar
Condenser outlet	38.7℃, 0.368bar
Turbine discharge pressure	**bar**
HP	77.07, 49.02
IP	21.36, 9.515
LP	5.013, 1.323, 0.5771, 0.2473, 0.069
TTD(FWH1-FWH7)	℃
FWH1	1.1
FWH2	0
FWH3	1.1
FWH4	-2.8
FWH5	-2.8
FWH6	-2.8
FWH7	-2.8

Fig. 2-1 shows the process flow diagram of the steam cycle. The steam cycle consists of two high-pressure (HP), two intermediate-pressure (IP), and five low-pressure (LP) steam turbines with a gross efficiency of 41.4%. It was assumed that the steam cycle employed a standard vacuum condensing cycle. The low-pressure steam from the LP turbine is expanded to 68.9 mbar and its corresponding temperature is 39 ℃. Seven feed water heaters (FWH) are used to preheat the water delivered to the steam-generating boiler. Preheating the feed water reduces the irreversibility involved in steam generation and thus improves the thermodynamic efficiency of the system [32]. A pair of heater blocks was used to simulate a FWH to establish the terminal temperature difference (TTD). The TTD can be expressed as follows:

$$TTD = T_{sat} - T_{fw} \qquad (2\text{-}1)$$

Where T_{fw} is the temperature of the feed water leaving the tubes and T_{sat} is the condensation temperature of the extracted steam in the closed FWH.

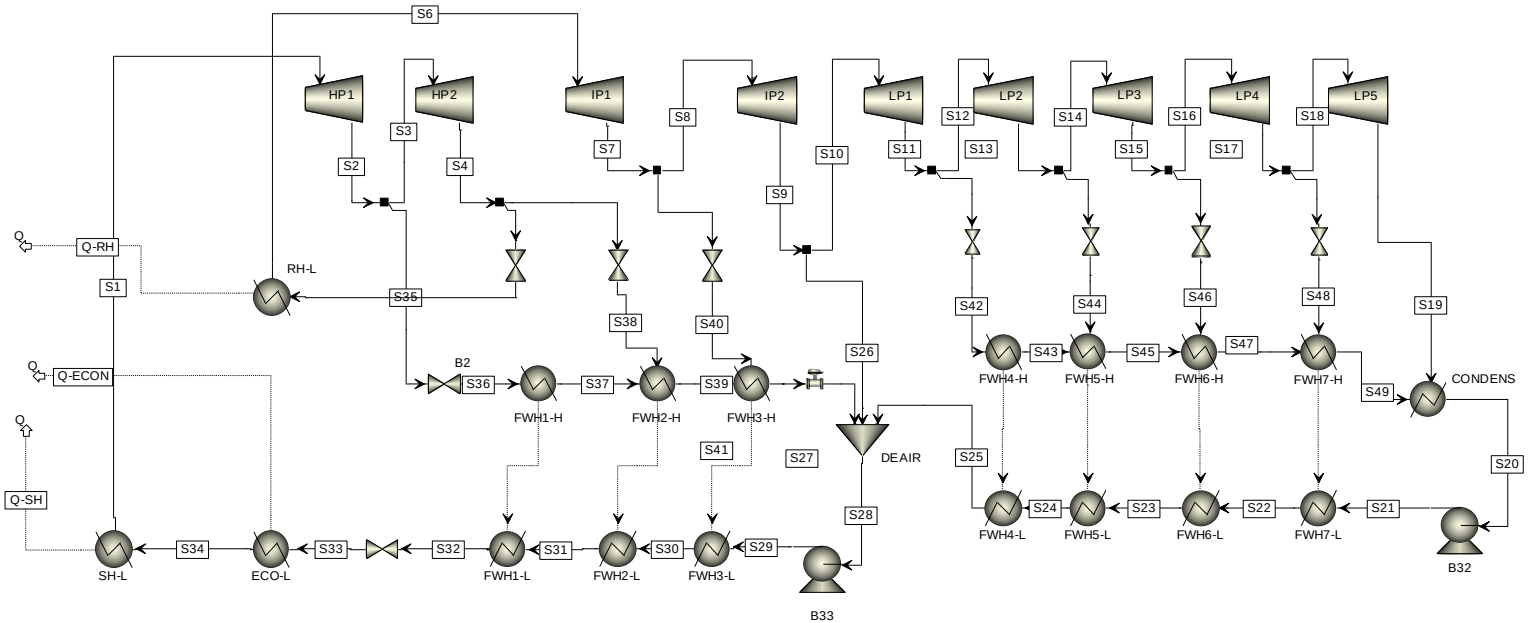

Fig. 2-1 Process flow diagram of steam cycle

In order to predict coal consumption as well as the heat duty of economizer, super-heater, and reheater, coal combustion unit was also modeled based on simulation data shown in DOE/NETL report [31]. The coal combustion unit is consisted of coal dryer, burner, steam generators, particulate control, and flue gas desulfurization (FGD). Illinois No. 6 bituminous coal was used as design coal and its charactoristics are presented in the Table 2-2. The HHV and LHV in the table represent higher heating value and lower heating value of the coal, respectively.

Fig. 2-2 indicates the process flow diagram of coal combustion process. In Aspen Plus, R-Gibbs model was used to simulated coal combustion. However, it cannot be done directly, because coal is a nonconventional component. Before feeding the coal to burner, the raw coal is decomposed to the components in the ultimate analysis using R-Yield model. The heat of reaction associated with the decomposition is added to burner using Q-DECOMP steam. The flue gas goes through the super-heater (SH-1), reheater (RH), economizer (ECON), cyclone (CYCLONE), a fabric filter (BAG-FILT), and electrostatic precipitator(ESP), and flue gas desulfurization (FGD). The composition and temperature of the flue gas shows good agreement with the DOE/NETL report. The flue gas exhausted from the coal combustion unit is sent to CO_2 capture process in order to remove CO_2 from the flue gas.

Table. 2-2 Design coal characteristics

Proximate Analysis	**As-Received**	**Dry**
Moisture	11.12%	0.00%
Volatile Matter	34.99%	39.37%
Ash	9.70%	10.91%
Fixed Carbon	44.19%	49.72%
Total	100.00%	100.00%
Ultimate Analysis	**As-Received**	**Dry**
Carbon	63.75%	71.73%
Hydrogen	4.50%	5.06%
Nitrogen	1.25%	1.41%
Sulfur	2.51%	2.82%
Chlorine	0.29%	0.33%
Ash	9.70%	10.91%
Moisture	11.12%	0.00%
Oxygen	6.88%	7.74%
Total	100.00%	100.00%
Reported Heating Value	**As-Received**	**Dry**
HHV (Btu/lb)	11,666	13,126
LHV (Btu/lb)	11,252	12,660

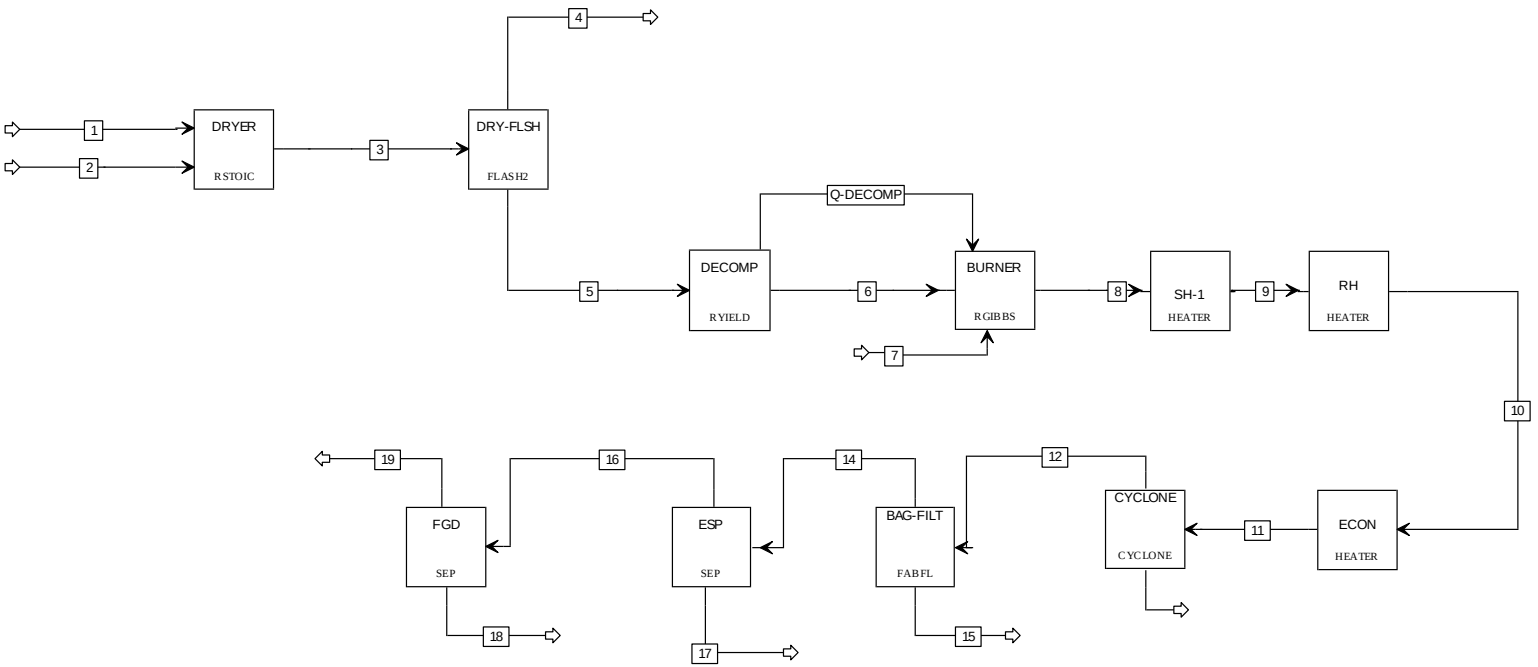

Fig. 2-2 Process flow diagram of coal combustion process

2.3. Post combustion CO_2 capture process modeling

To capture CO_2 of the flue gas generated from PC power plant, the post combustion CO_2 capture process using aqueous Mono-ethanolamine (MEA) was used because it is considered the most feasible option for CO_2 removal. An Aspen Plus^{TM} rate based model was built to identify the capture efficiency and process energy consumption, and the constructed model was validated with pilot plant data with similar flow gas composition and condition. Table 2-3 indicates the flue gas composition and condition adopted in this study.

Among the constituents of the flue gas, light gases such as N_2, CO_2 and O_2 were selected as Henry components and Henry's constants of these components were specified with water and MEA. Table 2-4 indicates the Henry's constant parameters of the light gases and Henry's constants can simply be calculated using Eq. (2-2) with parameters given in the table. The parameters of CO_2 in H_2O were obtained from the vapor liquid equilibrium (VLE) data of Takenouchi et al. [33], Tödheide et al. [34], Dodds et al. [35], Drummond [36], Zawisza et al. [37], Wiebe et al. [38] and Houghton et al. [39] and those in the MEA were regressed based on the work of Wang et al. [40].

$$\ln H_i^{Po} = C_1 + \frac{C_2}{T} + C_3 lnT + C_4 T \qquad (2\text{-}2)$$

Table. 2-3 Flue gas composition and its condition

Items	Value	Unit
Flue gas temperature	40	˚C
Flue gas Pressure	104.4	kPa
Flue gas flow rate	2307.05196	t/h
Flue gas composition(mole frac)		
N_2	0.728	
Ar	0.009	
CO_2	0.134	
H_2O	0.107	
O_2	0.022	

Table. 2-4 Henley's constant parameters of light gases

Henry's Component	**CO_2**	**CO_2**	**N_2**	**O_2**
Solvent	**H_2O**	**MEA**	**H_2O**	**H_2O**
Temperature units	K	K	K	K
a_{ij}	-145.316134	20.176	176.507	155.921
b_{ij}	765.888228	-1139	-8432.77	-7775.06
c_{ij}	32.2472704	0	-21.558	-18.3974
d_{ij}	-0.07395071	0	-0.008436	-9.44E-03

In this model, Electrolyte non-random two liquid model (E-NRTL) and Redlich-Kwong (RK) equation of state were used in order to predict thermodynamic property liquid and vapor, respectively. The NRTL interaction parameters between MEA and H_2O, and interaction energy parameters between H_2O and (MEAH+, HS-) were obtained from the work of Austgen et al. [26]. The rest of the interaction energy parameters such as H_2O-(MEAH+, HCO_3-), and H_2O - (MEAH+, MEACOO-), were regressed using the absorption heat data from Kim et al. [41], heat capacity data from Weiland et al. [42] and VLE data from Lee at al. [43] and Jou et al. [44]. The dielectric constants of non-aqueous solvents such as MEA were also calculated based on the work of Jean at al. [45].

Seven reaction models are involved in this study to describe the chemical reactions in the absorber and stripper. The power law expression is used for chemical reaction model. All reactions are assumed to be in chemical equilibrium except those of CO_2 with OH- and CO_2 with MEA. From Eq. (2-3) to (2-7), the equilibrium constants were calculated from the standard Gibbs free energy change. The equilibrium constants for Eq. (2-8) and (2-9) were taken from the work of Austgen et al. [26], and the kinetic parameters of these reactions were obtained from Hikita et al. [46]

$$H_2O + MEAH^+ \leftrightarrow MEA + H_3O^+ \quad (2\text{-}3)$$

$$2H_2O \leftrightarrow H_3O^+ + OH^- \quad (2\text{-}4)$$

$$HCO_3^- + H_2O \leftrightarrow {CO_2}^{2-} + H_3O^+ \quad (2\text{-}5)$$

$$CO_2 + OH^- \leftrightarrow HCO_3^- \quad (2\text{-}6)$$

$$HCO_3^- \leftrightarrow CO_2 + OH^- \quad (2\text{-}7)$$

$$MEA + CO_2 + H_2O \leftrightarrow MEACOO^- + H_3O^+ \quad (2\text{-}8)$$

$$MEACOO^- + H_3O^+ \leftrightarrow MEA + CO_2 + H_2O \quad (2\text{-}9)$$

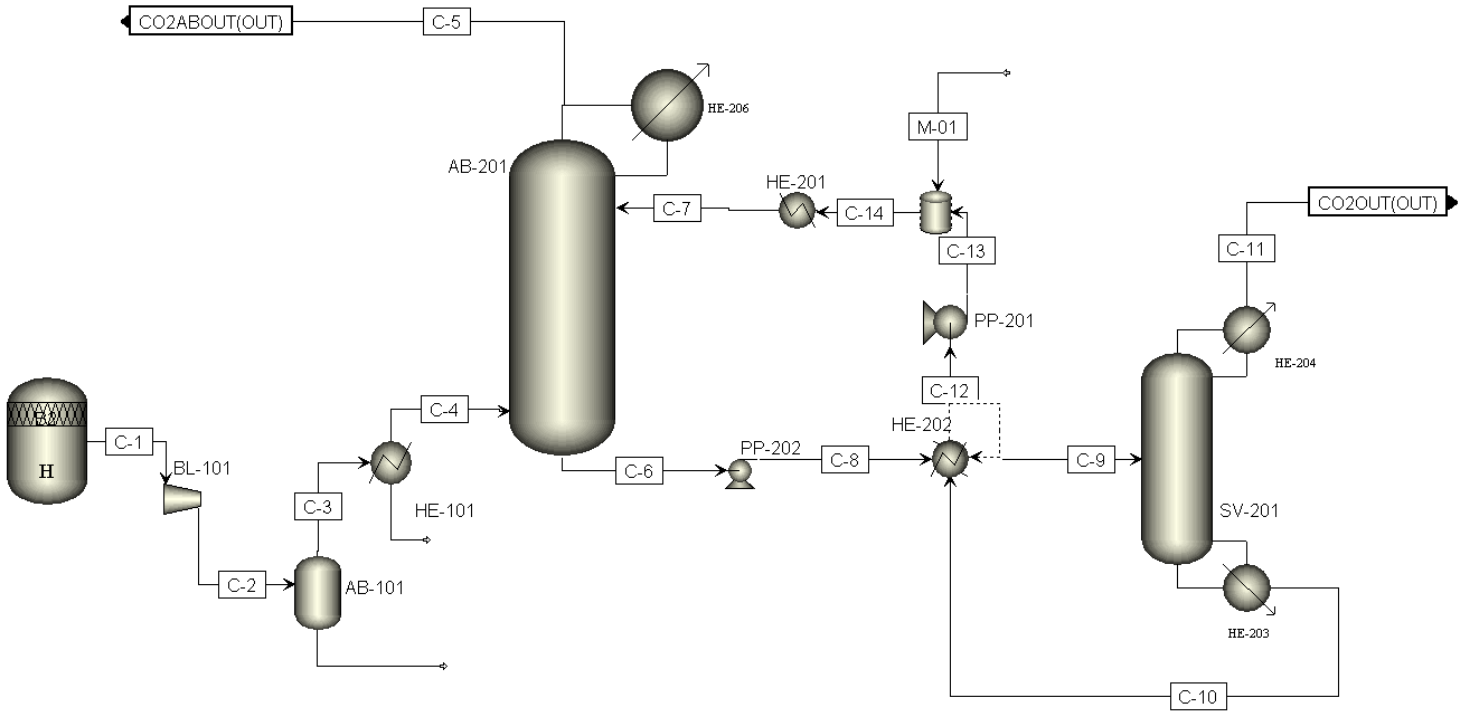

Fig. 2-3 Process flow diagram of post combustion CO2 capture process

Fig 2-3 indicates the process flow diagram of CO_2 capture process. The flue gas from the power plant, first, flows into the direct contact cooler (AB-101) where sulfur derivative residues are removed and is introduced to the absorber (AB-201). The flue gas in the absorber flows counter currently with the MEA solvent and chemically reacts with the solvent. The CO_2 lean stream is then partially condensed in condenser (HE-206) in order to recover water and the solvent, and remaining CO_2 lean flue gas is vent through stack. The rich amine stream from the absorber (C-6) is pumped to the top of the stripper through lean/rich amine heat exchanger (HE-202). Within the stripper, the MEA solvent is regenerated in the reboiler (HE-203) and CO_2 rich vapor is condensed in HE-204 in order to recover high purity CO_2 vapor. The lean amine stream from the stripper flows back to absorber via HE-202 in order to complete the cycle.

A 16.8 m and 11.75 m of Generic IMPT packing were used for absorber and stripper respectively. In order to estimate both interfacial area and mass transfer coefficient, HenleyIMTP [47] and Onda's correlation [48] were used for the absorber and the stripper, respectively. The temperature of rich amine stream exiting HE-202 and stripper operating pressure were decided as 93˚C and 1.35 bar, respectively based on the pilot plant operation data. It is assumed five pairs of absorbers and strippers are required to remove CO_2 from the flue gas generated from 660MW PC power plant. The column

diameters of both the absorber and stripper were recalculated assuming constant superficial velocity. The superficial velocity, 4 ft/s, was obtained from the pilot plant operation and it is fell within the typical range suggested by Wankat [49]. The column diameter was calculated as follows:

$$D = \sqrt{\frac{4V}{\dot{\rho} v \pi}} \qquad (2\text{-}10)$$

Where V, $\dot{\rho}$, and v are the volumetric flow rate of the gas, the molar gas density, and the superficial gas velocity, respectively. The column diameters of the absorber and stripper were determined to be 13.1 and 11.5 m.

In order to access the process performance, solvent regeneration energy and exergy loss were evaluated. The solvent regeneration energy can be calculated using Eq. (2-11).

$$E = \frac{\Delta H_L \cdot m_{steam}}{m_{CO_2}} \qquad (2\text{-}12)$$

Where ΔH_L, m_{steam}, and m_{CO_2} indicate the latent heat of steam, steam mass flow rate and captured CO_2 flow rate. The exergy analysis of the process can be done by evaluating irreversibility of the system (Eq. (2-13)).

$$\dot{I} = \dot{E}_Q + \sum \dot{E}_{in} - \sum \dot{E}_{out} - \dot{E}_W \qquad (2\text{-}13)$$

Here the irreversibility ($\dot{I}$) is defined as loss of available work. The exergy, $\dot{E}$, of each stream can be calculated using Eq. (2-14). Detailed results of the process performance evaluation are presented in Section 2.5

$$\mathrm{E}_i = \dot{m}[(H_{stream} - H_0) - T_0(S_{stream} - S_0)] \qquad (2\text{-}14)$$

2.4. CO_2 liquefaction process modeling

In this section, a liquefaction process of CO_2 rich stream from the capture process is proposed. This process is also modeled with Aspen Plus^{TM}, but Soave Redlich-Kwong (SRK) Equation of State was employed for describing thermodynamic behavior of high purity CO_2 [27]. A number of previous studies indicated that SRK equation predicts CO_2 or CO_2 mixture phase behavior the most precisely at high pressure [50, 51]. However, SRK equation with improper water-CO_2 binary interaction parameter often fail to predict their solubility [52]. In this study, the SRK equation is modified with binary interaction parameter (k_{ij}) of 0.193 in the Van der Waals mixing rule which is reported by Heggum et al [53].

The condition of the product for the liquefaction process was set near 6.5 bar and -52℃. It was decided based on the vessel pressure of the CO_2 transportation carrier. Commercially available large capacity tanks are usually operated within the pressure range of 5 to 7 bar [54], and numbers of studies indicate that 6.5 bar is a feasible condition for CO_2 ship transportation [55-57]. It is, also, the operating condition of the intermediate storage terminals which link the continuous liquefaction process to discrete ship transportation [58].

The feed stream in this study is the product stream of the post combustion capture process. It is mainly composed of CO_2, water and possibly traces

amount of amine solvent. SO_X and NO_X can be involved in the flue gas. However, the post combustion capture process can treat these gases until only a negligible amount remains. Volatile gases such as nitrogen or argon can increase the required liquefaction energy, and they should be removed during or before the CO_2 liquefaction process. With experience previously gained from other industrial projects, the CO_2 product stream from the post combustion process usually contains scarce amounts of volatile gases. However, additional distillation columns may be required when the CO_2 feed stream is coming from a pre-combustion process where the flue gas contains relatively larger amounts of volatile gases.

During the CO_2 liquefaction process, the water content in the liquid stream should be removed in order to avoid hydrates, freezing of water and corrosion. Li et al. indicated that liquid CO_2 containing 100 vppm of water lies on the liquid-hydrate equilibrium line near the target pressure and temperature [51]. In this study, it is assumed that the water contents in the liquid CO_2 stream should be less than 50 vppm. This specification is far lower than necessary from a thermodynamic point of view. Aspelund et al. insists hydrates and ice problems do not occur until the water content reaches 500vppm [59].

Table 2-5 indicates the composition of the feed stream and specification of the process input. It is also assumed that cold cooling water (10℃) is readily

available. The input feed stream is the product stream of the amine based post combustion CO_2 capture process, and its flow rate is 432.76 t/h which is equivalent to the 92.8% of a 661MW coal power plant CO_2 generation. 0.85 for Log Mean Temperature Difference (LMTD) correlation factor for seawater heat exchanger and iso-enthalpic expansion for Joule-Thomson valve are also assumed throughout the process simulation.

Table. 2-5 Gas Quality and Input Data for CO_2 Liquefaction Process

Input Stream Composition	Value	Unit
CO_2	95.0	mol %
H_2O	5.0	mol %
Volatiles	Trace	mol %
Process Input Data		
Compressor Efficiency	82	%
Pump Efficiency	85	%
Seawater HX		
Pressure Drop	0.5	Bar
MITA(Minimum Internal Temperature approach)	5	˚C
Process HX		
Pressure Drop	0.1	Bar
MITA(Minimum Internal Temperature approach)	3	˚C

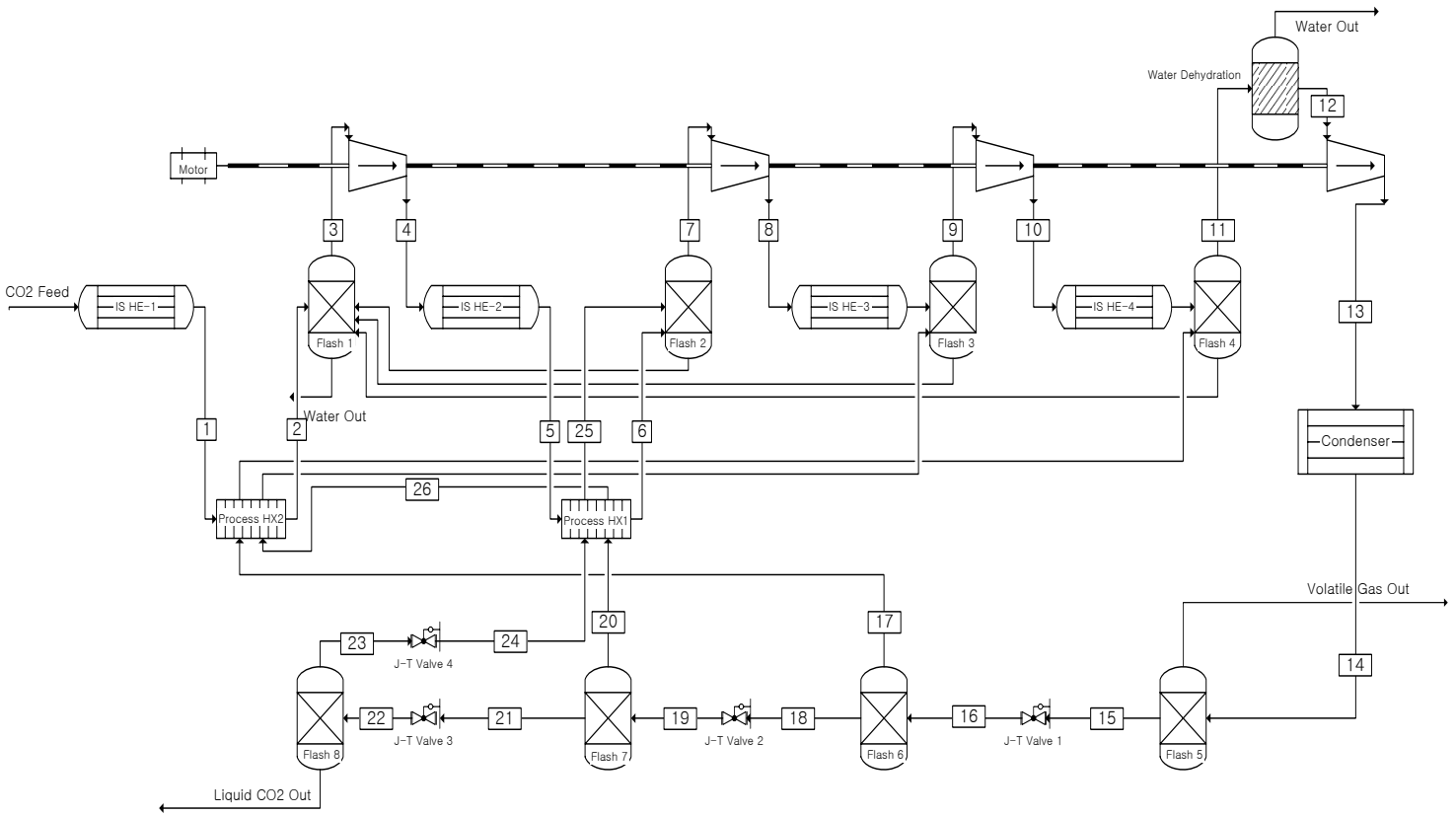

Fig. 2-4 Flow diagram of CO2 liquefaction process

Fig.2-4 shows the flow diagram of CO_2 liquefaction process. This process employs a four-stage compressor, four inter stage heat exchangers (IS HX-X) and two process heat exchangers. The CO_2 feed stream is compressed using the four stage compressor. The pressurized CO_2 feed stream is subsequently introduced to a condenser and liquefied. Inter stage heat exchangers lower the vapor CO_2 stream temperature to reduce the compressor energy consumption. The cold liquid CO_2 stream is finally sent to a Joule-Thomson (J-T) valve, and a low-pressure liquefied CO_2 stream is obtained through iso-enthalpic expansion. The liquefied CO_2 stream from the Joule-Thomson valve is recovered as a product and the effluents of the vapor stream from the expansion are used for lowering the CO_2 input stream temperature and recycled back to the compressor. In comparison with the conventional liquefaction processes [28], the pressurized CO_2 expansion is performed via multi stages. The conventional process employs direct expansion from high pressure liquefied CO_2 stream to low pressure CO_2 product stream. Consequently, most CO_2 vapor stream generated from the expansion are recycled back to second stage of compressor and flows through rest of the stages. Energy consumption and exergy loss, however, can be reduced by applying multi-stage expansion. In this process, the recycle ratio which directed to the second stage of the compressor can be reduced by adopting multi-stage expansion and energy consumption of the compressor can

eventually be reduced.

A number of liquid-vapor separation drums are installed to ensure no liquid entrainment enters the CO_2 compressor. It is the simplest way to remove components with lower boiling point than that of gaseous CO_2. In this process, water is the main component removed through the flash drums. The recovered water is subsequently sent to flash 1 in order to recover the dissolved CO_2 in the water at high pressure. For a CO_2 liquefaction process with an operating pressure higher than 30 bar, the specification of the water contents suggested by Austegard et al. can only be achieved through the flash drum separation without a dehydration column [59]. However, this process employs a dehydration column in order to lower the water content to less than 50 vppm. A Triethylene Glycol (TEG) drying column [60] or molecular sieve[61] can be applied for the dehydration unit.

The amount of seawater required for cooling and condensing the CO_2 gas streams was calculated based on the value of the LMTD correction factor (F_T) [62]. The LMTD correction factor can be expressed as follows in equation (2-15):

$$F_T = \frac{\sqrt{R^2+1}\ln\left[\frac{(1-S)}{(1-RS)}\right]}{(R-1)\ln\left[\frac{(2-S(R+1-\sqrt{R^2+1}))}{(2-S(R+1+\sqrt{R^2+1}))}\right]} \quad (2\text{-}15)$$

, where

$$R = \frac{T_{hot\ in} - T_{hot\ out}}{T_{cold\ out} - T_{cold\ in}}$$

$$S = \frac{T_{cold\ out} - T_{cold\ in}}{T_{hot\ in} - T_{hot\ out}}$$

In typical heat exchanger applications, 0.85 or higher F_T values are desirable because small errors in R and S can result in F_T values much lower than anticipated [63]. Thus, an F_T value of 0.85 was used throughout the process design and the corresponding amount of seawater was calculated for cooling the gaseous CO_2 vapor stream.

The multi-stream heat exchangers, that lower the stream temperature flowing into flash 1 and 2, utilize the vapor streams from the J-T expansions as refrigerant. A spiral wound, plate-frame, or brazed aluminum heat exchanger can be used for a multi-stream heat exchanger [64]. In this study, a spiral wound heat exchanger was used for the multi-stream heat exchanger, which is commonly used in LNG liquefaction.

The heat duty of the process heat exchanger 1 was determined by the temperature of the vapor stream 6, and the temperature of the stream was set

at 3℃. If the stream temperature is too low to maintain the vapor or liquid phase, problematic ice or hydrate formation may occur. Song et al. indicated that icing problem would occur at -8℃ and 6.9 bar with 1/10 of the water content used in this study [65]. Even if the solubility of water in CO_2 gas increases with lower pressure and higher temperatures [66], the temperature of the stream is kept above the freezing point of water to maintain the secure process operation.

Process heat exchanger 2 lowers the temperature of stream 1 entering flash 1. The cold vapor stream 20 from the J-T valve 2 is sent to process heat exchanger 2 after it lowers temperature of the stream 5 to 3℃ in process heat exchanger 1. Another cold vapor stream 17 from the J-T valve 1 is also supplied to the heat exchanger 2 as coolant. Process heat exchangers can be avoided in this process by mixing the cold vapor stream with the CO_2 feed stream entering each the compressor stage. However, direct mixing of cold CO_2 streams may cause problems such as the formation of local ice or of hydrates.

The compression ratio of each stage of the compressor was determined by solving non-linear programming.

$$\min J = W_1(r_1) + W_2(r_2) + W_3(r_3) + W_4(r_4); \quad with \quad W_i = \frac{q_i(r_i)F_i}{\eta} \qquad (2\text{-}16)$$

$$s.t.\ 1 \le r_i \le 4 \quad i = 1,\ 2, 3, 4$$

$$\prod_{i=1}^{4} r_i = 51.8$$

The objective function is sum of all compression work where *W* and *r* represents the compression work and ratio of each compressor stage, respectively. According to Seider et al., the maximum compression ratio of each stage can reach up to 4 [63]. The optimum compression ratio was calculated using the MATLAB^{TM} optimization solver with trusted region sequential quadratic programming (SQP) algorithm. The detailed result of the evaluation are presented in Section 2.5.

2.5. Base case simulation result

The process performances of the base case and combined Rankine cycle are indicated in Table. 2-6. As shown in the tables, the gross power outputs of the steam cycle in the base case are 661 MW without CO_2 capture process. The steam flow rate is consistently decreasing as the steam supplied for feed water heating. Fig. 2-5 shows the *T-S* diagram for the steam cycle. The cycle can be represented as S-1 → S-2 → S-4 → S-6 → S-7 … → S-19 → S-20 … → S-32 → S-34 → S-1.

The commonly used steam cycle efficiency is defined as:

$$\eta_{th} = \frac{W}{m_f \cdot LHV} \qquad (2\text{-}17)$$

Where η_{th}, W, m_f and LHV indicates the gross efficiency of the steam cycle, generated power, fuel mass, and the lower heating value of the fuel, respectively. The coal consumption of the power plant, 219.6 t/h is obtained from DOE/NETL report [31]. The gross efficiency of the steam cycle was evaluated as 41.4 %. The efficiency of the steam cycle is significantly reduced when the post combustion CO_2 capture process is introduced. The steam utilized for CO_2 capture solvent regeneration has pressure of 4.45 bar, thus it should be extracted from the first stage of low pressure steam turbine. The exhaust steam from the 2nd to 5th stages of low pressure turbine too low to be utilized for the solvent regeneration. The amount of 705.21 t/h

steam is extracted for solvent regeneration and it reaches about 50% of total exhausted steam from the first stage of LP turbine. The power generation from the steam cycle is reduced to 555.7 MW and the cycle efficiency is decreased to 32.1%. The power de-rate of the cycle is evaluated as about 15.4%

Table. 2-6 Power cycle performance of base case

Turbine	Input P (Bar)	Input Temp (ºC)	Output P (bar)	Output Temp (ºC)	Flow Rate (t/h)	Power Output (MW_e)
HP1	242.35	598.89	77.07	418.4	1891.05	157.77
HP2	77.07	418.4	49.02	357.53	1740.04	50.28
IP1	49.02	621.11	21.36	496.12	1547.73	111.11
IP2	21.36	496.12	9.52	388.6	1425.23	86.01
LP1	9.52	388.6	5.01	322.78	1425.09	51.24
LP2	5.01	322.78	1.32	206.6	1316.14	82.07
LP3	1.32	206.6	0.58	143.9	1268.72	42.01
LP4	0.58	143.9	0.25	87.74	1224.91	35.94
LP5	0.25	87.74	0.07	38.71	1174.30	44.57
Total						661.00

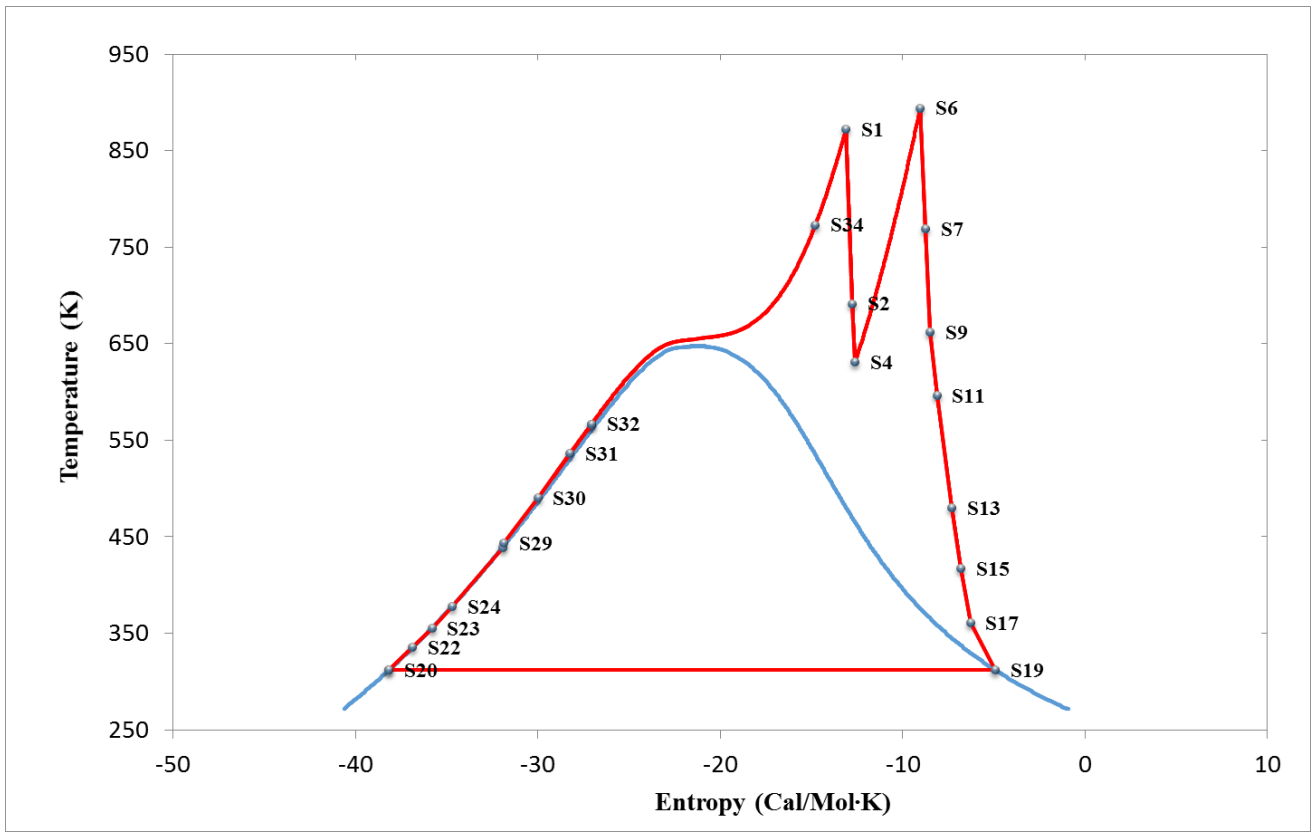

Fig. 2-5 T-S diagram of the steam cycle

The rate based CO_2 capture model is validated using pilot plant operation data. The pilot plant is located in Boryeong coal power plant in Republic of Korea. The differences of the composition of each component between the pilot plant data and simulation lies within 2%. Several methods can be used for model validation, but in this study, the internal temperature profile data and regeneration energy were evaluated. There are six and five thermocouples are located in the absorber and stripper, respectively. In order to match the simulated temperature profile with the experimental data, mass transfer coefficient method, interfacial area factor, and heat transfer factors are manipulated. The absorber temperature profile is the most precisely predicted with mass transfer area factor of 0.6 and HenleyIMTP correlation method. The absorber model was able to remove the same amount of CO_2 from the flue gas with the same 3.73 L/Sm^3 liquid to gas ratio as the operation data. For the stripper model, Onda's correlation predicts the temperature profile within the column the most precisely with the interfacial area factor of 0.41 and heat transfer factor 0.05. The regeneration energy of the column was evaluated as 3.72 GJ/ton CO_2, and it is about 97% of operation data.

Fig. 2-6 indicates the temperature profile of the absorber and stripper. As indicated in the figure, the simulation results of both the absorber and the stripper demonstrate good agreement with experimental data. Because of the

exothermic nature of the Eq. 2-8, the temperature within the column increases as the flue gas flows upward and opposite behavior can be observed in the stripper. Since both columns utilize the cooling water with 35˚C, top temperatures of both columns are fixed at 40˚C .

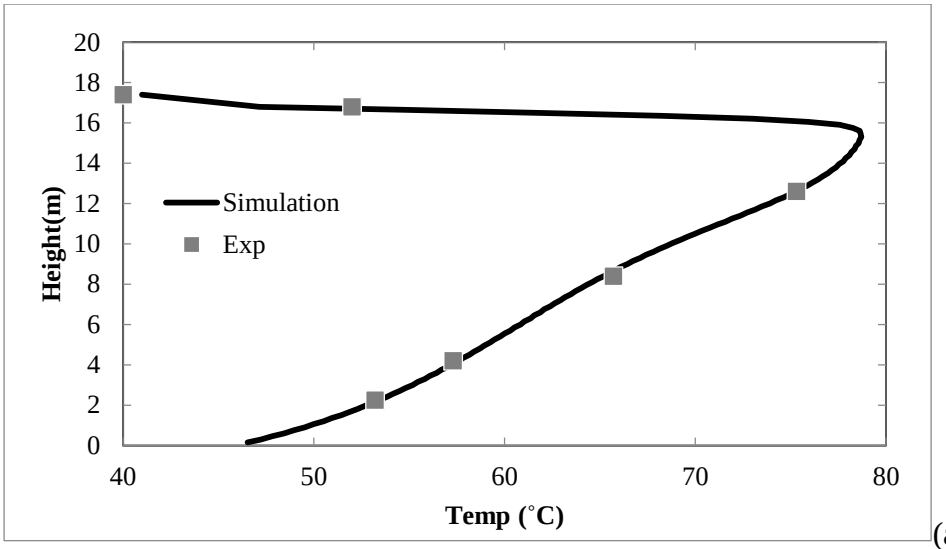

(a) CO_2 capture process absorber temperature profile

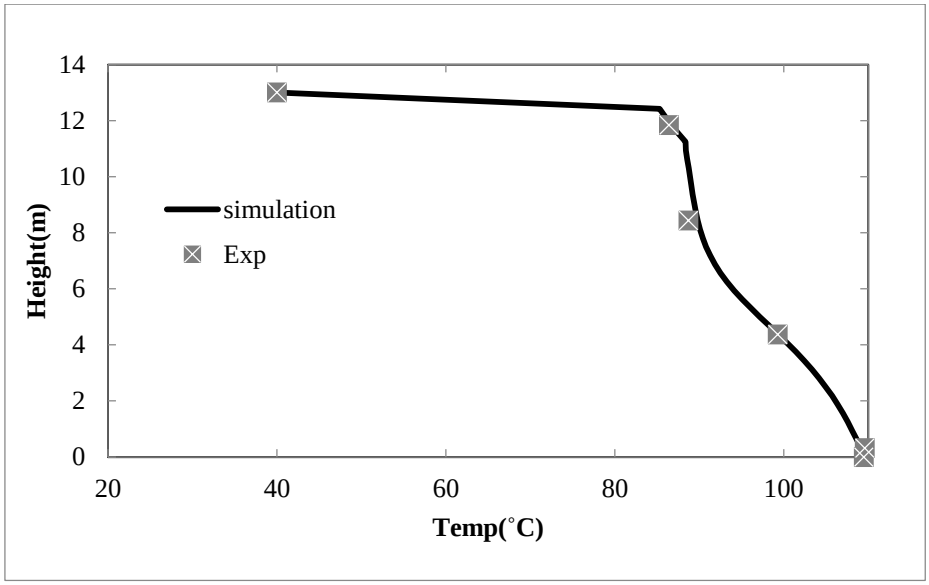

(b) CO_2 capture process stripper temperature profile

Fig. 2-6 CO_2 capture process column temperature profiles

The exergy analysis on the CO_2 capture process was also performed in order to identify the major units which contribute the exergy loss the most. Fig. 2-7 indicates the exergy loss of the unit operations in the CO_2 capture process. Among the six major unit operations, the AB-201, SV-201, and HE-202 occupies more than 86 % of the total exergy loss. Total irreversibility generated from the system was identified as 204.66 Kcal/Kg CO_2 and power consumptions of PP-201 and PP-202 were 1.44 and 1.77Kcal/Kg CO_2, respectively.

Several improvement can be made to reduce both energy consumption and exergy loss of the process. In the base case study, the temperature of the rich amine steam exiting the HE-202 was fixed at 93˚C, in order to prevent corrosion or degradation of the solvent. The exergy loss of the stripper can be improved by implementing advanced process configuration such as heat exchanger network or vapor recompression. In this study, lean vapor compression and mechanical vapor compression methods are employed to reduce the irreversibility of the stripper. Detailed approaches, modeling and simulation results are presented in Chapter 3

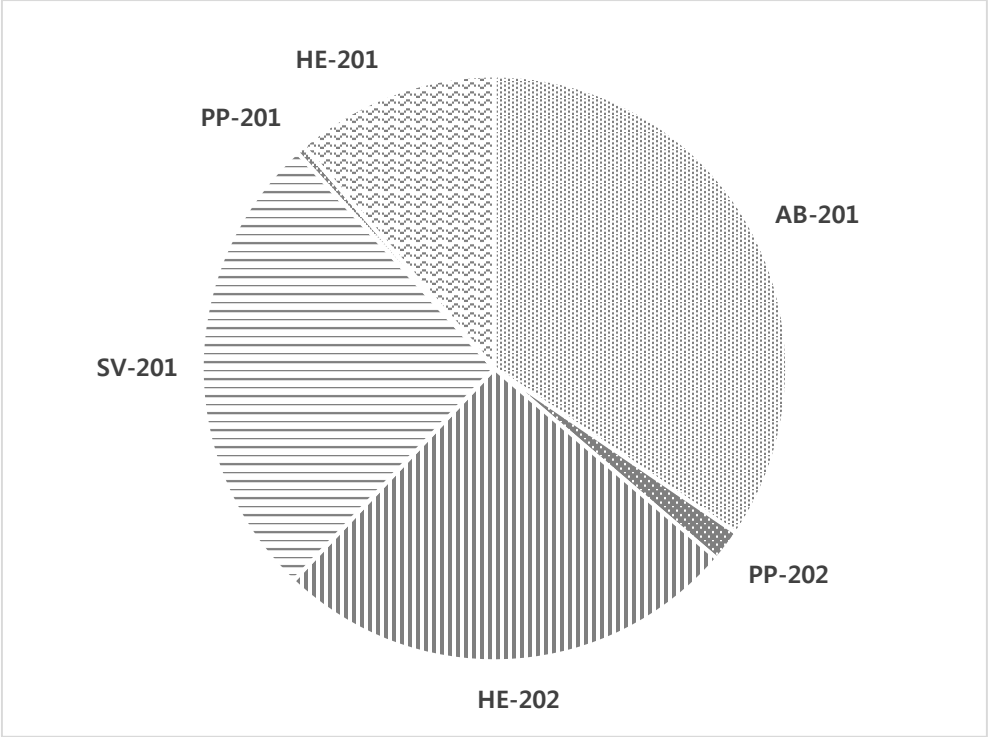

Fig. 2-7 Exergy loss of the unit operations in CO_2 capture process

Fig. 2-8 depicts the operating lines for the CO_2 liquefaction process. As indicated in the figure, this process employs multi-stage expansion. The main advantage of the multi stage expansion is reducing vapor CO_2 stream recycle ratio directed to second or third stage of the compressor. When the liquid CO_2 product stream is generated from the single expansion, the CO_2 vapor generated from the expansion has the same pressure as the CO_2 product. This vapor stream has to recycle back to the second stage of compressor and brings increments on second, third and fourth stage of the compressor work duty. If the product stream is generated from the multi stage expansion, fraction of the CO_2 vapor stream still remains in high pressure, and it can be recycled back to either third or fourth stage of the compressor directly. Using this method, the operation energy of the compressor can be reduced by reducing the flow rate introduced to second and third stage of the compressor.

The cold CO_2 vapor streams generated from the multistage expansion were used to cool down the temperature of both stream 1 and 5. As a result, the workloads for the first and second stages of the compressor were reduced and it eventually resulted in the compressor utilizing a smaller amount of operation energy than that of alternative process 1. The temperature of the CO_2 vapor stream leaving the process heat exchanger 1 was set at 3℃ in order to avoid the formation of ice or hydrates and that of the process heat

exchanger 2 was 5.4 ℃.

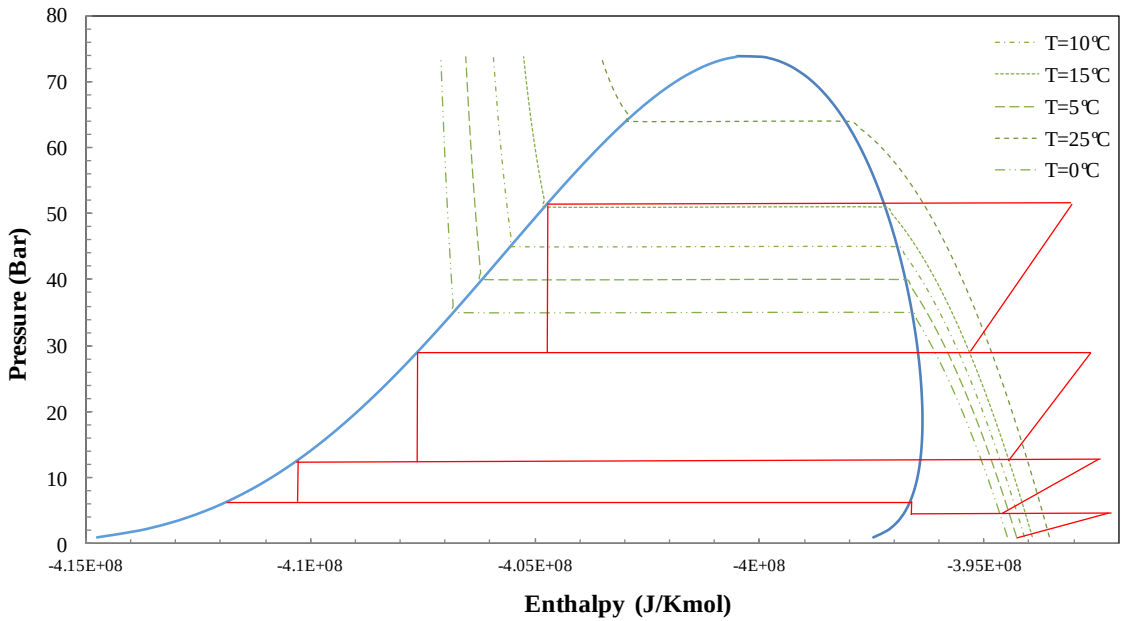

Fig. 2-8 Pressure enthalpy diagram of CO_2 and the operating line of the CO_2 liquefaction process

The compression ratios and discharge pressure on each compressor stage are presented in Table 2-7. The optimized compression ratios were calculated using MATLAB^{TM} solver with Aspen plus simulation model by solving Eq. (2-16). The amount of work to achieve the same compression ratio generally increases as the starting pressure rises because fraction of water is removed though intercooling in each feed stream of the compressor. Therefore, the optimized compression ratio became smaller as the feed stream proceeded through the compressor. Fig. 2-9 indicates the total operation energy of each CO_2 liquefaction system. This process consumes about 8.2% less operation energy than that of the conventional CO_2 liquefaction process proposed by Aspelund et al [59], and their energy consumption is 98.1 kWh/Tonne CO_2.

The net efficiency of the base case is defined as

$$\eta_{th} = \frac{W_{gross,Capture} - E_{liquefaction}}{m_f \cdot LHV} \qquad (2\text{-}19)$$

Where $W_{gross,Capture}$, and $E_{liquefaction}$ indicate gross power output from the steam cycle with CO_2 capture process, and electric energy consumption of the CO_2 liquefaction process. The net power generation of the base case are evaluated as 513.2 MW. The thermal efficiency of the base case is 32 %.

Table. 2-7 Optimized Compression ratio and pressure on each compressor stage

Stage	Pressure (bar)	Compression ratio
Feed	1.0	
Stage 1	4.0	4.0
Stage 2	12.9	3.7
Stage 3	29.2	2.4
Compressor Out	51.8	1.8

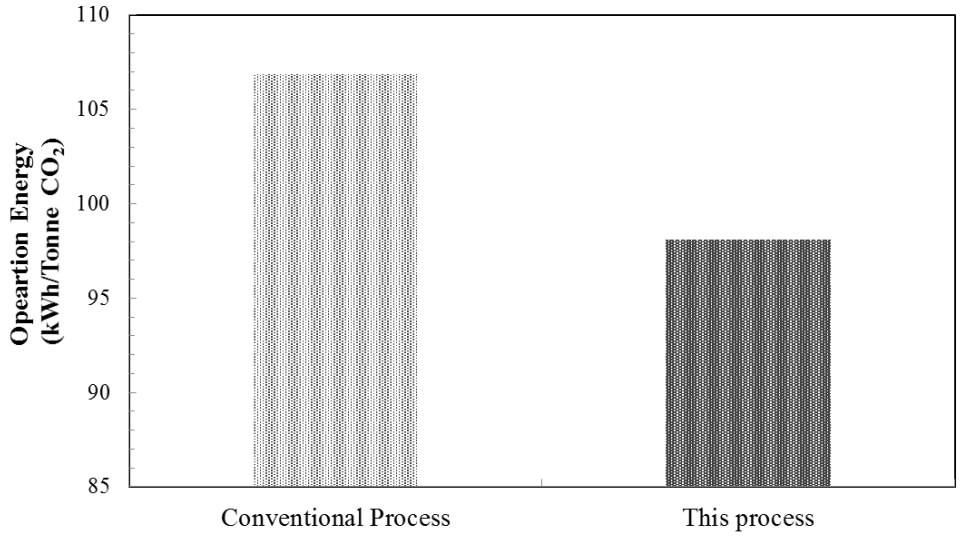

Fig. 2-9 Operation energy consumption of CO_2 liquefaction process

CHAPTER 3. Modified CO_2 Capture Process Design and Optimization

3.1. Overview

In this chapter, CO_2 capture process is modified in order to reduce both energy consumption and process irreversibility. Because the stripper in the CO_2 capture process consumes the operation energy the most, the process modification is mainly focused on retrofitting of stripper configuration. Two vapor recompression processes are introduced to the stripper configuration: mechanical vapor recompression (MVR) and lean vapor recompression (LVR). By employing MVR process, the latent heat of the steam, which is originally wasted in the condenser, can be utilized for the rebolier heat source. The LVR reduces both condenser and reboiler duty, thus exergy loss and energy consumption of the process can be reduced. Additionally, the minimum temperature of the lean/rich amine heat exchanger was decided as 5˚C, instead of fixed rich amine outlet temperature, 93˚C in the base case process. The CO_2 product steam is compressed to 6.5 bar through MVR process. As a result, the CO_2 liquefaction process is no longer required but directly utilized for organic Rankine cycle heat source.

3.2. Lean vapor recompression process

Fig. 3-1 depicts process flow diagram of LVR process. This process requires an expansion valve, a flash separator and steam compressor in conventional CO_2 stripper. The lean amine stream (C-10) regenerated from the reboiler is expanded via V-101 valve and send to flash separator. The resulting vapor stream is compressed to the stripper bottom pressure and feeds to the stripper base. Additional compressor is required to recover the pressure loss resulted from the expansion. Because of the isentropic expansion in the V-101, the liquid lean amine (LVR-2) temperature is decreased compared with the base case. As a result, both heat duty of HE-202 and rich amine stream (C-9) temperature are decreased. However, the total amount of enthalpy recovered from hot lean amine stream should be maintained the same.

$$\mathrm{m}_{C-10,bc}\,\mathrm{C}_p\Delta T_{C-10} = \mathrm{m}_{LVR-2}\mathrm{C}_p\Delta T_{LVR-2} + \mathrm{m}_{LVR-3}\Delta H_{Vap} \qquad (3\text{-}1)$$

Where $\mathrm{m}_{C-10,bc}$, m_{LVR-2}, and m_{LVR-3} indicate mass flow rate of stream C-10 of the base case, LVR-2, and LVR-3 of the LVR process, respectively. C_p and ΔH_{Vap} represent heat capacity and heat of vaporization of the stream. Eq. (3-1) implies, the amount of the heat recovered from the lean amine stream is the same regardless of the LVR process implementation.

However, the temperature decreases of the feed stream (C-9) reduces

cooling duty of the condenser (HE-204), and the reboiler heat duty can be further decreases, accordingly. In spite of the reboiler heat duty decreases, additional electricity is needed to drive LVR compressor. Also, the stripper needs to accommodate a slightly higher vapor flow compared with that of the base case[67].

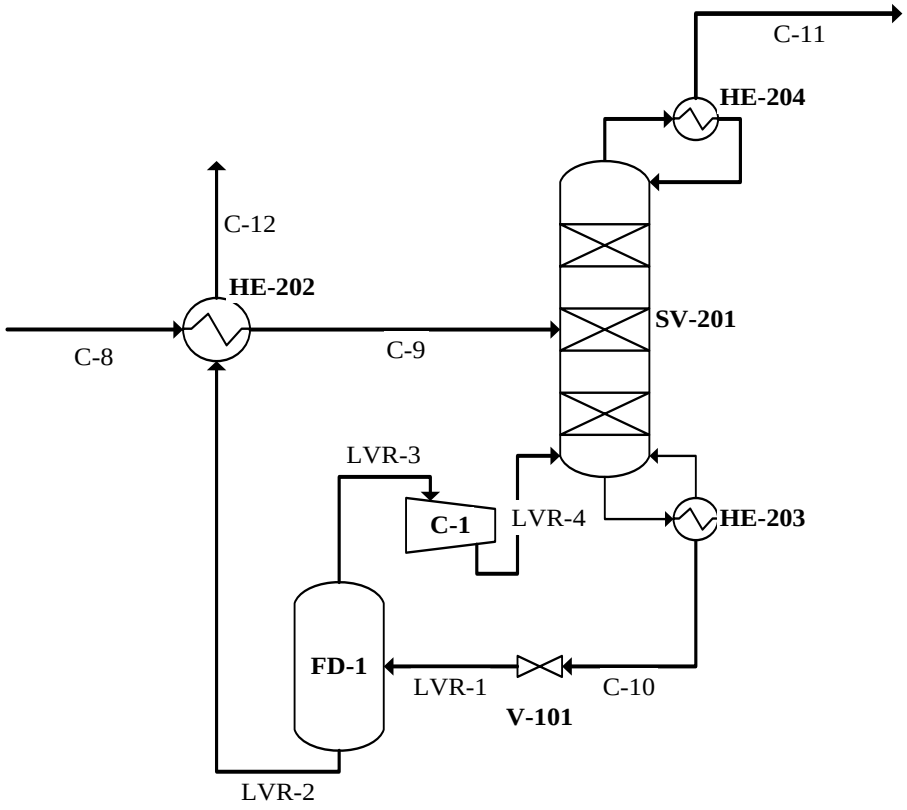

Fig. 3-1 Process flow diagram of the CO2 stripper lean vapor recompression

The main design variables of LVR process are stripper pressure, lean amine expanding pressure, and minimum temperature approach of lean/rich amine heat exchanger. For the simplicity and operability, the vacuum expansion at the expansion valve (V-101) was not considered in this study. Consequently, the minimum pressure of the lean vapor stream from the flash column is decided as 1 bar. The minimum temperature approach of the base case, 16.5˚C can be reduce when the LVR process is implemented because of the temperature reduction of the rich amine stream (C-9) according to the Eq. (3-1). The maximum rich amine temperature and minimum temperature approach are assumed 97˚C and 5˚C, respectively for preventing solvent degradation and process efficiency. The pressure of the stripper is decided to minimize total energy consumption (i.e. reboiler heat duty and compressor work), and it can be obtained by solving following optimization problem.

$$\text{Minimize } W_{total} \qquad (3\text{-}2)$$

subject to

$$W_{total} = W_{eq,reboiler} + W_{compresser}$$

$$T_{bottom} \leq 120℃$$

$$T_{rich} \leq 97℃$$

$$P_{LVC-1} \geq 1\ bar$$

Where W_{total}, $W_{eq,reboiler}$, and $W_{compresser}$ represent total work of the stripper, equivalent reboiler work, and LVR compressor work. The equivalent reboiler work can be calculated using gross efficiency of the steam cycle and compressor work.

$$W_{eq,reboiler} = Reboiler\ Heat\ Duty \times \eta_{th} \quad (3\text{-}3)$$

The results of the optimization are described in the section 3-3. The irreversibility of the units consisting LVR process are included for the exergy analysis of the stripper. The exergy and irreversibility of each unit were calculated using Eq. (3-4) and (3-5)

$$\dot{I} = \dot{E}_Q + \sum \dot{E}_{in} - \sum \dot{E}_{out} - \dot{E}_W \quad (3\text{-}4)$$

$$E_i = \dot{m}[(H_{stream} - H_0) - T_0(S_{steam} - S_0)] \quad (3\text{-}5)$$

3.3. Mechanical vapor recompression process

The largest operating energy consumption for implementation of CO_2 capture process is the solvent regeneration energy. Consequently, recovery of available energy within the battery limit is vital to obtain technical and economic feasibility of implementation of the capture process. Among the several engineering improvement, the mechanical vapor recompression (MVR) process is considered one of the most feasible options to recover large amount of waste heat.

The overhead vapor steam of the stripper generally contains more than 30

mole% of water. In the base case stripper configuration, the latent heat of the steam is wasted in the condenser. However, the latent heat can be utilized by adding additional pressure on the overhead vapor stream and exchanging heat. Fig. 3-2 indicates the T-S diagram of typical MVR process. The overhead vapor stream is originally resigned at lower temperature than the rebolier temperature. However, the saturation temperature of the vapor stream increases as the pressure increases (dashed line) and the latent heat of the steam in the overhead steam can be utilized for the reboiler heat source.

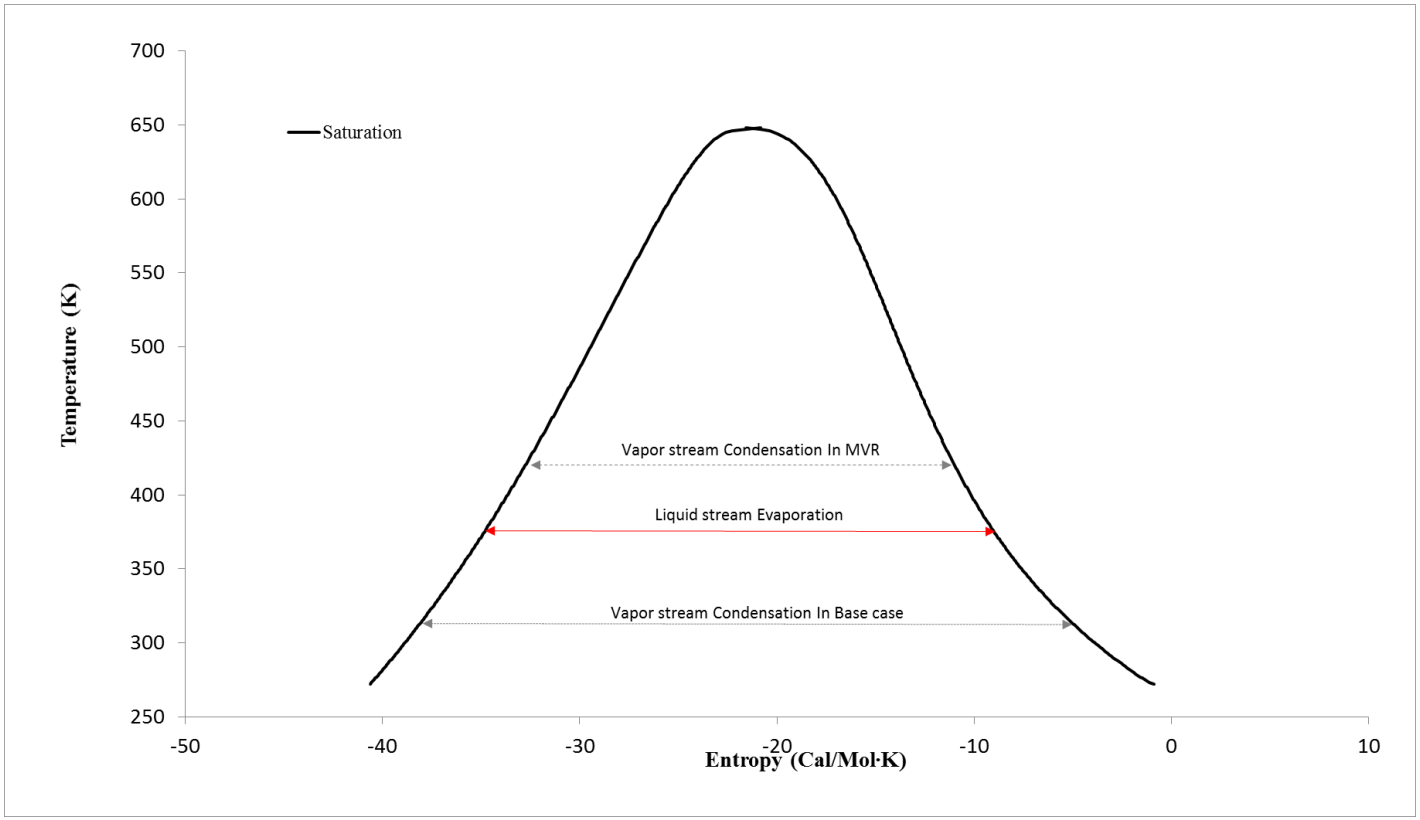

Fig. 3-2 T-S diagram of typical MVR process

Fig. 3-3 shows process flow diagram of the stripper with MVR process. For the MVR process, a two stage compressor, a multi stream heat exchanger, four flash columns and a dehydration column are added to the conventional stripper configuration. The overhead vapor stream (M1) is first compressed in the first stage of the compressor and utilized as the heat source of the multi stream heat exchanger, HE-M1. Then, it flows to the flash column F-M1 for phase separation. The vapor stream, M4, is introduce to the second stage of the compressor (C-M2). For the second stage of the compressor, the same procedure is proceeded, repeatedly. The output pressure of the last stage of compressor is fixed at 6.5 bar, which is the CO_2 product pressure of the liquefaction process in the base case study. The liquid stream from each flash column is sent to F-M5 in order to recover liquid stream, M23, and the liquid stream flows into the stripper as reflux. Because the pressures of liquid streams coming into the F-M5 are higher than that of the stripper, the pressures of these streams are lowered to the stripper pressure. Small amount of vapor is generated by liquid stream expansion, and the vapor stream is introduce to the top of the stripper to lower the stage temperature. The temperature of pressurized CO_2 rich vapor stream (M12) is further lowered to 40˚C to remove water residue from the product stream. The water contents in the stream is lowered to the desire level, 50 ppmv, in the dehydration column, then the CO_2 rich stream (M16) is introduced to organic Rankine

cycle as a heat source. Both condenser and reboiler are able to reduce their heat duty as much as the heat duty of the HE-M1.

The compressor ratio of MVR compressors are optimized by solving Eq. (3-6).

$$\text{Minimize } Z \tag{3-6}$$

subject to

$$Z = W_1(\gamma_1) + W_2(\gamma_2)$$

$$W_i = m(H_{in} - H_{out}) = m\frac{(H_{sin} - H_{out,s})}{\eta_{comp}}$$

$$1 \le \gamma_i \le 2.5$$

$$\prod_{i=1}^{3} \gamma_i = 6.5/P_{str}$$

Where W_i, γ_i, P_{str}, and m indicate the compressor work of i^{th} stage, pressure ratio, stripper pressure and CO_2 rich vapor stream flow rate, respectively. The maximum compression ratio of the H_2O and CO_2 mixture, 2.5, is decided based on industrial experience. The compressor efficiency, η_{comp}, and the minimum temperature of heat exchangers are assumed as 0.72 and 5˚C, respectively.

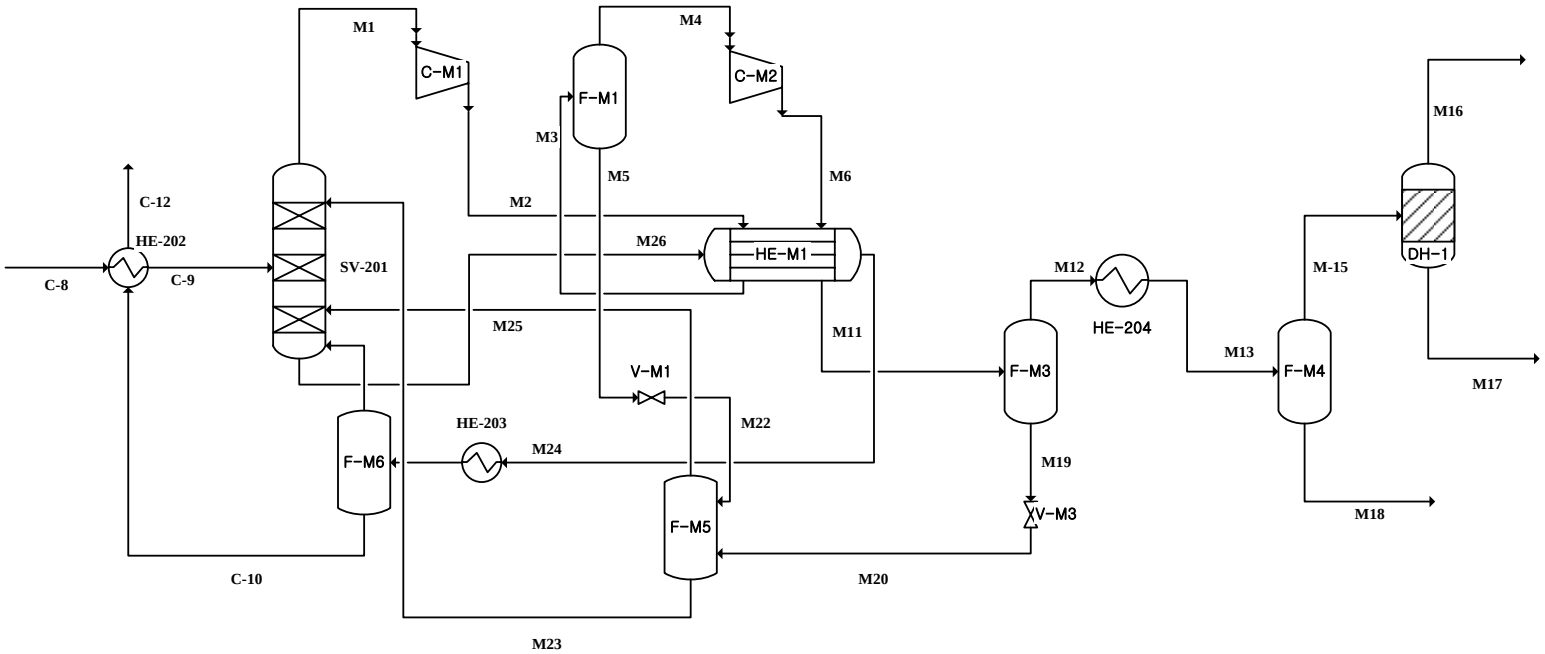

Fig. 3-3 Process flow diagram of the CO2 stripper with mechanical vapor compression process

3.4. Modified CO_2 capture process simulation result

3.4.1. Lean vapor recompression

The input parameters and effect of LVR process are summarized in Table 3-1. While main input parameters are unchanged from the base case, the rich amine temperature exiting HE-202 is lower in the LVR process. The enthalpy of hot lean amine stream is mainly recovered by steam generated from expansion, and only fraction of hot lean amine stream enthalpy is recovered through lean rich amine heat exchanger. Consequently, the stream C-9 has lower temperature then that of the base case.

As indicated in Eq. (3-1) the total amount of recovered heat from the hot lean amine stream is the same as the base case. Consequently, the temperature of lean amine stream (C-12) exiting lean rich amine heat exchanger is the same for both base case and LVR process (64˚C). The temperature of the overhead vapor stream, however, is decreased in the LVR process. As a result, the condenser duty is reduced as compared with base case, and the reboiler heat duty is also decreased accordingly. As indicated in the work of Sanchez et al., the vapor flow rate is slightly increased in the LVR process and it reaches about 8% [67]. Therefore, bigger column may be required for the implementation of LVR process.

Table. 3-1 Input parameters and results of the stripper with LVR process

	Base Case	**LVR**
Input Parameters		
Stripper P (bar)	1.36	1.36
Rich Amine T (˚C)	93.00	85.6
Condenser T (˚C)	40.00	40.0
Lean Amine Stream Expention P (bar)	-	1.00
Steam P (bar)	4.45	4.45
Result		
Reboiler T (˚C)	111.00	111.00
Regeneration E (GJ/ton CO_2)	3.72	3.47
Overhead Vapor Stream T (˚C)	86.32	81.9
Condenser Duty (GJ/Ton CO_2)	-0.78	-0.55
Steam Requirement (Ton/Ton CO_2)	1.73	1.59
Bottom Vapor Flow Rate (M^3/Sec)	47.75	51.80

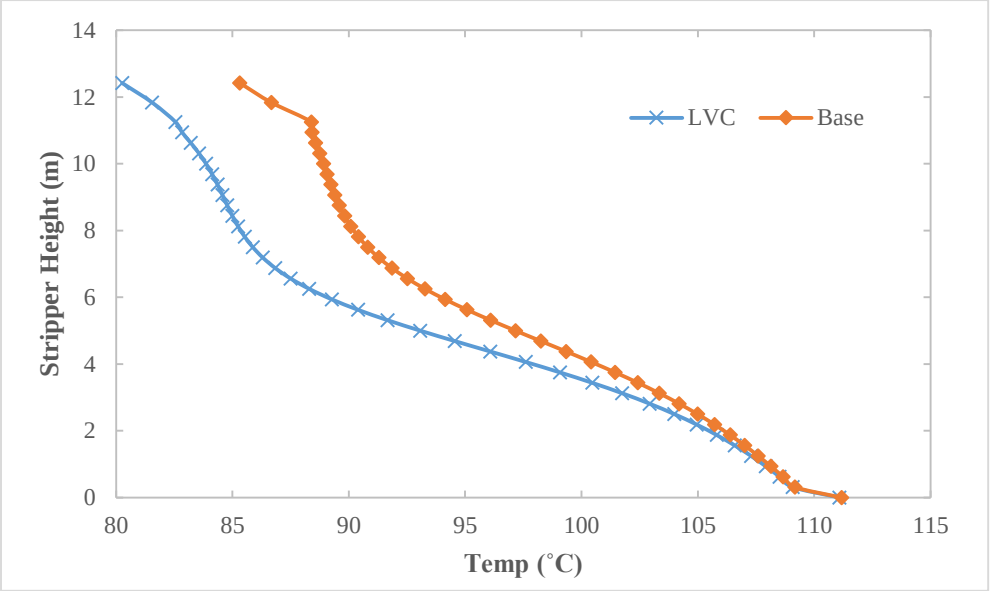

Fig. 3-4 Stripper temperature profile of LVR process

Fig. 3-4 shows the temperature profile of the stripper both in base case and LVR process. In spite of the same reboiler temperature, the top temperature of the stripper is reduced in LVR process due to the low rich amine stream temperature. As a result, the condenser heat duty is reduced by 0.23 GJ/Ton CO_2.

The reboiler heat duty of the LVR process are also decreased by 7 % with respect to the base case. This operation energy reduction can be further improved by reducing minimum temperature approach. Fig. 3-5 shows effect of minimum temperature approach on the solvent regeneration energy consumption. As depicted in the figure, the solvent regeneration energy of the reboiler is gradually decreased as the minimum temperature decreases. The monotonic decrease of the regeneration energy indicates that small minimum temperature is always favorable to reduce the solvent regeneration energy. In this study, however, the minimum temperature approach of HX-202 was selected as 5˚C with consideration of safety and operability of the process. Additionally, the upper limit of the hot rich amine stream temperature is selected as 97˚C in order to prevent possible degradation or corrosion. By reducing minimum temperature approach to 5˚C, the solvent regeneration energy can be lowered to 3.13GJ/Ton CO_2 and it only occupies only 84% of the energy requirement in the base case study.

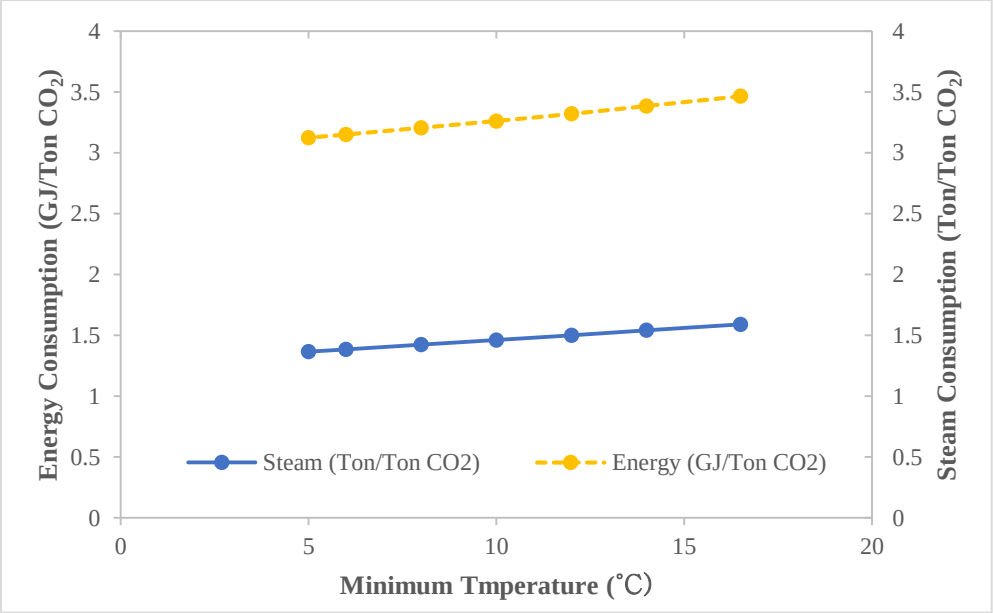

Fig. 3-5 Effect of the minimum temperature approach on the reboiler energy consumption and the steam consumption

Fig. 3-6 show heat curves of the both cases with minimum temperature 16.5 and 5˚C. The hot curves of the both cases are completely overlapped but the heat duty of hot curve with smaller minimum temperature is higher than that of the bigger minimum temperature. The temperature of the rich amine stream (C-9) rises to 96.2˚C and that of the lean amine stream (C-12) falls to 53.8˚C. Because of the high temperature of rich amine stream, phase change can be occurred and it may cause mechanical and operational problems within the heat exchanger HE-202. The vapor phase formation within the stream C-9 can be avoided by increasing input pump discharge pressure. The discharge pressure of PP-202, was increased from 2.5 bar to 4.5 bar, and no phase change was observed within the HE-202. The heat duty of the HE-202 with the 5˚C minimum temperature approach increases about 27% as compared with that of the 16.5˚C, and it indicates that the heat recovery from the hot lean amine stream can be greatly improved by adopting LVR process.

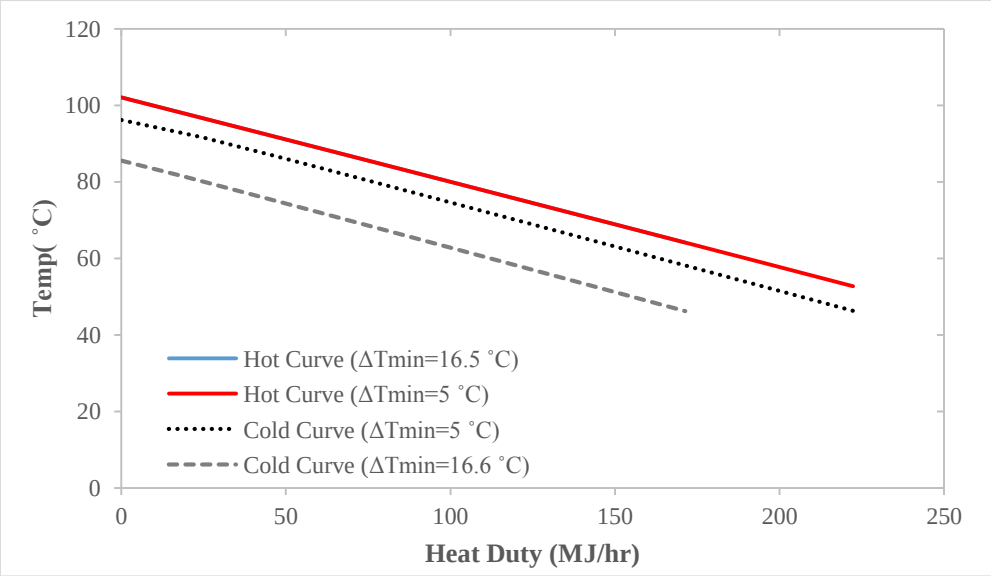

Fig. 3-6 Heat curves of the HE-202 with minimum temperature approach of 16.5 and 5˚C

The operating pressure of the stripper column is an important design variable. In the study of Abu-Zahra et al., increasing column pressure can lower both solvent regeneration energy and cooling water usage[1]. However, column pressure increment inevitably increases reboiler temperature, and it accelerates the solvent degradation. Lepaumier et al, conducted experimental study, and it showed that the MEA solvent degradation with 50% loading can be reached to 13% at 135˚C in a week [68]. In this study, however, the residence time of the MEA solvent in the stripper is far less than a week, and the CO_2 loading is comparably smaller than the 50%. As indicated in the Eq. (3-2) the maximum temperature of the reboiler is decided as 120˚C in order to prevent MEA solvent degradation.

Fig 3-7 shows the stripper pressure effects on the solvent regeneration and lean vapor compressor energy. The higher the stripper operation pressure was selected, the less the solvent regeneration energy consumed and the opposite behavior can be observed from the lean vapor compressor. For the total work calculation, the equivalent work of the reboiler is much more influential than compressor work. As a result, total work of the Eq. (3-2) appears at the position where the reboiler temperature constraint is bounded. The minimum reboiler heat duty and corresponding compressor work from the optimized LVR process are 2.83 GJ/Ton CO_2, and 0.070 GJ/Ton CO_2, respectively. With the gross efficiency of the steam cycle which was calculated in chapter

2, total work at the optimum pressure, 1.83 bar, is 1.24 GJ/Ton CO_2. The base case solvent regeneration energy, 3.72 GJ/Ton CO_2, corresponds to the 1.54 GJ/Ton CO_2 of the equivalent work.

The result indicates that the operation energy of the CO_2 capture process using MEA can be saved about 19% by adopting the LVR process and proper parameter optimization. Aside from the energy saving, the exergy loss of the stripper can be also achieved through the LVR process implementation. The exergy loss of the stripper is reduced from 224 MJ/Ton CO_2 to 91.4 MJ/Ton CO_2. The reduction of the exergy loss of the stripper mainly comes from the heat duty reduction of both the reboiler and condenser. Since the amount of cooling water and steam utilized in the CO_2 stripper are decreased, the exergy loss of these units are also decreased. The exergy loss of lean/rich amine heat exchanger is also decreased because of the minimum temperature approach decreasing. The exergy loss was originally 221 MJ/Ton CO_2 and it is reduced to 162 MJ/Ton CO_2.

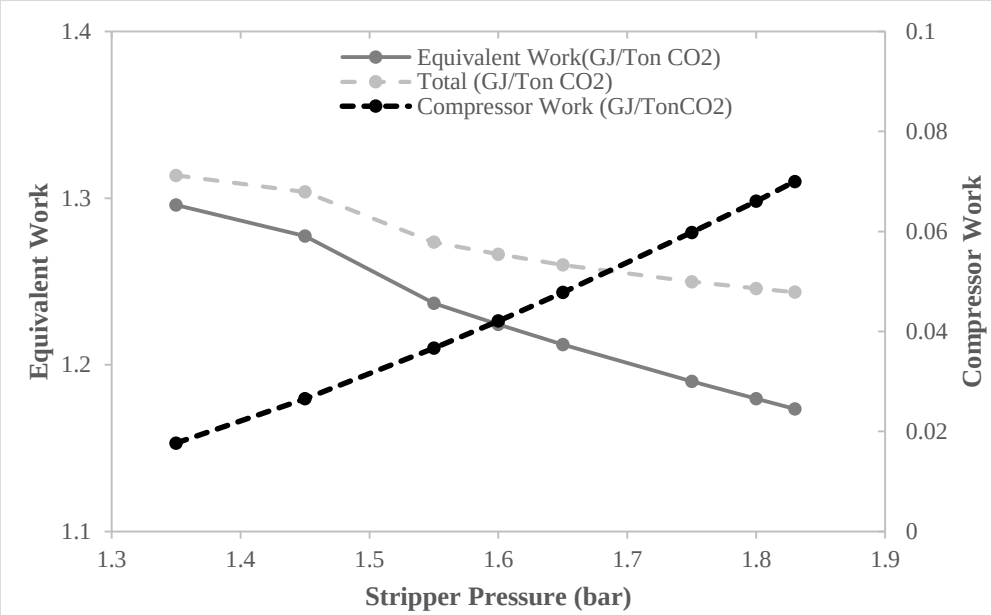

Fig. 3-7 Stripper operating pressure effect on the solvent regeneration and lean vapor compressor energy.

3.4.2. Mechanical vapor recompression

Both the MEA solvent regeneration energy and the exergy loss of the stripper can be further improved by implementing mechanical vapor recompression (MVR) process. Table 3-2 summarizes the composition of the stripper overhead vapor stream (M1). About 38 mole % of water vapor is presented as vapor phase, and the latent heat of the water can be potentially utilized as heat source. The amount of latent heat utilized in MVR process is highly depended on the pressure of product steam. In this study, the product pressure was decided as 6.5 bar which is the minimum temperature to liquefy CO_2 with safety margin. Because of the low product stream pressure, only fraction of the potential latent heat can be recovered in this study. Even though the solvent regeneration energy can be further improved by increasing compressor discharge pressure, it is not considered in this study because of the necessity of the additional compressor installation.

Table 3-3 summarizes the input parameters and results of the modified CO_2 capture process (i.e. LVR and MVR installation on the base case capture process). The stripper pressure and lean rich amine heat exchanger minimum temperature approach are decided based on the LVR simulation results. According to the solution of the Eq. (3-2) the bottom temperature of the stripper is resigned at 120˚C. While the solvent regeneration energy remains the same, the amount of heat, 0.41 GJ/Ton CO_2, can be recovered from the

hot product stream. Consequently, the solvent regeneration energy is reduced by equivalent amount of the heat duty of HE-M1. Total compressor work, however, is increased as compared with the base case CO_2 liquefaction process. Here the total compressor work is defined as the summation of the compressor work of both LVR and MVR process. The main reasons of the work increase are the flow rate increase of overhead vapor stream due to the water contents, and its high temperature. Eq. (3-7) depicts the theoretical power consumption of the compressor.

$$\mathrm{W} = \frac{m\eta RT_{in}}{k-1}\left[\left(\frac{P_2}{P_1}\right)^{k-1/k} - 1\right] \qquad (3\text{-}7)$$

Where m, η, k, and T_{in} are the mass flow rate, isentropic efficiency, heat capacity ratio, and compressor inlet temperature, respectively. As the temperature or mass flow rate of compressor inlet stream increase, the compressor duty also increases according to Eq. (3-7). However, the compressor work rise is far smaller than solvent regeneration energy reduction. Each energy consumption of both base case and modified capture process presented in this chapter are described in Fig 3.8.

Table. 3-2 Composition of the stripper overhead stream

Component	Mole Fraction
MEA	0.00%
H2O	38.06%
CO2	61.93%
N2	0.01%
O2	0.00%
Total	**100.00%**

Table. 3-3 Composition of the stripper overhead stream

Input Parameters	Value
Stripper P (bar)	1.83
Rich Amine T (˚C)	97.00
Condenser T (˚C)	40.00
Lean Amine Stream Expention P (bar)	1.00
Steam P (bar)	4.45
Result	
Reboiler T (˚C)	120.00
Regeneration E (GJ/ton CO_2)	2.83
Overhead Vapor Stream T (˚C)	89.55
Condenser Duty (GJ/Ton CO_2)	0.54
Heat Rcover from MVR (Ton/Ton CO_2)	0.41
Compressor Work (KW/Ton CO_2)	104.06

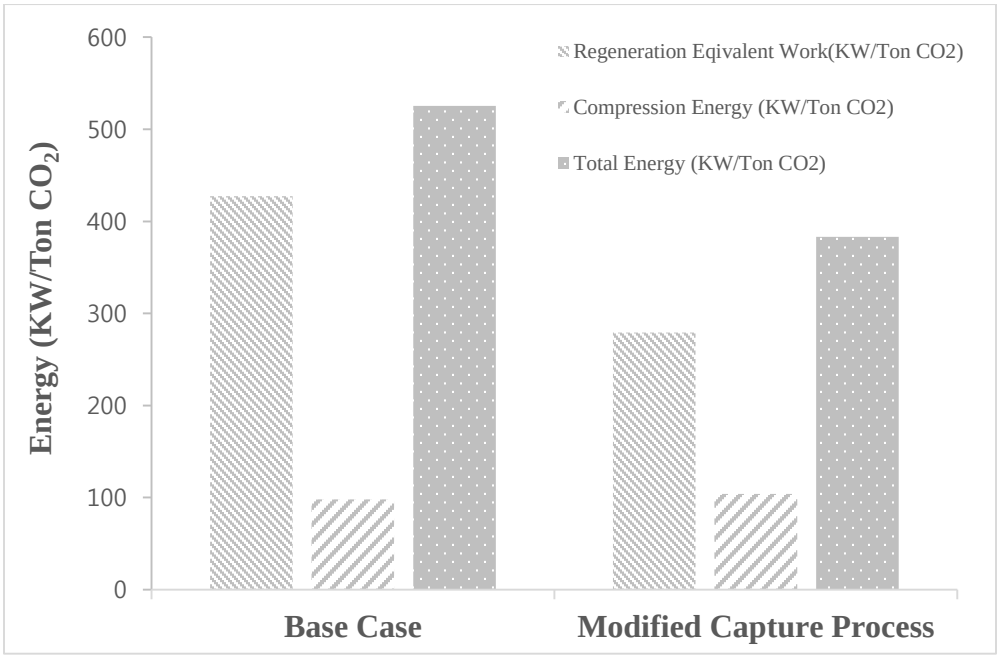

Fig. 3-8 Total energy consumption of the base case and modified capture process

The solvent regeneration energy of the modified CO_2 capture process is 279.2 kW/Ton CO_2 and it corresponds to about 65% of base case. Total energy consumption is also reduced about 27% of that in the base case study, and the relative decrease to the solvent regeneration energy is resulted from the compression work increment. The amount of required stream for solvent regeneration is decreased from 1.72 to 1.15 Ton/Ton CO_2.

The compressor work is minimized through compressor ratio optimization. Because the compressor inlet stream of the modified CO_2 capture process is not a pure substance, but binary mixture, high pressure ratio can no longer be achieved using single stage. From the industrial experience, water-CO_2 mixture can have 2.5 as its maximum compression ratio. From the Eq. (3-6), the optimum pressure ratios of C-M1 and C-M1 are tuned out to be 1.55 and 2.3 respectively and the minimized work is 84.6 kW/Ton CO_2. As compared with the pressure ratio evenly divided, the total compressor work exhibits about 10% less energy.

Exergy analysis was also performed over modified CO_2 capture process. As demonstrated in previous results, both condenser and reboiler heat duty were greatly reduced while additional the compression work introduced which was not used in the base case. Fig. 3-9 shows both exergy loss of each unit operation, and total exergy loss in comparison with the base case.

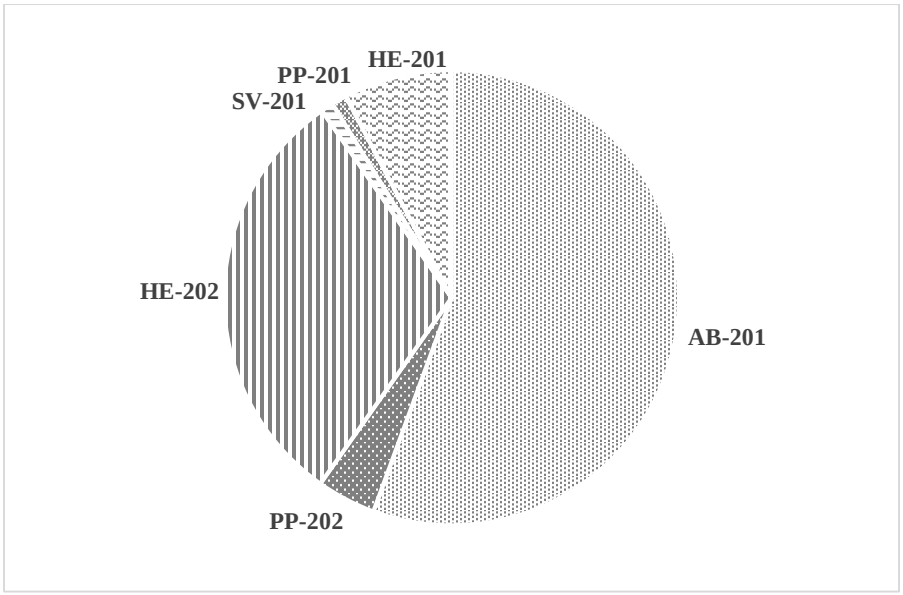

(a) Exergy loss in unit processes

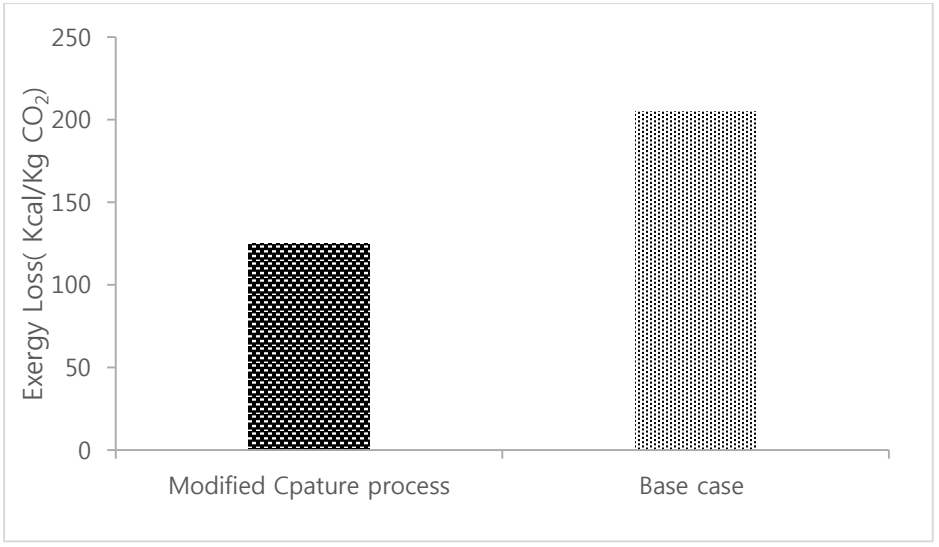

(b) Total Exergy loss of the base case and modified CO_2 capture process

Fig. 3-9 Exergy loss of each unit operation, and total exergy loss of the system

Fig.3-9 (a) shows that the exergy losses from the stripper (SV-201) and the lean rich amine heat exchanger are greatly reduced while that of absorber remains unchanged. The reduction of the irreversibility on the stripper is mainly resulted from the reduction of utility usage. Both condenser and reboiler heat duty of the stripper are reduced by employing vapor recompression process. Thus, subsequent hot and cold utility requirement are decreased as well. The irreversibility of HE-202 is also reduced by adjusting minimum temperature approach from 16.5 to 5^{o}C. Total exergy also shows noticeable amount of the reduction in the modified CO_2 capture process. As indicated in the Fig. 3-9 (b), the exergy loss of the modified CO_2 capture process is evaluated as 124.83 Kcal/Kg CO_2, and it is only 61% of that in the base case.

CHAPTER 4. Combined Rankine Cycle Design and Optimization

4.1. Overview

In this chapter, a combine Rankine cycle is modeled in order to produce additional power from the PC power plant. The combined cycle consists of a conventional stream cycle and an organic Rankine cycle (ORC). The ORC uses R601-R23-R14 ternary mixture as its working fluid and is integrated with a steam cycle as a bottoming cycle. The efficiency of the bottoming ORC is further improved by integrating it with liquefied natural gas (LNG) regasification process. By utilizing the hot and cold exergy of low-pressure steam and LNG that are initially wasted, the ORC is able to generate additional power without consuming fossil fuel. The CO_2 generated from the combined cycle is liquefied by utilizing its latent heat as a heat source for the working fluid. Consequently, the high pressure CO_2 vapor recovered from the modified CO_2 capture process can be liquefied without consuming additional energy. The nonisothermal condensing nature of the ternary mixture working fluid can reduce the exergy loss of the system, and the consequent power generation and efficiency of the ORC are significantly improved. Power generation from the ternary mixture ORC is increased by about 56% and 59% as compared with the pure and binary mixture ORCs, respectively. Important design parameters such as pump discharge pressure,

working fluid composition, and turbine inlet and outlet pressure are also optimized to recover the maximum power from the ORC.

4.2. Working fluid selection

In this study, an organic Rankine cycle is used for the bottoming cycle to recover the maximum power from cryogenic LNG. The composition of LNG adopted here is summarized in Table 4-1. Because LNG is not a pure substance, its temperature varies as it evaporates. In general, the more closely the temperature profile of a working fluid condensation process matches that of the LNG evaporation process, the more power can be recovered from the same amount of LNG evaporation. The thermodynamic properties of the cycles using a pure substance (propane), a binary mixture (water-ammonia), and a ternary mixture (R601-R23-R14), are shown in Fig. 4-1.

Table. 4-1 Composition of LNG

Component	Mole Fraction
N2	0.0007
CH4	0.8877
C2H6	0.0754
C3H8	0.0259
n-C4H8	0.0056
i-C4H8	0.0045
n-C5H12	0.0001
i-C5H12	0.0001
Total	**1**

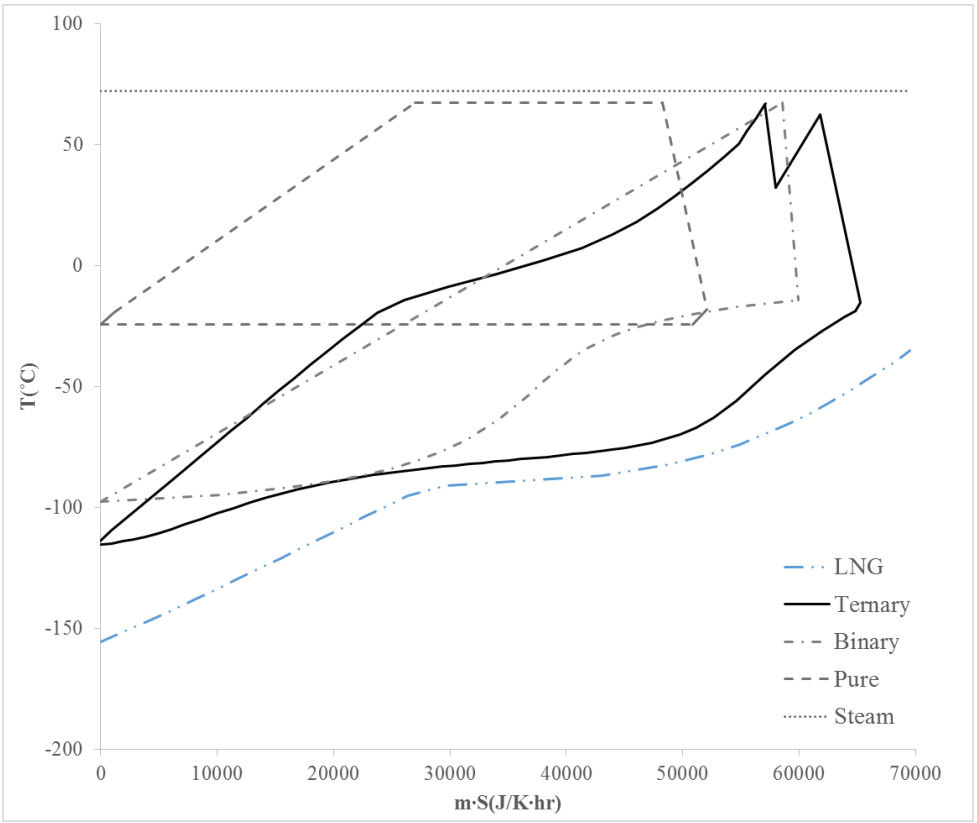

Fig. 4-1 T-S diagram of organic Rankin cycles

It can be seen that the cycle with the ternary mixture is more desirable than the cycles with a pure substance or a binary mixture because the ternary mixture cycle not only produces more power, but it also shows good agreement with the LNG evaporation temperature line. For a quantitative analysis of the potential work recovery from the LNG evaporation process, exergy analysis was performed using the following equations:

$$\mathrm{E}_i = (H_{out} - H_{in}) - T_0(S_{out} - S_{in}) \quad (4\text{-}1)$$

$$\dot{I} = \dot{E}_Q + \sum \dot{m}_{in}\dot{E}_{in} - \sum \dot{m}_{out}\dot{E}_{out} - \dot{E}_W \quad (4\text{-}2)$$

Here, the irreversibility ($\dot{I}$) is defined as the loss of available work, and it depends both on the condensation pressure and the composition of the ternary mixture. Along the working fluid condenser, irreversibility was calculated using Eqs. (4-1) and (4-2). The reference temperature, T_0, was selected as 300 K in this study. The enthalpy and entropy of hot and cold streams were calculated through Peng-Robinson equation of state (EoS) [69]. By varying the mole fraction of the ternary mixture and pressure, the minimum irreversibility and optimal mole fraction and pressure could be obtained. It is also assumed that all latent heat of the LNG should be recovered during the condensation process [Eq. (4-3)].

$$\mathrm{m}_{LNG}\Delta\mathrm{H}_{LNG} = \mathrm{m}_{wf}\Delta\mathrm{H}_{wf} \quad (4\text{-}3)$$

Nonazeotropic ternary mixtures of refrigerants are the potential candidates of the organic Rankine cycle. A total of 55 refrigerants were considered for the working fluid ternary mixture. Among these candidates, refrigerants were selected based on the thermodynamic properties (latent heat, density, and specific heat) suggested by Chen et al. [9]. Additionally, the normal boiling point difference was taken into account in order to make their temperature profile similar enough to the LNG evaporation curve. Refrigerants that have a high greenhouse potential, as well as those that have been designated as a controlled substance by the Montreal protocol, were excluded in this study. Taking into account physical properties and environmental impact, eight substances (listed in Table 4-2) were selected as components of the working fluid ternary mixture. There are 56 possible combinations of the ternary mixture with the listed refrigerants. However, only those combinations with a temperature difference between the bubble point and the dew point of more than 50 ℃ were considered as working fluid candidates in order to take advantage of nonisothermal condensing using LNG.

The heat curves of the 12 combinations of the ternary mixture along the working fluid condenser are presented in Fig. 4-2. The minimum temperature approach within the condenser is maintained as 5 ℃ throughout the irreversibility evaluation. To obtain a sufficient temperature glide during condensation, R-14 was selected as a light component (LC), and those with a

normal boiling point near –100 through –70 ℃ were considered as intermediate components (ICs). Similarly, substances with a high normal boiling point (close to or above 0 ℃) were selected as heavy components (HCs). As a result, all 12 combinations attained more than 50 ℃ temperature gliding, and consequent irreversibility can be reduced as compared with the pure or binary mixture working fluid condensation processes. Among these combinations, R601-R23-R14 exhibited the lowest irreversibility as it corresponds most precisely with the LNG evaporation heat curve. However, the best ternary mixtures shown in Figs. 4-2(a), 2(c), and 2(d) were also evaluated in the ORC in order to compare their performance with the R-601-R23-R14 mixture. The optimum composition, pressure, and corresponding irreversibility of the best ternary mixtures are listed in Table 4-3. HC MF, IC MF, and LC MF represent the heavy, intermediate, and light component mole fractions, respectively.

Table. 4-2 Refrigerants for ternary mixture working fluid combination

ASHRAE number	chemical formula	MM	NBP(˚C)	T_C(˚C)	P_C(Mpa)	LFL	ODP	GWP 100 yr
14	CF4	88	-128.1		3.75	none	0	5700
170	CH3CH3	30.07	-88.9	32.2	4.87	2.9	0	~20
23	CHF3	70.01	-82.1	25.9	4.84	none	0	12000
116	CF3CF3	138.01	-78.2	19.9	3.04	none	0	11900
30	CH2Cl2	84.93	40.2	237	6.08	13	0	10
601	CH3-CH2-CH2-CH2-CH3	72.15	36	196.6	3.37	1.4	0	11
245fa	CHF2CH2CF3	134.05	15.1	154.1	4.43	none	0	950
236fa	CF3CH2CF3	152.04	-1.4	124.9	3.2	none	0	9400

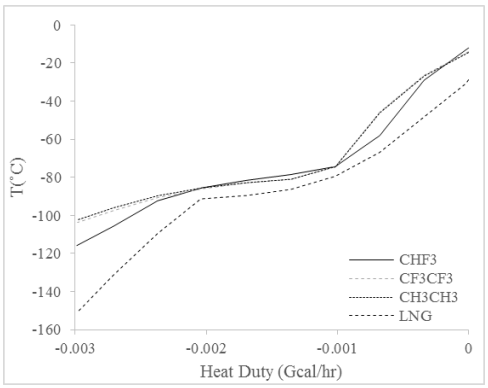

(a) R30(HC), R14(LC)

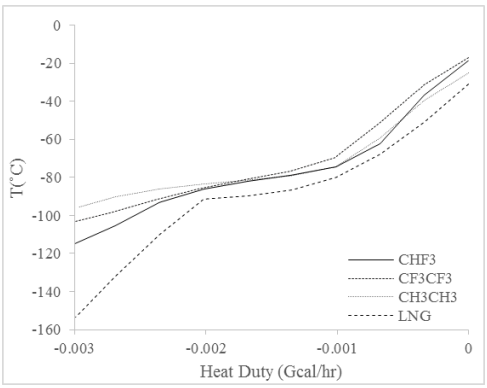

(b) R601(HC), R14(LC)

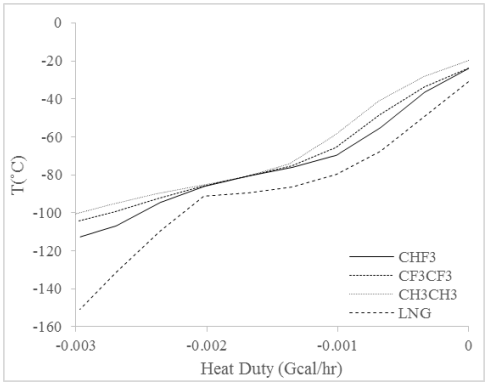

(c) R245fa(HC), R14(LC)

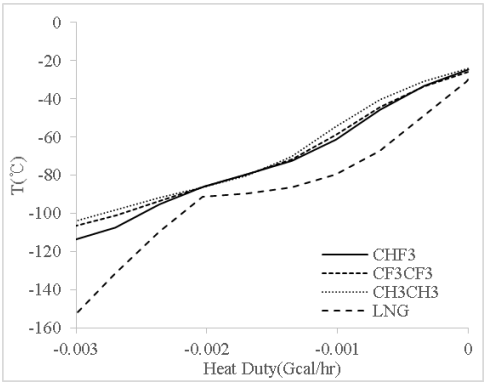

(d) R236fa(HC), R14(LC)

Fig. 4-2 Heat curve of the ternary mixture working fluid and LNG within the condenser.

Table. 4-3 Composition and pressure of the ternary mixture working fluid

Mixture	HC MF	IC MF	LC MF	Pressure (bar)	I (Kcal/Kmol LNG)
R30-R23-R14	0.068	0.680	0.252	1.60	393.34
R601-R23-R14	0.227	0.707	0.067	1.44	387.89
R245fa-R23-R14	0.092	0.624	0.284	1.70	415.41
R236fa-R23-R14	0.303	0.545	0.152	1.55	466.55

4.3. Process modeling and simulation

4.3.1. Design basis

To predict the thermodynamic properties (such as enthalpy and entropy) of the mixture, the Peng-Robinson equation of state, which is commonly used to describe the thermodynamic behavior of hydrocarbons and refrigerants, is used in this study [22, 70, 71]. A few assumptions were made in designing the ORC. First of all, all the evaporation enthalpy of LNG should be recovered in the working fluid condensation process in order to maximize the power generation. A minimum temperature approach of all heat exchangers is maintained at 5 ℃, and the isentropic efficiencies of turbines are chosen as 72%. It is also assumed that LNG evaporation takes place at 3 MPa, and pressure drops along the heat exchangers, flash separators, and pipeline are neglected. The low-grade heat for the working fluid evaporation is supplied from the low-pressure steam of the PC power plant. Most importantly, the working fluid is maintained in vapor phase across turbines in order to avoid mechanical and operational problems that may be caused by phase change within the turbine.

4.3.2. ORC process description

The ORC proposed in this study consisted of a working fluid condenser (HX1), a pump (P1), a preheater (HX2), an evaporator (HX3), a super heater (SH), a high-pressure turbine (T1), a reheater (RH), and a low-pressure

turbine (T2). A regenerator is not required in this process because the exhausting vapor from T2 is fully saturated. Fig.4-3 displays the process flow diagram and working fluid pathway of the ORC analyzed in this study. Once the R601-R23-R14 mixture is liquefied in HX1 (S1), it is then sent to P1 to be pressurized to the desired pressure, i.e., 33.9 bar.

Unlike the conventional Rankine cycle, the proposed ORC has a preheater (HX2) that employs captured CO_2 generated from the PC power plant as a heat source. The inlet CO_2 condition directly taken from the result of chaper 3, (6.5 bar and 40 ℃). By utilizing the latent heat of CO_2 to preheat the working fluid, not only is the low-pressure steam usage reduced, but the energy consumption for the CO_2 liquefaction process is also reduced, which is essential for the CO_2 transportation process. The working fluid from HX2 is then flowed through the evaporator (HX3) and SH to become vapor, and it is introduced to the two-stage turbine. To recover maximum work from the system, discharge pressures of P1 and T1 are optimized, and their optimum points are located at 33.9 and 16.5 bar, which makes the working fluid fully saturated at the exit of T2.

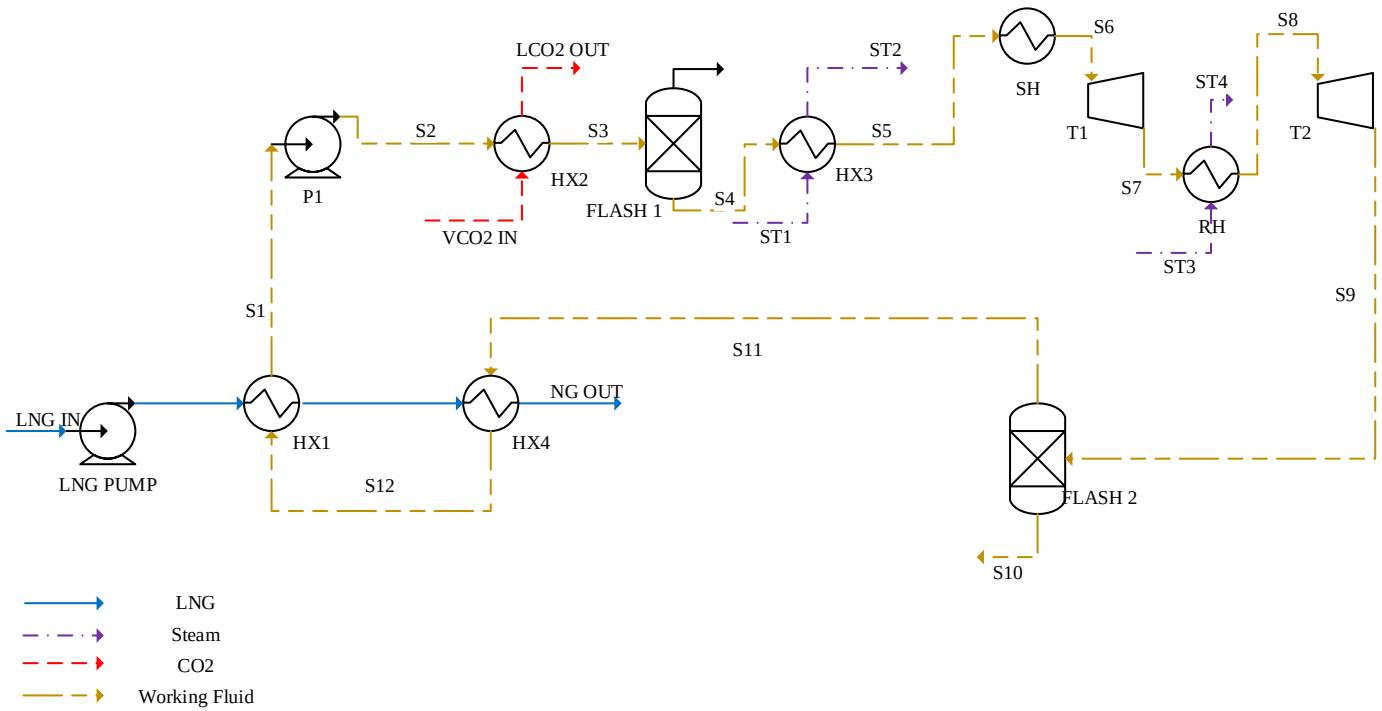

Fig. 4-3 Process flow diagram of ORC using ternary mixture working fluid.

4.4. Mathematical modeling

4.4.1. Condenser/evaporator

All the evaporation enthalpy should be utilized for the working fluid condensation while a minimum temperature approach, 5 ℃, is maintained within the heat exchanger. Therefore, the mass flow rate of the working fluid can be decided on the basis of the amount of available LNG. The latent heat of the working fluid mixture can be calculated using Eqs. (4-4) and (4-5),

$$l_v = \sum_{i=1}^{3} Y_i[\bar{H}_i^v(Y_i) - \bar{H}_i^l(X_i)] \quad (4\text{-}4)$$

The differential heat of vaporization, l_v, is defined as the amount of heat required to transfer one mole of a mixture of composition Y_i to vapor phase from an infinite liquid mixture of composition X_i [72]. The liquid and vapor mole fraction and enthalpy used in Eq. (4-4) are evaluated using the Peng-Robinson EoS. The total heat of vaporization can be calculated simply by integrating the differential heat of vaporization from the bubble point to the dew point. Using the latent heat calculated from Eqs. (4-4) and (4-5), the mass flow rate of the working fluid can be calculated using Eq. (4-3),

$$\Delta H = \int_{T_{Bubble}}^{T_{Dew}} l_v dT \quad (4\text{-}5)$$

The evaporator has similar criteria. However, sensible heat of both steam and the working fluid should be included because neither hot nor cold streams are in the saturated phase,

$$\dot{m}_{wf}(C_{p,l,wf}\Delta T + \Delta H_{wf} + C_{p,v,wf}\Delta T) = \dot{m}_{steam}(C_{p,v,steam}\Delta T + \Delta H_{steam}) \quad (4\text{-}6)$$

Once the mass flow rate of the working fluid and the steam are decided, the irreversibility of both the condenser and the evaporator is evaluated using Eq. (4-7),

$$\dot{I} = \sum \dot{m}_{in} E_{in} - \sum \dot{m}_{out} E_{out} \quad (4\text{-}7)$$

4.4.2. Reheater

The reheater in the ORC also utilizes low-pressure steam as its heat source. Since there is no phase change in the working fluid, the amount of steam required to increase the working fluid temperature can be calculated using Eq. (4-8),

$$\dot{m}_{wf} C_{p,v,wf}\Delta T = \dot{m}_{steam}(C_{p,v,steam}\Delta T + \Delta H_{steam}) \quad (4\text{-}8)$$

4.4.3. Preheater

The amount of CO_2 supplied to the preheater was calculated in Chapter 3. It is also assumed that all the CO2 captured from the capture process is utilized for working fluid preheating. The amount of CO_2 supplied to the ORC is 432.76 Ton/hr. In the same way as the reheater, there is no phase change in the working fluid within the preheater. As a result, the temperature of the working fluid exiting the preheater can be calculated using Eq. (4-9),

$$\dot{m}_{wf} C_{p,l,wf}(T_{out} - T_{in}) = \dot{m}_{steam}(C_{p,v,steam}\Delta T + \Delta H_{steam}) \quad (4\text{-}9)$$

The irreversibility over both the reheater and the preheater can also be calculated using Eq. (4-7).

4.4.4. Pump

The liquid-phase working fluid is assumed to be incompressible flow. As a result, the density and liquid volume are independent of pressure. By neglecting the kinetic and potential energy, the isentropic and actual pump work can be expressed by Eqs. (4-10) and (4-11), respectively,

$$\dot{W}_{pump,isen} = \dot{m}(H^S_{out} - H_{in}) = \dot{m}\frac{(P_{out} - P_{in})}{\rho} = \dot{V}(P_{out} - P_{in}) \quad (4\text{-}10)$$

$$\dot{W}_{pump,} = \dot{V}\frac{(P_{out} - P_{in})}{\eta_{pump}} \quad (4\text{-}11)$$

4.4.5. Turbine

The power generated by turbines is given by Eq. (4-12), and the nonideal expansion of the working fluid can be described based upon isentropic efficiency (Eq. (4-13)),

$$\dot{W}_{Turbine} = \dot{m}(H_{in} - H_{out}) = \dot{m}\frac{(H_{sin} - H_{out,s})}{\eta_{Turbine}} \quad (4\text{-}12)$$

$$\eta_{Turbine} = \frac{(H_{sin} - H_{out})}{(H_{sin} - H_{out,s})} \quad (4\text{-}13)$$

The irreversibility over the pump and turbine can be expressed as Eq. (4-14),

$$\dot{I} = \dot{m}(e_{out} - e_{in}) - \dot{W} = -\dot{m}T_0(S_{out} - S_{in}) \quad (4\text{-}14)$$

4.4.6. System efficiency

Total irreversibility and the net power of the ORC can be defined as

$$\dot{I} = \dot{I}_{HX1} + \dot{I}_{HX2} + \dot{I}_{HX3} + \dot{I}_{SH} + \dot{I}_{RH} + \dot{I}_{P1} + \dot{I}_{T1} + \dot{I}_{T2} \quad (4\text{-}15)$$

$$\dot{W}_{Net} = \dot{W}_{Turbine} - \dot{W}_{Pump} \quad (4\text{-}16)$$

For the ORC with a cold LNG utilization system, the power generation per unit of LNG vaporization is a more meaningful performance indicator than using power generation per unit heat source supplied. Therefore, Eq. (4-17), the net power per LNG, is used for system evaluation,

$$\dot{W}_{Net/LNG} = \frac{\dot{W}_{Net}}{\dot{m}_{LNG}} \quad (4\text{-}17)$$

Both the thermal efficiency and the exergy efficiency of the ORC are also calculated in order to give more detailed insights into the system,

$$\eta_{Th} = \frac{\dot{W}_{Net}}{\sum \dot{Q}_{IN}} \quad (4\text{-}18)$$

$$\eta_{ex} = \frac{\sum Exergy\ Output}{\sum Exergy\ Input} = 1 - \frac{\dot{I}}{\sum Exergy\ Input} \quad (4\text{-}19)$$

4.5. Result and Discussion

4.5.1. Cycle performance and optimization

The T-S diagram of the ORC is presented in Fig. 4-4. Nonisothermal condensation of the working fluid reduces the irreversibility of the system, and consequent power generation is increased as compared with the pure or binary substance ORC. The exergy loss during the evaporation process is higher than that in the ORC with a pure substance due to its nonisothermal evaporation. However, LNG exergy recovery should gain more attention because the evaporation system utilizes an abundant heat source of low-pressure steam, which could not have been fully utilized otherwise. Furthermore, the exergy recovery during the evaporation process can be improved by using different types of waste-heat sources such as low-temperature flue gas or geothermal energy, and it may make the irreversibility along the evaporator even lower than that with a pure substance [20, 71]. As shown in Fig. 4-4, the saturated working fluid mixture (S9) is condensed to complete liquid (S1) in HX 1.The composition of the working fluid is R601 = 0.00667, R 23 = 0.707, and R14 = 0.227 in mole fraction. The pressures of the hot and cold side of HX 1 are assumed to be 1.44 and 30 bar, respectively.

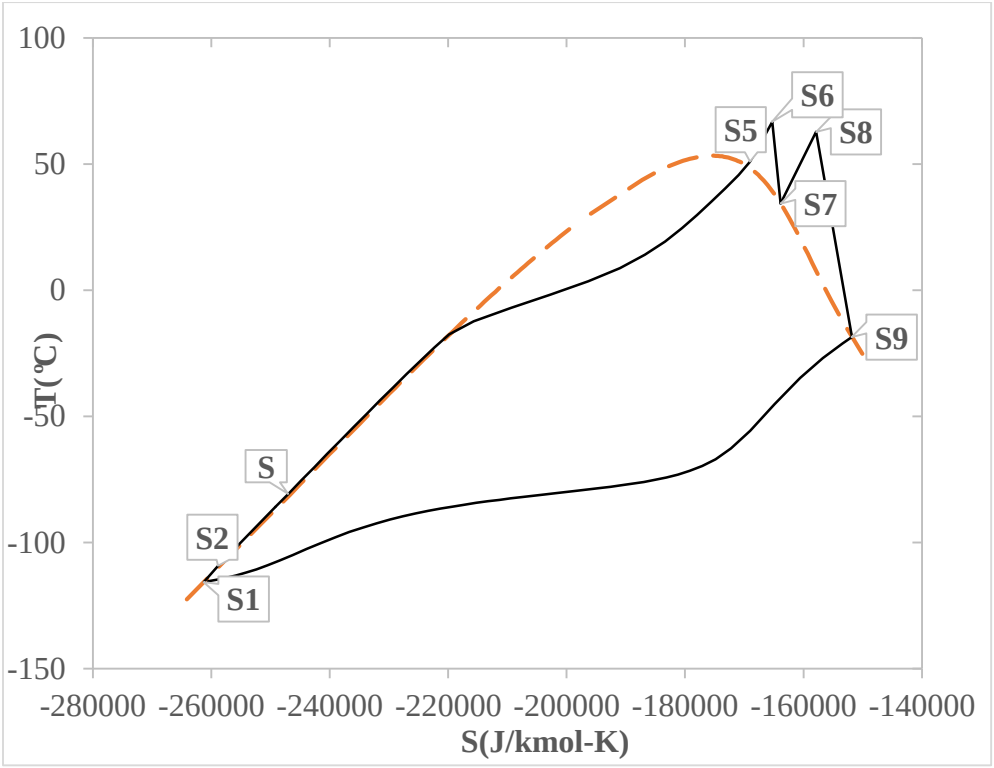

Fig. 4-4 T-S diagram of ORC using ternary mixture working fluid.

From the stream S1 to S2, the working fluid is pressurized from 1.44 to 33.9 bar. The discharge pressure of P1 is decided to generate the maximum power in the cycle. Generally, the maximum power can be recovered when the final discharged stream is at saturated phase. Fig. 4-5 shows total power generation vs. P1 discharge pressure and the corresponding T-S diagram. The power generation of the cycle increases as the P1 discharge pressure increases until 33.9 bar, as indicated in Fig. 4-5(a). However, the total power generation decreases rapidly beyond 33.9 bar because the turbine discharge stream (S9) starts to become liquefied. This tendency can be more clearly recognized in the T-S diagram of the cycle with a different P1 discharge pressure [Fig. 4-5(b)]. The solid line in Fig. 4-5(b) is fully saturated at the turbine exhausted stream (S9). However, this stream is superheated as the P1 discharge pressure is decreased, or phase change occurs in the stream when the P1 discharge pressure is higher than 33.9 bar. The areas between the evaporation and condensation curves are decreased by both 25 and 35 bar, as indicated in Fig. 4-5(b), and the consequent power generation with these pressures is also smaller than that with 33.9 bar.

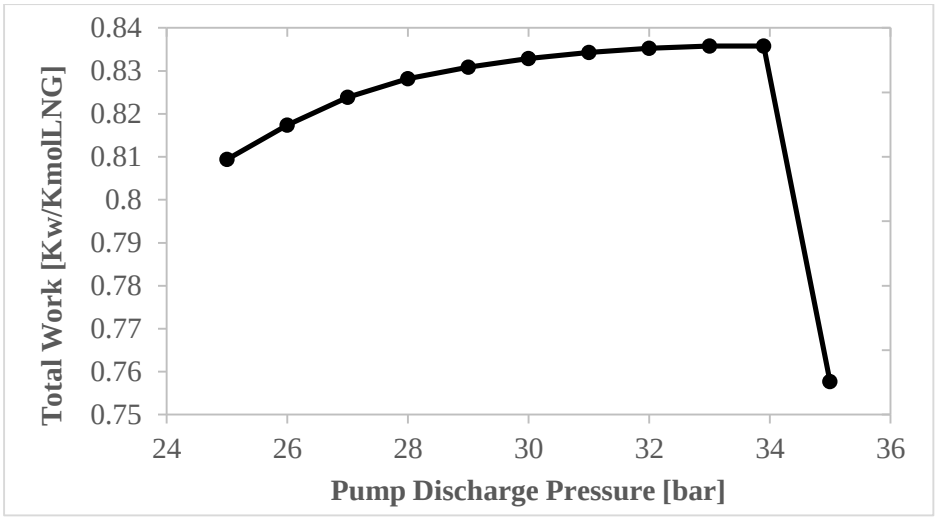

(a) Total power generation depending of P1 discharge pressure

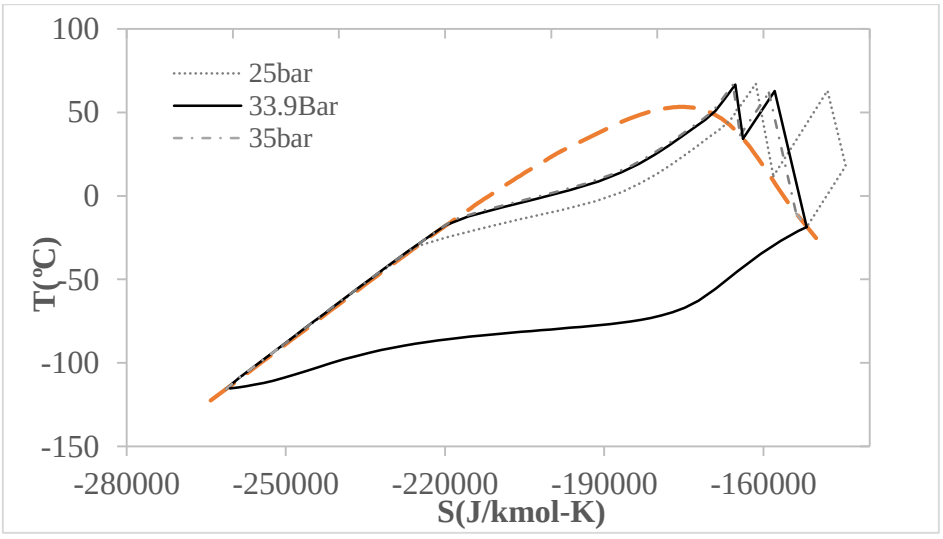

(b) T-S diagram of ORC with different P1 discharge pressure

Fig. 4-5 Total power generation vs. P1 discharge pressure change and corresponding T-S diagram of the ORC

The temperatures of super-heated stream (S6) and reheated stream (S8) are limited to 66.7 and 62.7 ℃ in order to keep the minimum temperature within SH and RH. Fig. 4-6 indicates the heat curve of the evaporator (a) and the reheater (b). The steam supplied at 87.7 ℃ and 0.25 bar is used as a heat source in both the evaporator and the reheater. Because of the isothermal condensation nature of the steam, the irreversibility of the process increases when the ternary mixture, instead of the pure substance, is used as the working fluid. The irreversibility of the evaporator is evaluated as 799.4 kcal/Kmol LNG. The sum of these values, however, is more than twice that of the condenser irreversibility and should be lowered to improve cycle efficiency. One of the possible solutions to lower the irreversibility is to use different types of heat sources such as flue gas or geothermal energy, which are nonisothermal heat transfer media. However, irreversibility optimization on the evaporator and reheater is not considered in this study because the proposed ORC utilizes an abundant low-grade heat source, which is considered free to use.

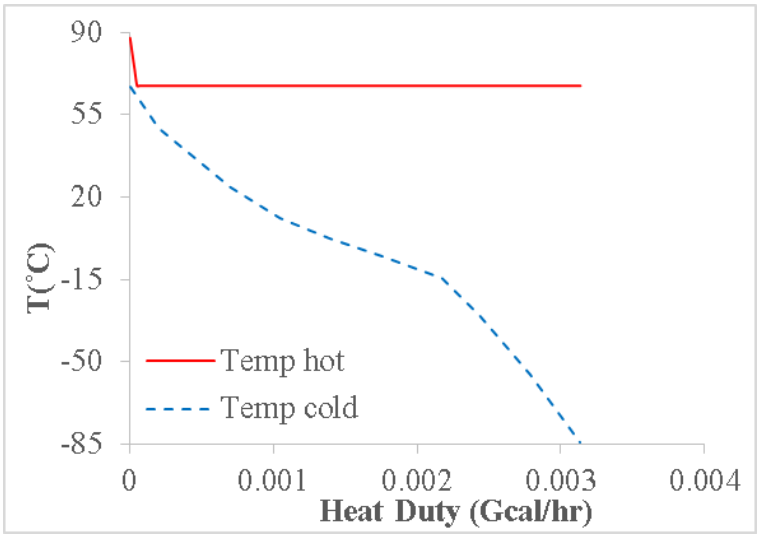

(a) Evaporator

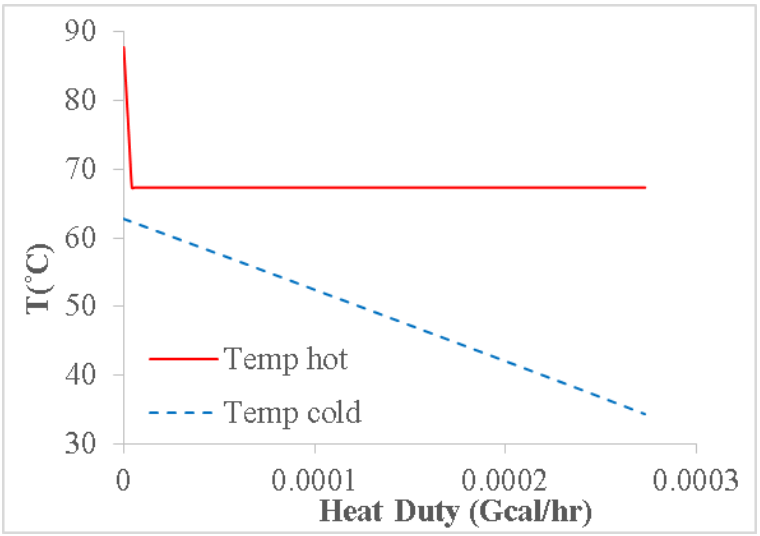

(b) Reheater

Fig. 4-6 Heat curve of evaporator and reheater

The power generation of T1 and T2 is 37.6 and 127.1 kJ/kg LNG, respectively. The intermediate pressure, 16.53 bar, is also decided at the point where the T1 discharge stream is fully saturated. The effect of intermediate pressure change is presented in Chapter 4.5.3.2

Fig. 4-7 illustrates the exergy loss of each unit in the ORC. The exergy loss of the evaporator, HX3, is highest among all the unit processes, and it makes up about 46% of the total exergy loss. Since the preheater and the evaporator employ isothermal condensing media for the working fluid heat source, the irreversibility of these unit processes is comparably high. Moreover, the minimum temperature of the preheater (40 ℃), HX2, is much higher than that of other heat exchangers in order to liquefy all CO_2 generated from the power plant, thus the irreversibility of HX2 is high for the amount of heat transfer. However, the irreversibility of those units can be reduced if nonisothermal heat transfer heat sources are used. In this manner, the exergy efficiency of the system can be further improved. The irreversibility of the condenser (HX3) is greatly reduced, and it accounts for only 23% of the total irreversibility. Because the ternary mixture temperature profile within HX3 shows good agreement with the LNG evaporation curve, the condenser irreversibility is reduced by 33% and 76% as compared with that of binary and pure working fluid ORCs.

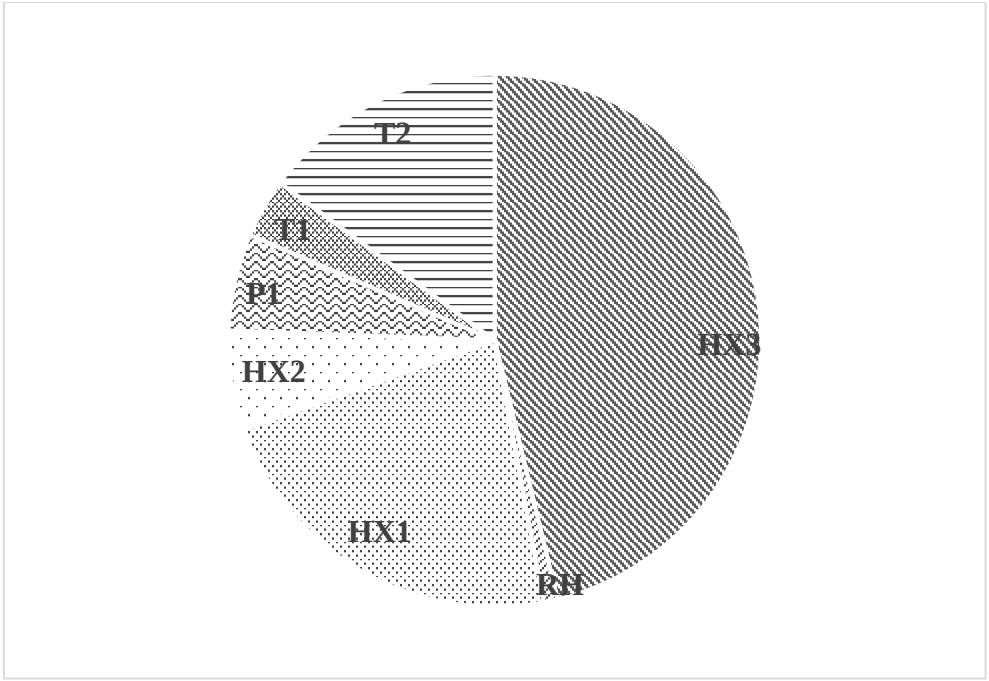

Fig. 4-7 Irreversibility of unit process.

Table 4-4 presents the performances of the ORC cycle using R601-R23-R14. It is assumed that 1620 t/h LNG is available for cold exergy utilization based on the Incheon LNG terminal regasification process operation data. The main heat source of the system is the low-pressure steam extracted from fourth stage of the steam turbine. When the low-pressure steam is extracted from the fourth stage of the turbine, the power generation of the ORC together with the steam cycle is maximized. By extracting the low-pressure steam from the fourth stage of the turbine, the steam cycle loses about 18.7 MW power generation. However, the power generation from the ORC is increased about 22.6 MW, thus the combined Rankine cycle can produce more power in comparison with waste-steam utilization. A detailed cycle performance depending on LP steam extraction location is provided in Section 4.5.3.1.

Table. 4-4 Evaluation result of ORC with R601-R23-R14 working fluid

Parameters	Value
Power Generation (MW)	74.10
Power/LNG (KJ/Kg LNG)	164.67
Irreversibility (Kcal/hr)	1135.13
ORC Thermal Efficiency	23.7%
ORC Exergy Efficiency	27.0%

The performance of the proposed cycle is compared with the ORC using a pure and a binary mixture. As indicated in Table 4-5, the ORC proposed in this study can produce more than 50% of the power from the same heat source and the cold sink. Both the thermal and exergy efficiency of the cycle are greatly improved based upon the total irreversibility decreases. The high power output of the proposed ORC is mainly due to the reduction of the irreversibility on HX1. The thermal efficiency of the ORC is relatively lower than the conventional Rankine cycle because exergy transfer of the working fluid to the cold sink, which is usually higher than that of a hot source in wet fluid, is included for the heat input in Eq. (4-18).

Although the exergy efficiency of the ORC, 27.0%, can be further improved by using higher-pressure steam and removing the preheater, it is not desirable in this study. When LP steam higher than 0.25 bar is implemented as the ORC heat source, the power decrease in the steam cycle is overwhelmed by the power increase in the ORC, even though the ORC itself has higher exergy efficiency. Moreover, the utilization of the preheater can save a considerable amount of the CO_2-liquefaction process operation energy. By utilizing the latent heat of CO_2 to preheat the working fluid, the CO_2 can be liquefied without further compression, thus the CO_2 liquefaction energy, which is an inevitable process in the base case study, can be avoided.

Table. 4-5 Performance of ORCs with pure, binary and ternary mixture working fluid

	Pure (Propane)	**Binary (Water-Ammonia)**	**Ternary (R601-R23-R14)**
Power Gen. (KJ/Kg LNG)	105.7	103.7	164.7
Thermal Efficiency	15.2%	14.9%	23.7%
Exergy Efficiency	15.0%	19.1%	27.0%
I_{cond} (Kcal/kmol LNG)	1634.7	581.5	389.2
I_{total} (Kcal/kmol LNG)	2111.8	1908.2	1729.7

4.5.2. Cycle performance of different ternary mixtures

The ORC proposed in this study is also evaluated using three other combinations of ternary working fluids, which exhibit minimum irreversibility in Fig. 4-2. The ORC with the ternary mixture of R601-R23-R14 produces the highest net power to the semblance of irreversibility evaluation in Fig. 4-2. The net power production of the cycle, however, depends not only on the irreversibility of the condenser but also on the other thermophysical properties, and most importantly on the amount of heat transfer in the evaporator. For example, the power generation of the cycle with the R245fa-R23-R14 mixture is higher than that with R30-R23-R14 in spite of the higher irreversibility on the condenser. As indicated in Fig. 4-8, the steam requirement of the R245fa-R23-R14 mixture for working fluid evaporation is higher than that of the R30-R23-R14 mixture, and it mainly depends on thermophysical properties such as latent heat, specific density, heat capacity, and pressure. Although the ternary mixture, R601-R23-R14, used in this study exhibits both the minimum irreversibility and the maximum power production (as well as the thermal efficiency), the thermophysical properties and exergy transfer along the evaporator should also be considered when a different working fluid is selected for the cycle employing both a heat source and a cold sink at the same time.

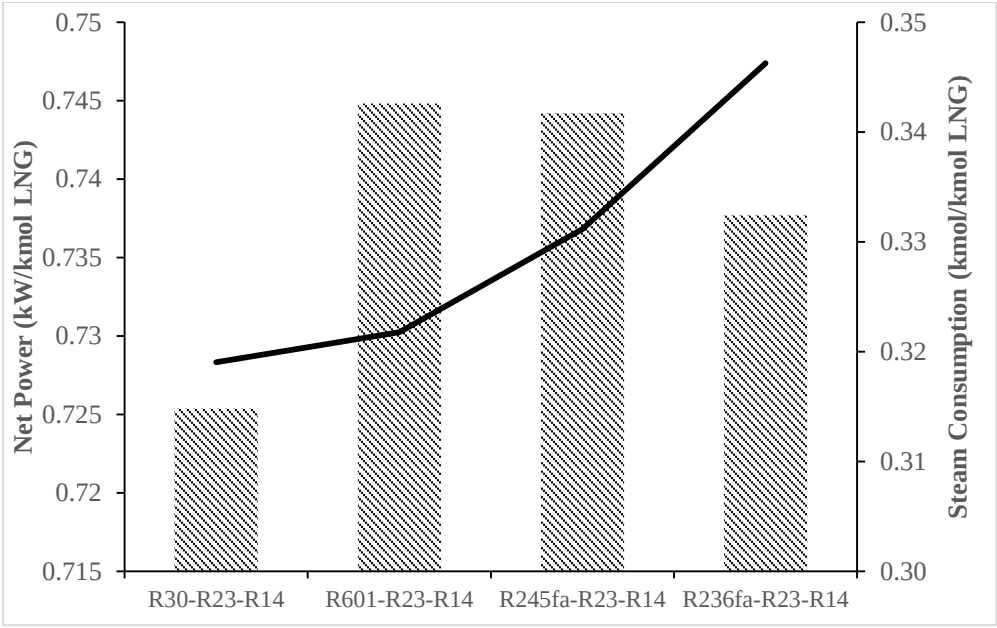

Fig. 4-8 Net power generation of ORCs using ternary mixture working fluids.

4.5.3. Sensitivity analysis

4.5.3.1. Steam temperature

The power generation of both the ORC and the steam cycle depends highly on the steam extraction location of the steam cycle. The higher the pressure of steam extracted from the steam cycle for the ORC heat source is, the less power is generated from the steam cycle, whereas the power generation from the ORC increases. Fig. 4-9 shows power generation of both the steam cycle and the ORC. The pressures in the figure correspond to the output steam pressure of fifth-, fourth-, third-, and second-stage turbines. Except for the steam temperature, most of the variables do not changed in the sensitivity study. For example, the minimum temperature approach of the heat exchangers is maintained at 5˚C. Since the same working fluid is used for the steam temperature sensitivity analysis, the turbine discharge pressure is maintained 1.44 bar. Pump discharge pressures are selected based on the same criteria proposed in chapter 4.5.1 where the turbine discharge fluid is fully saturated. The total power generation, 601.0 MW, is maximized when the steam is extracted from the fourth stage of the turbine.

The thermal efficiency of the combined Rankine cycle is also calculated using Eq. (4-18). The $\sum \dot{Q}_{IN}$ of the cycle is defined as the summation of heat transfer of the ORC working fluid to the LNG and the higher heating value (HHV) of coal. The solid line in Fig. 4-9 indicates the thermal

efficiency of the combined Rankine cycle. In the same manner as the power generation, thermal efficiency reaches the maximum when the steam is extracted from the fourth stage of the steam turbine, and the corresponding efficiency is about 37.6%.

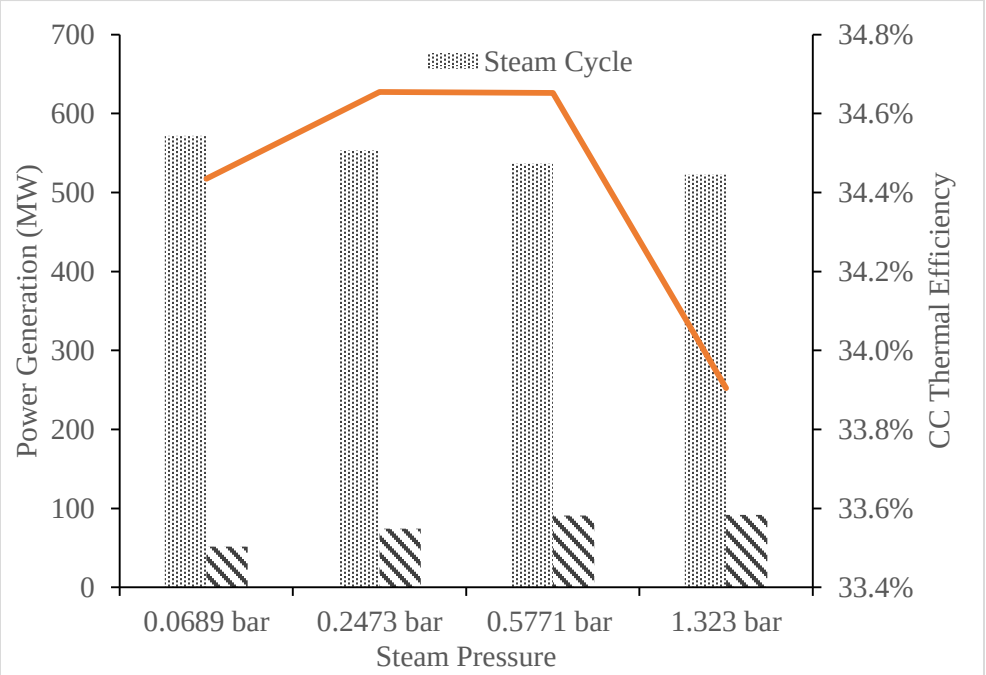

Fig. 4-9 Power generation of combined Rankine cycle depending on the steam extraction location.

4.5.3.2. Intermediate pressure

The dependence of net power generation as well as thermal efficiency on the intermediate pressure of the turbine is also investigated in this study. In many studies, the maximum power production is achieved when a turbine exhaust stream is in a fully saturated phase. However, it is not necessarily true all the time because this tendency can change depending on the types and properties of the working fluid. For example, a turbine exhaust stream cannot be saturated when dry fluids are employed for a cycle, thus the maximum power production occurs with superheated turbine exhaust stream.

Fig. 4-10 presents the relationship between intermediate pressure and power generation. Similar to the steam temperature sensitivity analysis, design variables except the intermediate pressure are unchanged with respect to the base case (e.g. minimum temperature, pump discharge pressure, and turbine discharge pressure). As indicated in the figure, the net power generation as well as the thermal efficiency are decreased with an increase in intermediate pressure. With an intermediate pressure of 16.55 bar, the T1 exhaust stream is in a saturated vapor phase. Subsequently, the T1 exhaust stream is superheated as the intermediate pressure increases. As a result, the amount of heat transfer in RH is reduced and the power generation is also decreased. Therefore, the discharge pressures of T1 and T2 are chosen at the points where the exhaust stream is in a saturated vapor phase.

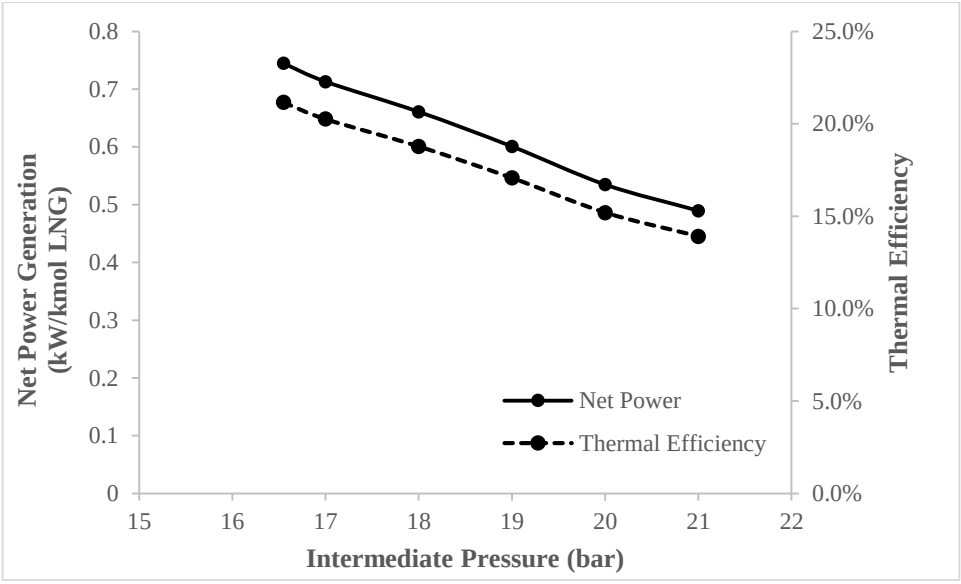

Fig. 4-10 Power generation and thermal efficiency of ORC according to the T1 discharge pressure.

4.5.3.3. Working fluid composition

The composition of the working fluid is decided based on the exergy loss of the condenser (HX3). Even though the condenser supplies more than 80% of the total exergy input, the maximum power generation does not necessarily take place with the same working fluid composition because other exergy input through the preheater or the evaporator may have a significant effect on power generation. Sensitivity analysis was done near the optimum point calculated in Section 2. Similar to the previous sensitivity studies, most of the design variables are maintained the same. However, both the pump discharge pressure and intermediate turbine pressure should be adjusted as the composition of the working fluid changed. The pump discharge pressure and intermediate pressure are decided at the place where the working fluid from the first and second stages of the turbine is fully saturated.

Fig. 4-11 indicates the gross power generation in the ORC vs. working fluid mole fraction. The maximum power, 0.8357 kW/kmol LNG, is generated with the same mole fraction as that with the lowest condenser irreversibility. As indicated in the figure, the power generation is generally increased as the mole fraction of R14 and R23 increases. However, it starts to decrease beyond the point R601 = 1, R23 = 3.4, and R14 = 10.6, and it is mainly caused by the temperature crossover within the HX1. As the mole faction of light and intermediate components increases, the temperature of the working

fluid in the condenser decreases more rapidly (high C_p), and Eq. (3) is no longer satisfied to keep the minimum temperature approach within HX 1. Consequently, the exergy input of the HX1 is eventually decreased and the resulting power generation is also decreased.

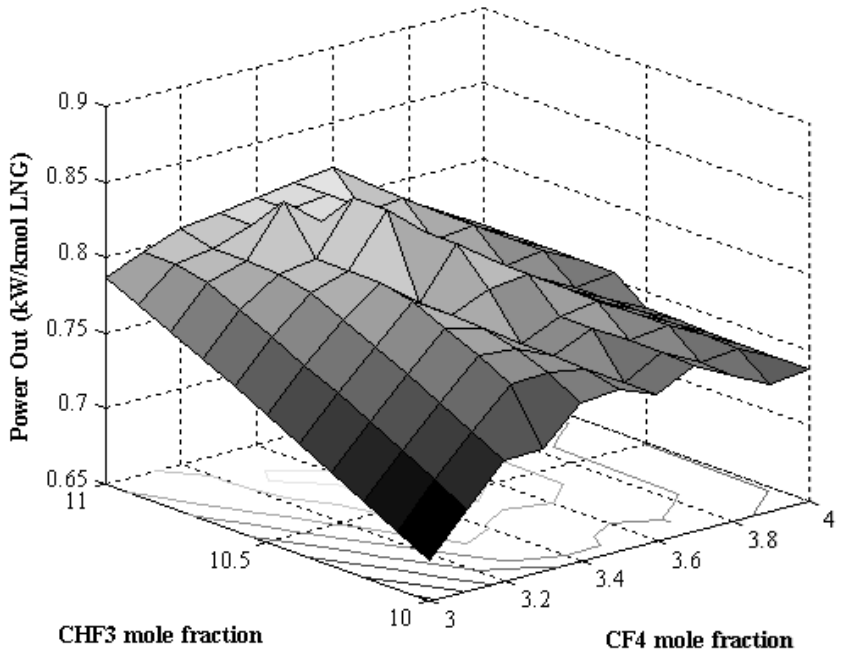

Fig. 4-11 Gross power generation according to the composition of working fluid

4.6. Performance summary of the combined rankine cycle

In this section, quantitative comparison between the combined Rankine cycle with modified CO_2 capture process and base case is presented. Table 4-6 summarized the process performance of base case and combined Rankine cycle. The most importantly, power generation of the combined Rankine cycle is increased about 17% as compared with that of the base case. Power de-rate of the plant is also decreased from 22% to 9%. Both CO2 capture energy reduction and additional power generation from the bottoming ORC contribute to the power de-rate reduction. Thermal efficiency of the combined Rankine cycle is also improved by 5.5%. Together with the modified configuration of the CO_2 capture process and combined Rankine cycle, it makes economically and technically more feasible to implementing CCS technology on the coal combustion power plant

Table. 4-6 Performance summary of the base case and the combined Rankine cycle

	Base case	**Combined Rankine cycle**
Gross Power Generation(MW)	661.0	661.0
Steam cycle power reduction (MW)	105.3	89.1
Steam extraction for CO2 capture (t/h)	705.2	471.5
Steam extraction for bottoming cycle (t/h)	-	556.1
Amount of CO2 capture (Ton)	432.8	432.8
CO2 capture Energy (GJ/Ton CO2)	3.7	2.4
Compression Energy (MW)	42.5	45.0
Bottoming cycle power production (MW)	-	74.1
Net Power Generation (MW)	513.2	601.0
Coal Consumption(t/h)	219.6	219.6
Thermal Efficiency	32.1%	37.6%

CHAPTER 5. Implementation of Scattered Search for Simulator Based Non Convex Problem

5.1. Overview

The algorithm describe in this chapter is a heuristic design to find global optima for non-convex problem with many constraints and variables. Although many process simulator provide sequential quadratic programming (SQP) based process optimizers, they are often failed to find the global optimum with multi variable non convex problem. For example, the pressure ratio optimization shown in chapter 2 and 3 can be successfully solved through SQP algorithm, but the irreversibility optimization in chapter 4 cannot be performed due to the presence of numbers of local optima. The scattered search algorithm proposed in this chapter chooses multiple starting points decided based on the single variable gradients. From each starting point, the local optimum can be found using SQP algorithm provided by MATLAB^{TM}. Among the local optima, the minimum value were selected as global optimum candidate and verified though iterations. Rastrigin's function was evaluated using the proposed method in order to show the efficiency and accuracy of the algorithm as an examples. Also, the solution of irreversibility minimization problem demonstrated in chapter 4 was provided in this chapter.

5.2. Local optima calculation: Sequential Quadratic Programming

The general non-linear minimization problem can be represented using Eq. (5-1).

$$\text{minimize } f(x) \tag{5-1}$$

Where n-dimensional vector x returns a scalar value f(x) subject to constraints on the allowable x (Eqs. (5-2) and (5-3)).

$$G_i(x) = 0 \quad i=1,\ldots,m_e \tag{5-2}$$

$$G_i(x) \leq 0 \quad i= m_e,\ldots,m \tag{5-3}$$

The optimization problem stated above can be transform to an easier sub problem that is solved through the basis of an iterative process. The Karush-Kuhn-Tucker (KKT) equations are the necessary condition for optimality for constrained optimization problem. If the optimization problem is a convex problem, the KKT equations are both necessary and sufficient for a global solution point.

$$\begin{gathered}\nabla f(x^*) + \sum_{i=1}^{m} \lambda_i \cdot \nabla G_i(x^*) = 0 \\ \lambda_i \cdot \nabla G_i(x^*) = 0 \quad i=1,\ldots,m_e \\ \lambda_i \geq 0 \quad i= m_e+1,\ldots,m\end{gathered} \tag{5-4}$$

The KKT equations can be expressed as Eq. (5-4). Constrained quasi-Newton methods can successfully obtain the solution of KKT equations as well as the Lagrangian multiplier. The method suggested by Biggs [73], Han [74], and Powell [75] based on Newton's method for constrained optimization perform the constrained optimization in the similar way of unconstrained optimization. With the Hessian function of the Lagrangian function (Eq. (5-5)), a quadratic programming sub problem, Eq. (5-6), can be formulated whose solution is used for search direction.

$$L(\mathrm{x},\lambda) = \mathrm{f}(\mathrm{x}) + \sum_{i=1}^{m} \lambda_i \cdot \mathrm{G}_i(x) \tag{5-5}$$

$$\begin{gathered} \min \frac{1}{2} d^T H_k d + \nabla \mathrm{f}(x_k)^T d \\ \nabla \mathrm{g}_i(x_k)^T d + \mathrm{g}_i(x_k)^T = 0,\ i=1,\ldots,m_e \\ \nabla \mathrm{g}_i(x_k)^T d + \mathrm{g}_i(x_k)^T \leq 0,\ i= m_e,\ldots,m \end{gathered} \tag{5-6}$$

This QP problem can be simply solved and the solution of the problem is used to update initial solution.

$$x_{k+1} = x_k + \alpha_k d_k \tag{5-7}$$

The step length parameter α_k is determined by an appropriate line search procedure so that a sufficient decrease in a merit function is obtained.

5.3. Scattered search for global optimum

Although the SQP algorithm introduced in chapter 4.2 can successfully obtain optimum value, it often fail to find global optima when local optimum exist. The scattered search algorithm can overcome the trap in local optimum efficiently, by evaluating multiple starting point within the test subset S. The optimization problem presented here has the same mathematical from of Eq. (5-1) to (5-3). Also, it is assumed that global optimum occurs in the interior of S. The local optimum point which can be obtained from the SQP algorithm is denoted by L. The simplest method to find global optimum through multiple start points are finding local optima from uniformly distributed points in S, and compare the value of L from each of these. As the number of points increase to infinity, the optimum value approach to a global solution [76]. This procedure, however, is very inefficient because many starting points may go through the unnecessary calculation and converge to the same solution. Therefore, it is the most important step to choose proper starting points

In this study, the starting points of the optimization problem satisfied the conditions specified in Eqs. (5-8) and (5-9)

$$\left(\frac{df}{dx_i}\right)_{x_i=x_i^*} = 0, \qquad i = 1, \dots, m \tag{5-8}$$

$$\left(\frac{d^2f}{dx_i{}^2}\right)_{x_i=x_i^*} \geq 0, \qquad i = 1, \dots, m \tag{5-9}$$

With the solution of the single variable local optimum obtain from the Eqs. (5-8) and (5-9), the starting point grid can be generated accordingly. The starting point grid has m-dimension, and each dimension has the same number of points with the solution of Eqs. (5-8) and (5-9). In this study, the distance between the nearby solutions in the single variable search is defined as critical length. For example, x_1 and x_2 has 13 and 7 local optima in the following Rastrigin's function, and 91 starting points are selected accordingly. While evaluating single variable local optima, the rest of the variables resign in the maximum or minimum of the subset S.

$$f(x) = 20 + \frac{x_1^2}{5} + \frac{x_2^2}{10} - 10(cos2\pi\frac{x_1}{5} + cos2\pi\frac{x_2}{10}) \qquad (5\text{-}10)$$

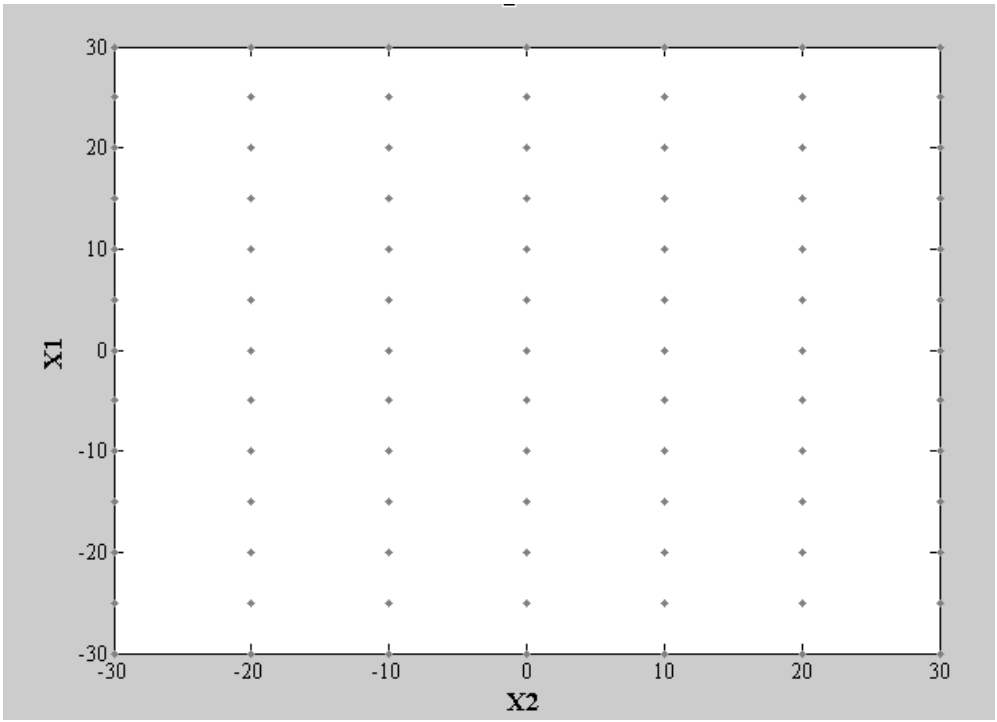

Fig. 5-1 Starting point grid of Rastrigin's function

Once the starting point grid is obtained, objective function f is evaluated through SQP algorithm. The points are sorted in accordance with their L values and the same procedure is repeated with reduced sample and critical length. For each iteration, single variable search is performed and the critical length is reduced by half. When the global optimum occurs at the same place with the previous iteration, the optimization is terminated.

5.4. Case study with Rastrigin's fucnction

In order to show the efficiency and accuracy of the proposed algorithm, the minimum point of Rastrigin's function was evaluated using the scattered search algorithm. The Rastrigin's function is a non-convex function used as a performance test problem for optimization algorithms [77].

$$f(x) = 20 + \frac{x_1^2}{10} + \frac{x_2^2}{10} - 10(cos2\pi\frac{x_1}{10} + cos2\pi\frac{x_2}{10}) \qquad (5\text{-}11)$$

The test ranges of x_i are selected as $-30 \leq x_i \leq 30$. Eq. (5-11) represents the Rastrigin's function, and Fig. 5-2 shows the 3D-surface and contour of it. As indicated in the figure, there are 49 local optima within the subset S, and the global minimum occurs at the location of (0,0) with the value of 0.

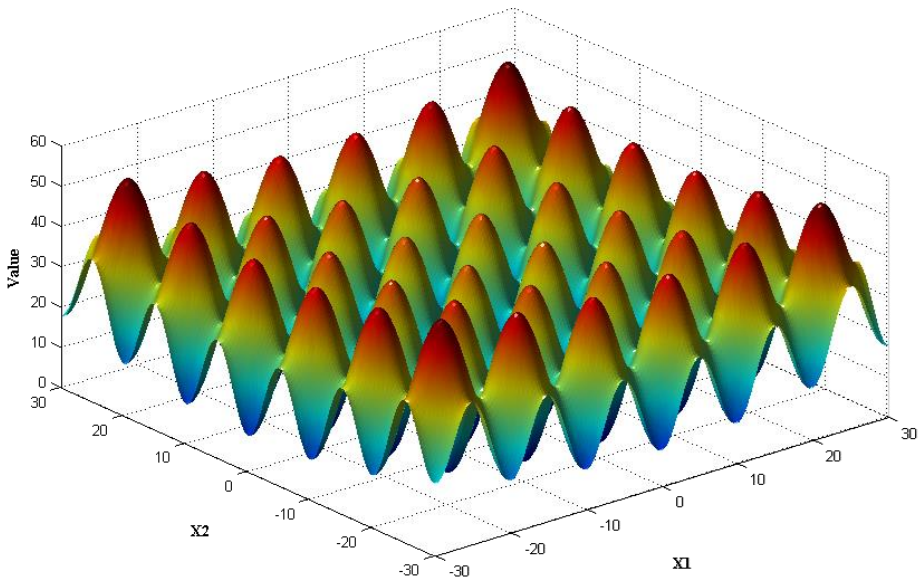

(a) 3D plot of Rastrigin's function

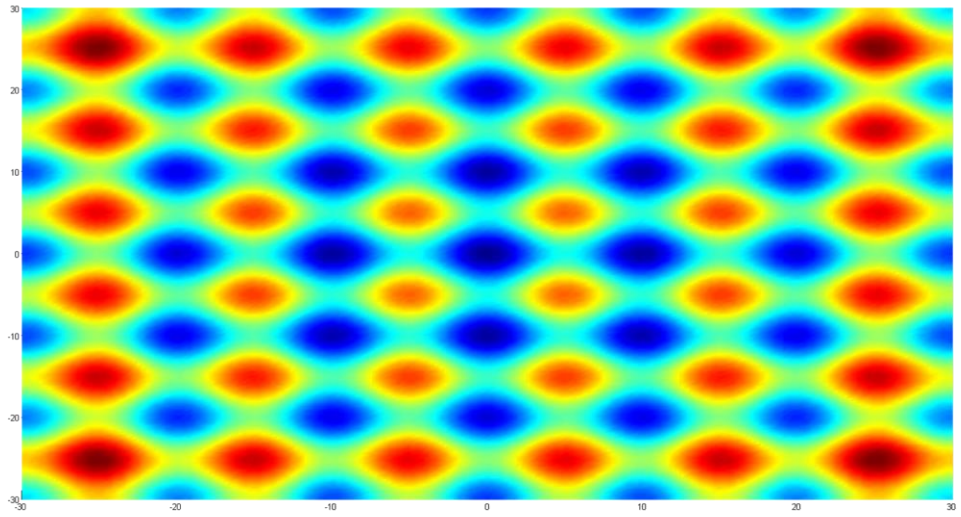

(b) Contour of Rastrigin's function

Fig. 5-2 3D plot and contour of Rastrigin's function

Using Eqs. (5-8) and (5-9), seven local minimum points were found for each x_1 and x_2. Fig. 5-3 depicts behavior of Rastrigin's function depending on single variable and initial starting points of the scattered search method. There are 49 starting points exist and from each starting point local optima were calculated. Once the local optima were obtained, the search domain is reduced by half toward the minimum value of the local optimum, and the critical length is also decreased by half. With two iteration step, the scattered search algorithm was converged at (0, 0), and the minimum value is turned out to be 0.

Several other method were also tested to find the global optimum of Rastrigin's function. These algorithm include fminunc, patternsearch, and genetic algorithm provided by MATLAB™. As presented in Fig. 5-2, one solution is better if the objective function value is closer to 0. Table. 5-1 summarizes the results.

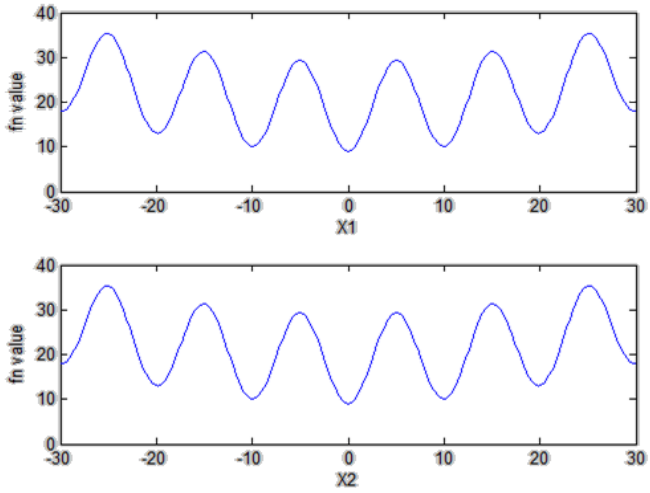

(a) Single variable responds of Rastrigin's function

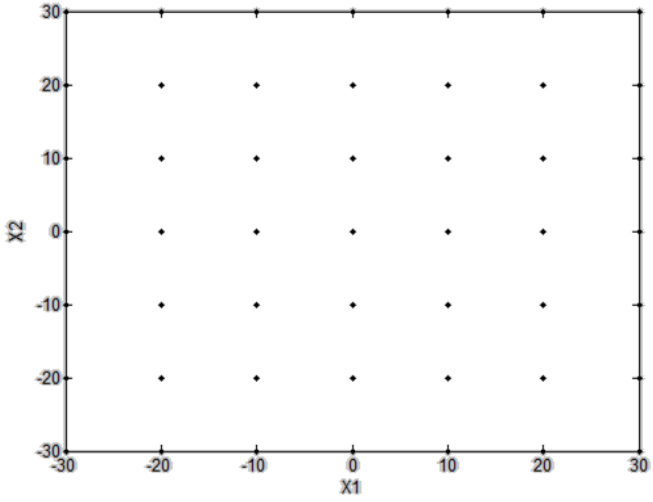

(a) Starting points for scattered search

Fig. 5-3. Single variable responds and starting points of Rastrigin's function optimization

Table. 5-1 Results of Rasfrigin's function optimization with different algorithms

Results	Fminunc	Patternsearch	GA	Scatttered Search
Initial Points	[20, 30]	[20, 30]	[20, 30]	-
Solution	[19.9 29.9]	[19.9 9.9]	[9.9 0]	[0 0]
Objective	12.9	5	1	0
Number of Iteration	15	174	1040	474

The results of the Rasfrigin's function evaluation show typical behavior except scattered search. Fminunc find the solution the most quickly, but could not explore outside of this basin at all. Patternsearch takes more iteration than fminunc and searches through more basin. Consequently, it arrives at a better solution than fminunc. GA takes many more evaluation than pattern search. GA is a stochastic algorithm, so its result change with every run leading better solution than pattern search. However, extra steps may require to arrive the solution. Scattered search proposed in this study shows even better result than GA with smaller iteration steps. Since this algorithm select most probable initial points, both efficiency and accuracy are greatly improved as compared with other optimization methods.

5.5. Implementation of scattered search on irreversibility minimization

The irreversibility minimization problem presented in chapter 4 can be solved using scattered search algorithm. Since there exist numbers of local optima, the SQP algorithm embedded in Aspen Plus may not effective to find the global optimum solution.

$$\begin{gathered} \text{minimize } f(x_1, x_{2,} x_3, p) \\ x_1, x_2, x_3, p \geq 0 \\ x_1 + x_2 + x_3 = 1 \\ \mathrm{m}_{LNG}\Delta\mathrm{H}_{LNG} - \mathrm{m}_{wf}\Delta\mathrm{H}_{wf} \geq 0 \end{gathered} \tag{5-12}$$

The irreversibility minimization problem with , R601-R23-R14 mixture can be represented using Eq. (5-12). The objective function, f, is the irreversibility of the condenser. In order to calculate the irreversibility, thermodynamic properties such as enthalpy, and entropy and stream information along the condenser should be calculated. These information can be calculated using Commercial software, Aspen Plus™, and imported to the MATLAB. Consequently, a scalar value of irreversibility obtained with four variable x_1, x_2, x_3, and p.

From the equality constraint, the variable x_3 can be eliminated. Single variable responds of the rest of the variables are presented in Fig. 5.3.

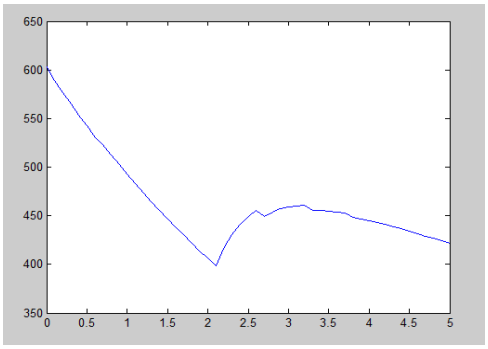

(a) x1

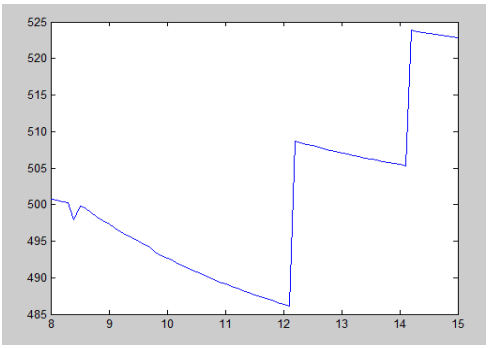

(b) x2

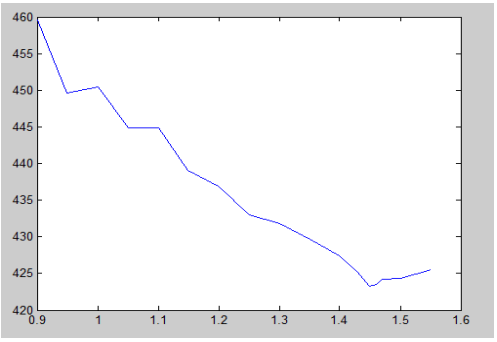

(c) P

Fig. 5-4 Single variable respond of objective function f

There are 27 starting points for scattered search. With these starting points, the minimum irreversibility occurs at x1=3.4, x2=10.6, and P=1.44. The objective function value reaches 387.89 Kcal/Kmol LNG. By utilizing scattered search method proposed in this chapter, both accuracy and efficiency of the condenser irreversibility problem are greatly improved.

CHAPTER 6. Concluding Remarks

6.1. Conclusions

This thesis addressed design and optimization of low carbon emitting combined Rankine cycle. The combined Rankine cycle is consisted of the coal combustion unit, steam cycle, CO_2 capture process, and multi component ORC. The coal combustion model and steam cycle are designed based on the literature data, and CO_2 capture process is based on the pilot plant operation data

In order to minimized the exergy loss and solvent regeneration energy, both lean vapor recompression and mechanical vapor recompression process are adopted. The compression ratio and the stripper operating condition are also optimized in this study. As a result of introducing vapor recompression to CO_2 capture process both total energy consumption and the exergy loss are reduced 27% and 39%, respectively. Consequently, the steam consumption of the CO_2 capture process is reduced by 33%.

The efficiency and power de-rate of the power plant can be further improved by integrating steam cycle with organic Rankine cycle. The ORC proposed in this study utilizes LNG cryogenic exergy and wasted low pressure steam. By using ternary mixture working fluid, the both power generation and exergy loss is greatly improved as compared with pure or binary mixture ORC. In addition, an energy intensive liquefaction process

can be avoided by utilizing vapor CO_2 coming from the capture process as heat source of the preheater. 74MW of additional electricity can be produced from ORC without consuming additional coal, thus both cycle efficiency and power de-rate resulted from CO_2 capture process installation are greatly improved.

In this thesis, a scattered search algorithm which can be easily apply for searching global optima using process simulator. Based on the single variable local optimum information, this method selects deterministic starting point and find the local optimum using sequential quadratic programming method. By repeating the same procedure in the reduced searching area, reliable global optimum point can be obtained. In comparison with genetic algorithm, the proposed method is able to find the optimum point with less than half iteration steps with the better accuracy.

6.2. Future work

Several topics are suggested for future study. First of all, the exergy loss of the CO_2 capture process can be further reduced by implementing advanced configuration or different CO_2 solvents. Secondly, the ORC can produce more power with different substances. Even though more than 55 possible working fluids were reviewed and 12 combinations of the ternary mixture were modeled and optimized, the irreversibility of the condenser can be further reduced with different substances or combinations of working fluid mixtures. For example, substances with high greenhouse potential were excluded in this study, but if the addition of a small amount of these substances can reduce the irreversibility of the system, these substances should be carefully examined and researched. Another point to be considered for the future study is exergy minimization on the evaporator and reheater of the ORC. In this study, more than 45% of the exergy loss comes from the evaporator and reheater. Although the exergy optimization of these units is beyond the scope of this study, because of the abundant low-pressure steam utilization, the exergy efficiency of the system can be greatly improved by optimizing these units. One of the possible ways to reduce the exergy loss in these units is to utilize heat sources with nonisothermal heat transfer, such as flue gas or geothermal energy. With a proper selection of the heat source, further improvement in both the exergy efficiency and power generation of

the ORC with R601-R23-R14 can be expected.

The combined Rankine cycle proposed in this study is mainly focused on the preliminary design. Consequently, further research should be conducted in order to develop it to the front end engineering design. First of all, equipment sizing and cost evaluation are required. According to the equipment sizing and cost information, economic evaluation can be done in order to determine the feasibility of the proposed process. Secondly, control scheme design and robustness evaluation of the process should be carried out. In this stage, dynamic model construction and simulation are required and operation philosophy can also be obtained. Finally, safety analysis is required to identify potential risk and hazards of the process. Risk and hazard analysis of the process including HAZOP study should be carried out and the results should be provided in the front end engineering design. With the future studies, process flow diagram and pipe and instrumentation diagram can be obtained, and these information can be used for the real world implementation of the proposed combined Rankine cycle.

Nomenclature

PC	pulverized coal
LNG	liquefied natural gas
E	exergy (Kcal)
H	enthalpy (Kcal)
T	temperature (℃)
T_0	reference temperature (℃)
S	entropy (Kcal/℃)
$\dot{I}$	irreversibility generation rate (Kcal/hr)
$\dot{E}$	exergy transfer rate (Kcal/hr)
$\dot{m}$	mass transfer rate (kg/hr)
ΔH	latent heat (Kcal)
LC	light component
IC	intermediate component
HC	heavy component
MF	mole fraction
HP	high pressure
IP	intermediate pressure
LP	low pressure
MEA	monoethanol amine
l_v	differential heat of vaporization (Kcal)
Y	vapor composition of mixture
X	liquid composition of mixture
$\bar{H}$	enthalpy per mole (Kcal/mole)
EoS	equation of state
C_p	specific heat
e	exergy per unit mass (Kcal/kg)
$\dot{W}$	power (KW)
$\dot{Q}$	heat transfer rate (Kcal/hr)
P	pressure (bar)
HHV	higher heating value
Greek symbols	
η	efficiency of turbine and pump
Subscripts and superscripts	
Q	heat transferred to cycle
W	work generated
wf	working fluid

l	liquid
v	vapor
Dew	dew point
Bubble	bubble point
s	isentropic
Th	thermal
Ex	exergy

References

[1] Abu-Zahra MR, Schneiders LH, Niederer JP, Feron PH, Versteeg GF. CO_2 capture from power plants: Part I. A parametric study of the technical performance based on monoethanolamine. International Journal of Greenhouse Gas Control. 2007;1:37-46.

[2] Abu-Zahra MR, Niederer JP, Feron PH, Versteeg GF. CO_2 capture from power plants: Part II. A parametric study of the economical performance based on mono-ethanolamine. International journal of greenhouse gas control. 2007;1:135-42.

[3] Alie CF. CO2 capture with MEA: integrating the absorption process and steam cycle of an existing coal-fired power plant: University of Waterloo; 2004.

[4] Mimura T, Simayoshi H, Suda T, Iijima M, Mituoka S. Development of energy saving technology for flue gas carbon dioxide recovery in power plant by chemical absorption method and steam system. Energy Conversion and Management. 1997;38:S57-S62.

[5] Romeo LM, Bolea I, Escosa JM. Integration of power plant and amine scrubbing to reduce CO_2 capture costs. Applied Thermal Engineering. 2008;28:1039-46.

[6] Desideri U, Paolucci A. Performance modelling of a carbon dioxide removal system for power plants. Energy Conversion and Management. 1999;40:1899-915.

[7] Van Wagener D, Gupta A, Rochelle G, Bryant S. Amine Solvent Regeneration for CO2 Capture Using Geothermal Energy with Advanced Stripper Configurations. Oil & Gas Science and Technology–Revue d'IFP Energies nouvelles. 2013.

[8] Jassim MS, Rochelle GT. Innovative absorber/stripper configurations for CO2 capture by aqueous monoethanolamine. Industrial & Engineering Chemistry Research. 2006;45:2465-72.

[9] Chen H, Goswami DY, Stefanakos EK. A review of thermodynamic cycles and working fluids for the conversion of low-grade heat. Renewable and Sustainable Energy Reviews. 2010;14:3059-67.

[10] Chacartegui R, Sánchez D, Muñoz J, Sánchez T. Alternative ORC bottoming cycles for combined cycle power plants. Applied Energy. 2009;86:2162-70.

[11] Vélez F, Segovia J, Chejne F, Antolín G, Quijano A, Carmen Martín M. Low temperature heat source for power generation: exhaustive analysis of a carbon dioxide transcritical power cycle. Energy. 2011;36:5497-507.

[12] Baik Y-J, Kim M, Chang K-C, Lee Y-S, Yoon H-K. Power enhancement potential of a mixture transcritical cycle for a low-temperature geothermal power generation. Energy. 2012;47:70-6.

[13] Roy J, Mishra M, Misra A. Parametric optimization and performance analysis of a waste heat recovery system using Organic Rankine Cycle. Energy. 2010;35:5049-62.

[14] Dai Y, Wang J, Gao L. Parametric optimization and comparative study of organic Rankine cycle (ORC) for low grade waste heat recovery. Energy Conversion and Management. 2009;50:576-82.

[15] Hung T-C. Waste heat recovery of organic Rankine cycle using dry fluids. Energy Conversion and Management. 2001;42:539-53.

[16] Wang J, Yan Z, Wang M, Li M, Dai Y. Multi-objective optimization of an organic Rankine cycle (ORC) for low grade waste heat recovery using evolutionary algorithm. Energy Conversion and Management. 2013;71:146-58.

[17] Xi H, Li M-J, Xu C, He Y-L. Parametric optimization of regenerative organic Rankine cycle (ORC) for low grade waste heat recovery using genetic algorithm. Energy. 2013;58:473-82.

[18] Qiang W, Yanzhong L, Jiang W. Analysis of power cycle based on cold energy of liquefied natural gas and low-grade heat source. Applied thermal engineering. 2004;24:539-48.

[19] Shi X, Che D. A combined power cycle utilizing low-temperature waste heat and LNG cold energy. Energy conversion and management. 2009;50:567-75.

[20] Wang J, Yan Z, Wang M, Dai Y. Thermodynamic analysis and optimization of an ammonia-water power system with LNG (liquefied natural gas) as its heat sink. Energy. 2013;50:513-22.

[21] Yanni L, Kaihua G. Efficiency of power generation by LNG cold energy. Power and Energy Engineering Conference (APPEEC), 2010 Asia-Pacific: IEEE; 2010. p. 1-4.

[22] Liu Y, Guo K. A novel cryogenic power cycle for LNG cold energy recovery. Energy. 2011;36:2828-33.

[23] Szargut J, Szczygiel I. Utilization of the cryogenic exergy of liquid natural gas (LNG) for the production of electricity. Energy. 2009;34:827-37.

[24] Choi I-H, Lee S, Seo Y, Chang D. Analysis and optimization of cascade Rankine cycle for liquefied natural gas cold energy recovery. Energy. 2013;61:179-95.

[25] Rao W-J, Zhao L-J, Liu C, Zhang M-G. A combined cycle utilizing LNG and low-temperature solar energy. Applied Thermal Engineering. 2013;60:51-60.

[26] Austgen DM, Rochelle GT, Peng X, Chen CC. Model of vapor-liquid equilibria for aqueous acid gas-alkanolamine systems using the electrolyte-

NRTL equation. Industrial & engineering chemistry research. 1989;28:1060-73.

[27] Soave G. Equilibrium constants from a modified Redlich-Kwong equation of state. Chemical Engineering Science. 1972;27:1197-203.

[28] Aspelund A, Jordal K. Gas conditioning—The interface between CO_2 capture and transport. International Journal of Greenhouse Gas Control. 2007;1:343-54.

[29] Freguia S, Rochelle GT. Modeling of CO2 capture by aqueous monoethanolamine. AIChE Journal. 2003;49:1676-86.

[30] Lee U, Yang S, Jeong YS, Lim Y, Lee CS, Han C. Carbon Dioxide Liquefaction Process for Ship Transportation. Industrial & Engineering Chemistry Research.

[31] Ciferno J. Pulverized Coal Oxycombustion Power Plants. 2008.

[32] Elliott TC, Kao Chen, Robert Swanekamp Standard handbook of powerplant engineering. New York, NY 10011: McGRAW-Hill; 1989.

[33] Takenouchi S, Kennedy GC. The binary system H 2 O-CO 2 at high temperatures and pressures. American Journal of Science. 1964;262:1055-74.

[34] Tödheide K, Franck E. Das Zweiphasengebiet und die kritische Kurve im System Kohlendioxid–Wasser bis zu Drucken von 3500 bar. Zeitschrift für Physikalische Chemie. 1963;37:387-401.

[35] Dodds W, Stutzman L, Sollami B. Carbon dioxide solubility in water. Industrial & Engineering Chemistry Chemical & Engineering Data Series. 1956;1:92-5.

[36] Drummond SE. Boiling and mixing of hydrothermal fluids: chemical effects on mineral precipitation: Pennsylvania State University; 1981.

[37] Zawisza A, Malesinska B. Solubility of carbon dioxide in liquid water and of water in gaseous carbon dioxide in the range 0.2-5 MPa and at temperatures up to 473 K. Journal of Chemical and Engineering Data. 1981;26:388-91.

[38] Wiebe R, Gaddy V. The solubility of carbon dioxide in water at various temperatures from 12 to 40 and at pressures to 500 atmospheres. critical phenomena*. Journal of the American Chemical Society. 1940;62:815-7.

[39] Houghton G, McLean A, Ritchie P. Compressibility, fugacity, and water-solubility of carbon dioxide in the region 0–36 atm. and 0–100 C. Chemical Engineering Science. 1957;6:132-7.

[40] Wang Y, Xu S, Otto F, Mather A. Solubility of N_2O in alkanolamines and in mixed solvents. The Chemical Engineering Journal. 1992;48:31-40.

[41] Kim I, Svendsen HF. Heat of absorption of carbon dioxide (CO2) in monoethanolamine (MEA) and 2-(aminoethyl) ethanolamine (AEEA) solutions. Industrial & engineering chemistry research. 2007;46:5803-9.

[42] Weiland RH. Physical properties of MEA, DEA, MDEA and MDEA-based blends loaded with CO2: Gas Research Institute; 1996.

[43] Lee JI, Otto FD, Mather AE. Equilibrium between carbon dioxide and aqueous monoethanolamine solutions. Journal of Applied Chemistry and Biotechnology. 1976;26:541-9.

[44] Jou FY, Mather AE, Otto FD. The solubility of CO2 in a 30 mass percent monoethanolamine solution. The Canadian Journal of Chemical Engineering. 1995;73:140-7.

[45] Dean J. Lange's Handbook of Chemistry, 14th edn., 1992. McGraw-Hill, New York, NY.

[46] Hikita H, Asai S, Ishikawa H, Honda M. The kinetics of reactions of carbon dioxide with monoisopropanolamine, diglycolamine and ethylenediamine by a rapid mixing method. The Chemical Engineering Journal. 1977;14:27-30.

[47] Hanley B, Chen CC. New mass-transfer correlations for packed towers. AIChE journal. 2012;58:132-52.

[48] Onda K, Takeuchi H, Okumoto Y. Mass transfer coefficients between gas and liquid phases in packed columns. Journal of Chemical Engineering of Japan. 1968;1:56-62.

[49] Wankat PC. Separation process engineering. Prentice Hall. London, UK: Prentice Hall; 2007.

[50] Coutinho JAP, Kontogeorgis GM, Stenby EH. Binary interaction parameters for nonpolar systems with cubic equations of state: a theoretical approach 1. CO2/hydrocarbons using SRK equation of state. Fluid phase equilibria. 1994;102:31-60.

[51] Li H, Yan J. Evaluating cubic equations of state for calculation of vapor-liquid equilibrium of CO2 and CO2-mixtures for CO2 capture and storage processes. Applied Energy. 2009;86:826-36.

[52] Austegard A, Solbraa E, De Koeijer G, Mølnvik M. Thermodynamic Models for Calculating Mutual Solubilities in H_2O–CO_2–CH_4 Mixtures. Chemical Engineering Research and Design. 2006;84:781-94.

[53] Heggum G, Weydahl T, Roald W, Mølnvik M, Austegard A. CO2 conditioning and transportation. Carbon Dioxide Capture for Storage in Deep Geologic Formations. 2005;2:925-36.

[54] Mitsubush Heavy Industries L. Ship Transport of CO2;. 2004.

[55] Aspelund A, Mølnvik M, De Koeijer G. Ship Transport of CO_2: Technical Solutions and Analysis of Costs, Energy Utilization, Exergy Efficiency and CO2 Emissions. Chemical Engineering Research and Design. 2006;84:847-55.

[56] Barrio M, Aspelund A, Weydahl T, Sandvik T, Wongraven L, Krogstad H, et al. Ship-based transport of CO2. Proceedings of the 7th International Conference on Greenhouse Gas Control Technologie2004. p. 1655-60.

[57] Decarre S, Berthiaud J, Butin N, Guillaume-Combecave J-L. CO_2 maritime transportation. International Journal of Greenhouse Gas Control. 2010;4:857-64.

[58] Lee U, Lim Y, Lee S, Jung J, Han C. CO2 Storage Terminal for Ship Transportation. Industrial & Engineering Chemistry Research. 2012.

[59] Aspelund A, Jordal K. Gas conditioning--The interface between CO2 capture and transport. International Journal of Greenhouse Gas Control. 2007;1:343-54.

[60] Grynia EW, Carroll JJ, Griffin PJ. Dehydration of Acid Gas Prior to Injection. Acid Gas Injection and Related Technologies. 2010:107-27.

[61] Kidnay AJ, Parrish W, Parrish WR. Fundamentals of natural gas processing: CRC; 2006.

[62] Nagle WM. Mean temperature differences in multipass heat exchangers. Industrial & Engineering Chemistry. 1933;25:604-9.

[63] Seider WD, Seader JD, Lewin DR. Product & Process Design Principles: Synthesis, Analysis And Evaluation. Danver, MA: Wiley; 2009.

[64] FULTON S, COLLIE J. Confirm Complex Heat Exchanger Performance. Hydrocarbon Engineering. 1997;75:82.

[65] Song K, Kobayashi R. Water content of CO2 in equilibrium with liquid water and/or hydrates. SPE Formation evaluation. 1987;2:500-8.

[66] Diamond LW, Akinfiev NN. Solubility of CO2 in water from-1.5 to 100 C and from 0.1 to 100 MPa: evaluation of literature data and thermodynamic modelling. Fluid phase equilibria. 2003;208:265-90.

[67] Sanchez Fernandez E, Bergsma EJ, de Miguel Mercader F, Goetheer EL, Vlugt TJ. Optimisation of lean vapour compression (LVC) as an option for post-combustion CO_2 capture: Net present value maximisation. International Journal of Greenhouse Gas Control. 2012;11:S114-S21.

[68] Lepaumier H, da Silva EF, Einbu A, Grimstvedt A, Knudsen JN, Zahlsen K, et al. Comparison of MEA degradation in pilot-scale with lab-scale experiments. Energy Procedia. 2011;4:1652-9.

[69] Peng D-Y, Robinson DB. A new two-constant equation of state. Industrial & Engineering Chemistry Fundamentals. 1976;15:59-64.

[70] Angelino G, Colonna di Paliano P. Multicomponent working fluids for organic Rankine cycles (ORCs). Energy. 1998;23:449-63.

[71] Chen H, Goswami DY, Rahman MM, Stefanakos EK. A supercritical Rankine cycle using zeotropic mixture working fluids for the conversion of low-grade heat into power. Energy. 2011;36:549-55.

[72] Tamir A. Prediction of latent heat of vaporization of multicomponent mixtures. Fluid Phase Equilibria. 1982;8:131-47.

[73] Biggs M. Constrained Minimisation Using Recursive Quadratic Programming Some Alternative Subproblem Formulations: Numerical Optimisation Centre, Hatfield Polytechnic; 1973.

[74] Han S-P. A globally convergent method for nonlinear programming. Journal of optimization theory and applications. 1977;22:297-309.

[75] Powell MJ. A fast algorithm for nonlinearly constrained optimization calculations. Numerical analysis: Springer; 1978. p. 144-57.

[76] Ugray Z, Lasdon L, Plummer J, Glover F, Kelly J, Martí R. Scatter search and local NLP solvers: A multistart framework for global optimization. INFORMS Journal on Computing. 2007;19:328-40.

[77] Rastrigin L. Systems of extremal control. Nauka, Moscow; 1974.

요 약

이 논문은 액화 천연가스의 냉열을 사용하여 발전소의 효율을 향상시키고 온실가스의 배출을 최소화할 수 있는 복합 화력 발전 시스템의 설계와 최적화를 다루고 있다. 논문에서 제시하는 복합 화력 발전 공정은 보일러, 스팀 사이클, 이산화탄소 포집 공정, 유기 랜킨 사이클 (Organinc Rankine Cycle) 등의 단위공정으로 구성되며 각 단위공정의 최적화된 연계를 통하여 발전 효율 및 온실가스 제거율을 극대화하고 있다. 공정의 설계 및 최적화를 위해 순차적 모듈 구조의 상용 공정모사기를 이용하여 공정의 에너지 사용량 및 비가역성을 수치적으로 정의하고 이를 최적화 문제로 구성하였다. 또한 기존의 최적화 알고리즘의 한계를 극복하기 위하여 국소 최적해의 정보를 이용하는 Scattered Search Method를 제시하고 이를 활용하여 최적 설계를 가능하게 하였다.

우선, 논문에서는 화력발전소, 이산화탄소 포집공정 및 압축공정을 포함하는 전체 CCS Chain 의 모델링 및 공정 모사를 수행하였다. 이를 통하여 이산화탄소의 포집에너지 및 발전소 효율저하를 정량적으로 나타내었고 열역학적인 공정 분석을 통하여 대상공정의 개선점들을 제시하였다.

둘째, 발전소 및 액화 천연가스 재 기화 공정에서의 폐열을 이용하여 추가전력을 생산하고 증기 재 압축 공정을 통하여 이산화탄소의 포집에너지를 줄일 수 있는 새로운 공정을 개발하였다. 개발된 공정은 다성분계 작동유체를 사용하여 액화 천연가스 및 발전소 폐스팀으로

부터의 열회수를 극대화하며 이를 통하여 발전효율을 높일 수 있는 장점이 있다. 또한 기존의 이산화탄소 포집 공정에서 낭비되던 잠열 및 현열을 증기 재압축 공정에서 회수하여 포집공정에서 사용되던 증기 사용량을 기존 공정 대비 30% 이상 절감 시켰다.

마지막으로 다변수 비선형 Non-Convex 문제를 효과적으로 풀 수 있는 새로운 최적화 기법을 제시하였다. 제시된 최적화 기법은 국소해의 정보를 이용하여 최적화를 수행함으로써 기존의 최적화 방법론에 비해 풀이 시간 및 정확성을 획기적으로 향상시키고 동시에 풀이과정의 강건성이 높아지는 장점이 있다.

이 연구에서 제안하는 공정은 기존 CCS 기술의 문제점으로 지적되는 발전소의 효율저하를 절반 이하로 낮출 수 있다. 또한 공정 설계에 사용된 열역학적 최적화 기법 및 그 해결 알고리즘은 여러 화학공정에서 최적화된 공정 설계를 수행하는데 기여할 수 있을 것으로 판단된다.

주요어: 이산화탄소 포집, 액화 천연가스, 엑서지 분석, 최적화, 복합발전, 유기 랜킨 사이클, 다성분계 작동유체

학번: 2010-21006
성명: 이 웅